

THREAD-LIKE PARTICLES IN SHEARED SUSPENSIONS

A THESIS

by

Otto Lionel Forgacs, B.Sc.(Tech.), (Manchester)

Submitted to the Faculty of Graduate
Studies and Research of McGill University
in partial fulfilment of the requirements
for the degree of Doctor of Philosophy

Department of Chemistry,
McGill University,
Montreal, Canada.

August 1958.

ACKNOWLEDGEMENTS

The author wishes to express his sincere thanks to Dr. S.G. Mason for his valuable guidance and encouragement in this work, and for his constant readiness to discuss problems.

Grateful acknowledgement is also made to:

Dr. A.A. Robertson for many useful discussions;

the Consolidated Mining and Smelting Co. of Canada Limited for a fellowship during the session 1956-1957;

the National Research Council of Canada for a studentship during the session 1957-1958, and for a summer scholarship in 1957;

the Pulp and Paper Research Institute of Canada for financial assistance during the summer of 1956;

the Pulp and Paper Research Institute of Canada for laboratory accommodation and equipment, and for permitting the author liberal use of its service facilities. The co-operation of the Chemical Pulping and Physical Measurements Group in the preparation and routine testing of pulp samples is especially appreciated;

F.D. Rumscheidt for assistance in the photographic work;

Dr. S.G. Mason and A.P. Arlov for permission to include a paper, which was written with their co-authorship, as an appendix to this thesis.

FOREWORD

This thesis forms one of a series of fundamental investigations conducted in this laboratory in connection with the flow properties of papermaking pulp suspensions.

Previous studies have appeared in the scientific literature as a series of papers entitled "Particle Motions in Sheared Suspensions". These studies were reviewed recently in a paper by W. Bartok and S.G. Mason, "The Behaviour of Suspended Particles in Laminar Shear", presented at the Symposium on the Rheology of Disperse Systems, British Society of Rheology, September 1957 (in Press).

The structure of the thesis requires some explanation. The experimental work is presented in Parts II, III and IV. These parts have been written to achieve brevity without loss of clarity, and to make it possible for the work to be published in the scientific literature with little or no further modification. Each part is complete in itself, with its own introduction, experimental section, discussion, summary and bibliography.

The objectives of the work and a short review of the background is given in Part I.

A discussion of some broader aspects of the work, and

recommendations for further studies are given in Part V.

A paper dealing with a preliminary investigation of the behaviour of pulp fibres in sheared suspensions is included as Appendix I.

Appendix II contains additional information on the apparatus and the experimental technique.

For the benefit of readers unfamiliar with papermaking, a brief glossary of specialized terms used in Part IV is given as Appendix III.

TABLE OF CONTENTS

	Page
PART I	
GENERAL INTRODUCTION	
A. THE NATURE OF THE PROBLEM.....	1
B. PREVIOUS WORK.....	2
C. SCOPE OF THE THESIS.....	5
REFERENCES.....	7
PART II	
THREAD-LIKE PARTICLES: SPIN AND DEFORMATION	
A. INTRODUCTION.....	8
B. THEORETICAL.....	11
1. The Spin of Rigid Rods.....	11
2. The Forces Causing Deformation.....	13
(i) Burgers' Theory.....	13
(ii) Effect of Orientation on Axial Forces.....	17
(iii) Shear Induced Buckling.....	18
C. EXPERIMENTAL METHODS.....	26
D. RESULTS AND DISCUSSION.....	28
1. The Spin of Rigid Rods.....	28
2. The Onset of Bending.....	29
(i) Variation of η	31
(ii) Variation of r	31
(iii) The Elastic Constants.....	34
(iv) Orbits of Bent Particles.....	35
E. SUMMARY.....	38
REFERENCES.....	40
PART III	
THREAD-LIKE PARTICLES: FLEXIBLE ORBITS	
A. INTRODUCTION.....	41
B. EXPERIMENTAL PART.....	43
1. Apparatus and Materials.....	43
2. Method of Varying Particle Flexibility.....	45
C. RESULTS AND DISCUSSION.....	46
1. The Orbits of Deformable Threads.....	46
(i) Springy and Snake Orbits.....	46
(ii) Coiled Orbits without Entanglement.....	52
(iii) Coiled Orbits with Entanglement.....	59

TABLE OF CONTENTS (cont'd)

	Page
2. The Effect of Deformation on TG.....	63
(i) Preliminary.....	63
(ii) The Effect of Permanent Deformation.....	67
(iii) The Variation of TG with r.....	71
(iv) The Variation of TG with G.....	75
D. SUMMARY.....	81
REFERENCES.....	83

PART IV

THE FLEXIBILITY OF WOOD PULP FIBRES

A. INTRODUCTION.....	84
B. PRINCIPLES OF THE METHOD.....	85
1. General.....	85
2. Orbit Types.....	88
3. Theoretical Considerations.....	96
C. EXPERIMENTAL PART.....	99
1. Apparatus.....	99
2. Materials.....	99
3. Procedure.....	101
D. RESULTS.....	104
1. The Effect of Fibre Length.....	104
2. The Effect of Pulping Conditions.....	107
3. The Effect of Beating.....	121
4. The Effect of Moisture.....	131
E. DISCUSSION.....	135
F. SUMMARY.....	143
REFERENCES.....	144

PART V

GENERAL DISCUSSION AND RECOMMENDATIONS FOR FURTHER WORK

A. PREFERRED ORIENTATIONS OF FLEXIBLE PARTICLES.....	145
B. THE VISCOSITY OF SUSPENSIONS.....	146
C. THE WEISSENBERG EFFECT.....	153
D. THE FLEXIBILITY OF PULP FIBRES.....	154

TABLE OF CONTENTS (cont'd)

E. SUMMARY OF RECOMMENDATIONS FOR FURTHER WORK.....	155
REFERENCES.....	157
CLAIMS TO ORIGINAL RESEARCH.....	158

APPENDIX I

GENERAL BEHAVIOUR OF WOOD PULP FIBRES IN SHEARED SUSPENSIONS..	159
----------------------------------------------------------------	-----

APPENDIX II

A. THE COUETTE APPARATI.....	160
1. Principles of the Apparatus.....	160
2. Effective Shear Rate.....	161
3. Apparatus No. 1	164
4. Apparatus No. 2	165
5. Avoidance of Wall Effects and End Effects.....	175
6. Precision of Calculated Values of G.....	176
B. PHOTOGRAPHIC TECHNIQUES.....	176
C. PREPARATION OF FILAMENT SAMPLES.....	177
D. MEASUREMENT OF THE PERIODS OF ROTATION.....	178
E. VISCOSITIES OF SUSPENDING MEDIA.....	179
REFERENCES.....	181

APPENDIX III

GLOSSARY.....	182
---------------	-----

LIST OF TABLES

Table		Page
PART II		
I	$2M_{\max}$ at different values of C.....	21
II	Predicted and observed axial spin.....	30
III	The effect of viscosity on critical bending.....	32
IV	Comparison of E_b at various axis ratios with E.....	33
PART III		
I	Helix formation of elastomer filaments.....	58
II	The effect of flexibility on TG of pulp fibres.....	64
III	Variation of TG with r.....	72
PART IV		
I	Rotational orbits of rayon filaments in corn syrup....	98
II	Pulping condition.....	100
III	Reproducibility experiment.....	103
IV	Orbit distributions of Douglas Fir sulphite pulps.....	110
V	Orbit distributions for Black Spruce sulphite pulps...	111
VI	Orbit distributions of Black Spruce kraft pulps.....	112
VII	Orbit distributions in beater pulps.....	124
VIII	Effect of drying.....	132
APPENDIX II		
I	Dimensions and speeds of Couette cylinders.....	174
II	Viscosities of suspending media.....	180

LIST OF FIGURES

PART II		Page
Figure		
1	The spherical elliptical orbit of a rotating cylinder.....	9
2	The variation of $f(k)$ with k	14
3	Calculated variation of $2M$ with ϕ	19
4	The model rod used in the theory of shear-induced buckling.....	23
5	Polar plot of the loci of the ends of a Nylon filament during rotation.....	36
PART III		
1	Springy rotation.....	48
2	Snake rotation.....	50
3	Helix rotation viewed along the Z-axis.....	54
4	Helix rotation viewed along the Y-axis.....	56
5	Coil formation.....	61
6	TG vs. r - preliminary results.....	65
7	The effect of permanent deformation on r_e for rigid rotations in the XY-plane.....	69
8	TG vs. r	73
9	TG vs. G for rayon filaments undergoing snake rotations.....	77
10	TG vs. G for various deformable particles.....	79

LIST OF FIGURES (cont'd)

PART IV

1	The co-ordinate system in relation to the shear field.....	86
2	Schematic diagram of the rotational orbits of fibres in the XY-plane.....	91
3	Segmental bending: photomicrographs of spruce sulphite fibres in polarized light.....	93
4	The effect of fibre length on the orbit distributions	105
5	Orbit distribution vs. yield: Douglas Fir sulphite series.....	113
6	Orbit distribution vs. yield: Black Spruce sulphite series.....	115
7	Orbit distribution vs. yield: Black Spruce kraft series.....	117
8	Percent rigid orbits vs. Klason lignin content: spruce sulphite pulps.....	119
9	The development of flexible orbits vs. Canadian Standard Freeness.....	125
10	The frequency of flexible fibres vs. beating time...	127
11	Combined flexible orbits (III + IV + V) together with breaking-length and bulk vs. beating time.....	129
12	Photomicrographs of virgin, freeze dried, and oven dried fibres.....	133
13	The differential distribution of flexibility $D(f)$ vs. flexibility f	139
14	Δ and Klason lignin content vs. yield.....	141

LIST OF FIGURES (cont'd)

PART V

1	Graph of $(\alpha_0)^{1/2}$ vs. r	150
---	-------------------------------------------	-----

APPENDIX II

1	Principle of the Couette apparatus.....	162
2	Photograph of apparatus no. 1.....	166
3	Schematic diagram of the apparatus no. 1.....	168
4	Photograph of apparatus no. 2.....	170
5	Sectional diagram of the apparatus no. 2.....	172

LIST OF SYMBOLS

a'	=	semi-length of a cylindrical particle.
b'	=	semi-diameter of a cylindrical particle.
C	=	orbit constant.
c	=	concentration (Part V only).
E, E_b	=	tensile and bending moduli of elasticity.
F	=	axial force acting on the central cross-section of a rod.
G	=	velocity gradient.
He_n	=	Hermite function of order n .
I	=	moment of inertia.
\underline{l}	=	co-ordinate measured along the length of a rod.
M	=	orientation factor (Part II).
m	=	orientation factor (Part V).
N_a, N_b	=	r.p.m. of outer and inner Couette cylinders.
n	=	number of axial spins in time T .
R_a, R_b	=	radii of outer and inner Couette cylinders.
r	=	axis ratio of a cylindrical particle.
r_e	=	equivalent ellipsoidal axis ratio.
T	=	period of rotation about the Z-axis. Also period of circulation of a fluid drop.
t	=	time.
u, v, w	=	velocity components along the X-, Y- and Z-axes of the shear field.

LIST OF SYMBOLS (Cont'd)

X, Y, Z	=	cartesian co-ordinates.
α	=	angle between the tangents at the ends of a curved filament.
α_0	=	intrinsic viscosity.
β	=	r/r_e , a correction factor in the theory of viscosity.
ζ	=	a co-ordinate in the theory of buckling of a rod.
η	=	viscosity of suspending medium.
η_{sp}	=	specific viscosity.
θ, ϕ	=	colatitudinal and azimuthal polar co-ordinates (Z = polar axis).
λ	=	azimuthal angle (Y = polar axis).
ψ, k	=	parameters in the theory of axial spin.
Ω	=	angle of axial spin.
ω_s	=	angular velocity of spin.
ω_a, ω_b	=	angular velocities of the outer and inner Couette cylinders.

PART I

GENERAL INTRODUCTION

A. THE NATURE OF THE PROBLEM

The flow properties of a liquid containing particles in suspension differ from those of the pure liquid in a number of ways which depend principally on the characteristics and concentration of the particles.

In the presence of velocity gradients the particles undergo translational and rotational motions, and cause disturbances of the field of flow. In laminar shear flow, the disturbances cause local increases in the velocity gradient; these result in an increase in the rate of dissipation of energy and are manifested in an increase in the viscosity of the suspension over that of the pure suspending liquid (without particles).

If the particles are unsymmetrical or deformable, preferred orientations are established, which give rise to streaming birefringence and under certain conditions non-Newtonian behaviour. At sufficiently high concentrations, the flow behaviour of the suspensions is further complicated by particle interactions and the formation of aggregates and structures.

Many of the observed phenomena are not completely understood. Insight into the behaviour of suspensions can only be attained if the behaviour of the individual particles is known, but rigorous treatments using the methods of hydrodynamics have thus far been limited by the complexity of the problem to spheres (1), ellipsoids of revolution (2) and fluid drops

suffering small deformations (3). Even for these simple particles the treatments are limited to conditions at which the particles do not interact and do not possess Brownian motion. A knowledge of the motions of more complicated particles may, however, be achieved experimentally.

Previous work in this laboratory has dealt with the motions, orientations and interactions of rigid spheres (4, 5, 6), smooth rigid rods (4, 6, 7), fluid drops (8, 9) and rigid and flexible pulp fibres (10). In the present work, these studies have been extended to deformable thread-like particles.

B. PREVIOUS WORK

Einstein (1) in deriving his classical equation for the viscosity of suspensions of spheres from rigorous hydrodynamics, predicted that spheres rotate at an angular velocity

$$\omega = G/2 \quad (1)$$

where G is the velocity gradient. Jeffery (2) extended the treatment to prolate and oblate spheroids and deduced orbital motions which are discussed in detail in Part II. The forces acting on a prolate spheroid reduce to two couples, one tending to rotate the particle and the other tending to set its axis along the direction of flow of the liquid. As a result, the particle precesses in a spherical elliptical orbit about an axis normal to the directions of flow and of the gradient (i.e. about the Z-axis of Fig. 1, Part II).

In addition, the particle spins about its own axis. According to the equations of motion the angular velocity of both types of rotation depends on G , the particle axis ratio and the instantaneous orientation of the particle relative to the field of flow. The higher the axis ratio, the greater is the time the particle spends in the neighbourhood of the direction of flow.

Jeffery also calculated the contribution to viscosity made by the individual particles. This was shown to be least for the orbit in which the particle spins with its axis normal to the plane of the gradient (i.e. along the Z-axis of Fig. 1, Part II), and greatest for the orbit in which the particle rotates with its axis in the plane of the gradient (i.e. in the XY-plane). Jeffery assumed intuitively that prolate spheroids will drift into the orbit corresponding to the least contribution to viscosity. Saffman (11) claimed that such a drift may be explained by considering inertia terms which were neglected in Jeffery's treatment, but that the effect was too small to be observed experimentally.

The periodic rotations of ellipsoidal particles were first observed by Taylor (12) in a Couette apparatus in which the outer cylinder was rotated. Taylor found that the preferred orbit predicted by Jeffery was assumed after about 100 rotations, though the validity of this result has been questioned (11).

Eirich and co-workers (13, 14) and Binder (15) observed periodic rotations similar to those of prolate spheroids with rigid cylindrical particles made of glass, silk, rayon and human hair. Preferred orbits as predicted by

Jeffery were observed with particles of axis ratio less than 5.

Quantitative observations on particle rotations were first made by Trevelyan and Mason (4), using a twin-cylinder Couette device in which the cylinders were rotated in opposite directions. The validity of Eq. (1) for spheres was confirmed, although indirect proof had previously been provided by confirmation of the viscosity equation (16, 17). Mason and co-workers (4, 5, 6) also observed the rotations of rigid cylindrical particles made of glass, Dacron and Orlon. The spherical elliptical orbits described by these particles were found to be identical with those predicted for prolate spheroids (1) provided an equivalent ellipsoidal ratio (4) was used in the equations of motion instead of the true axis ratio of the particles. Despite extensive observations, Manley (7) was unable to find systematic drifts towards preferred orbits. However, the steady-state distribution of orbits at finite concentrations were found to lie between those calculated from the assumption of Jeffery, which has already been mentioned, and the assumption of Eisenschitz (19) that the particles are isotropically distributed before the onset of motion and thereafter retain their original orbits.

Taylor (3, 18) and Bartok and Mason (9) studied the motions and deformations of fluid spheres. Several results are of interest in connection with the present work, to which reference is made in Part III.

The rotations and spins executed by rigid and flexible wood-pulp fibres in laminar shear were described in a recent paper by Arlov, Forgacs and Mason (10). It was shown that when rigid, the fibres rotated in spherical elliptical orbits in the same general manner as smooth rigid rods. Flexible

fibres rotated in orbits which became more complicated the greater the degree of deformation.

Unlike rigid fibres, isolated flexible fibres rapidly assumed one of two preferred orbits. The period of rotation T of flexible fibres was substantially lower than for rigid rods of the same axis ratio. It has been shown theoretically and experimentally (4) that for rigid rods, the product TG is independent of G . With flexible fibres, TG increased appreciably with increasing G , an effect which appeared to be associated with an increase in the amount of deformation during rotation. The paper (10) on the motions of pulp fibres formed a starting point for the present work. It is included in the thesis as Appendix I.

C. SCOPE OF THE THESIS

The objectives of this work were:

- (i) To confirm quantitatively Jeffery's theoretical equation for axial spin.
- (ii) To determine the variables which govern the shear-induced deformation of thread-like particles.
- (iii) To study the motions of thread-like particles over a wide range of flexibility, and the effect of deformation on the periodic time of rotation.
- (iv) To develop a method of measuring the flexibility of wood-pulp fibres based on their behaviour in liquid shear.

The material is presented in three parts. Part II deals with axial spin of rigid particles and the critical conditions required

for shear-induced bending of a rod.

In Part III, the motions of thread-like particles are described, under conditions where various degrees of deformation occur. Parts II and III are of a fundamental nature, and the results are of general interest in connection with the flow of suspensions.

Part IV which utilizes the principles set forth in Parts II and III to obtain a "flexibility spectrum" for suspensions of wood-pulp fibres is of specific interest to pulp and paper technology.

REFERENCES

1. Einstein, A., Ann. Physik. 19:289 (1906);
84:591 (1911).
2. Jeffery, G.B., Proc. Royal Soc. (London) A 102:117 (1922).
3. Taylor, G.I., Proc. Royal Soc. (London) A 146:501 (1934).
4. Trevelyan, B.J. and Mason, S.G., J. Colloid Sci. 6, No. 4:354 (1951).
5. Manley, R.St.J. and Mason, S.G., J. Colloid Sci. 7, No. 4:354 (1952).
6. Bartok, W. and Mason, S.G., J. Colloid Sci. 12, No. 3:243 (1957).
7. Mason, S.G. and Manley, R.St.J., Proc. Royal Soc. (London) A 238:
117 (1956).
8. Manley, R.St.J. and Mason, S.G., Can. J. Chem. 33:763 (1955).
9. Bartok, W. and Mason, S.G., Forthcoming publication.
10. Arlov, A.P., Forgacs, O.L. and Mason, S.G., Svensk Papperstidn. 61,
No. 3:61 (1958). Also Appendix I of this Thesis.
11. Saffman, P.G., J. Fluid Mech. 1, Part 5:540 (1956).
12. Taylor, G.I., Proc. Royal Soc. (London) A 103:58 (1923).
13. Eirich, F., Margaretha, H. and Bunzl, M., Kolloid Z. 75:20 (1936).
14. Eirich, F., Reports on Progress in Physics 7:329 (1940).
15. Binder, A., J. Appl. Physics 10:711 (1939).
16. Vand, V., J. Phys. and Colloid Chem. 52:277 (1948).
17. Eirich, F., Bunzl, M. and Margaretha, H., Kolloid Z. 74:276 (1936).
18. Taylor, G.I., Proc. Royal Soc. (London) A 138:41 (1932).
19. Eisenschitz, R., Z. Phys. Chem. A 158:84 (1932).

PART II

THREAD-LIKE PARTICLES: SPIN AND DEFORMATION

A. INTRODUCTION

When a viscous liquid containing suspended particles is subjected to laminar shear, the particles undergo rotation and deforming stresses. Jeffery (1) predicted theoretically that the major axis of a prolate spheroid of axis ratio r_e rotates in a spherical elliptical orbit described by the equations:

$$\tan \theta = \frac{Cr_e}{(r_e^2 \cos^2 \phi + \sin^2 \phi)^{1/2}} \quad (1)$$

and
$$\tan \phi = r_e \tan 2\pi t/T \quad (2)$$

in a field of fluid shear defined by $u = Gy$, and $v, w = 0$ where u, v and w are respectively the components of velocity of the undisturbed liquid along the X-, Y- and Z-axes of the co-ordinate system shown in Fig. 1. θ and ϕ are the spherical polar co-ordinates of the major axis of the spheroid and C is the orbit constant which is related to the eccentricity of the spherical elliptical path described by the ends of the particle axis. T is the period of rotation about the Z-axis and is given by

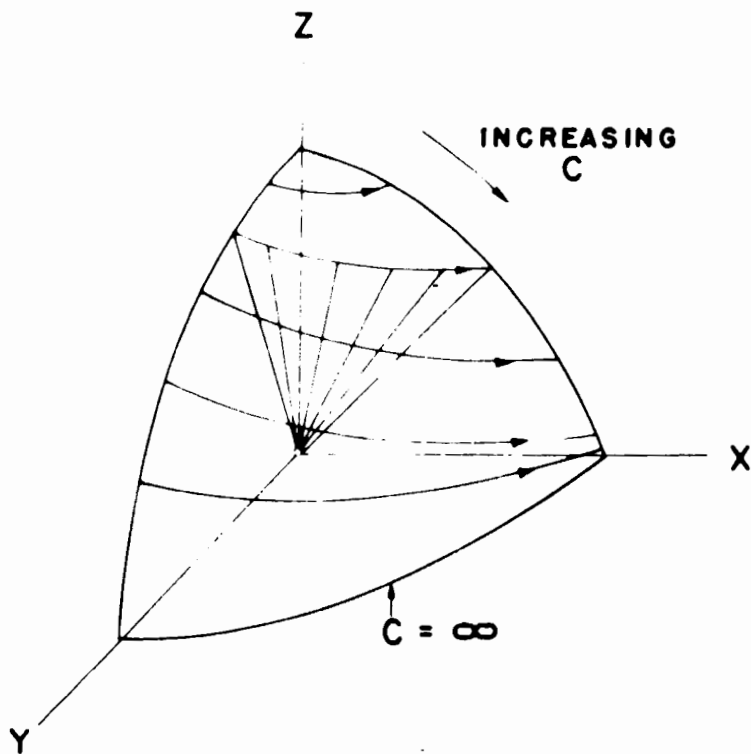
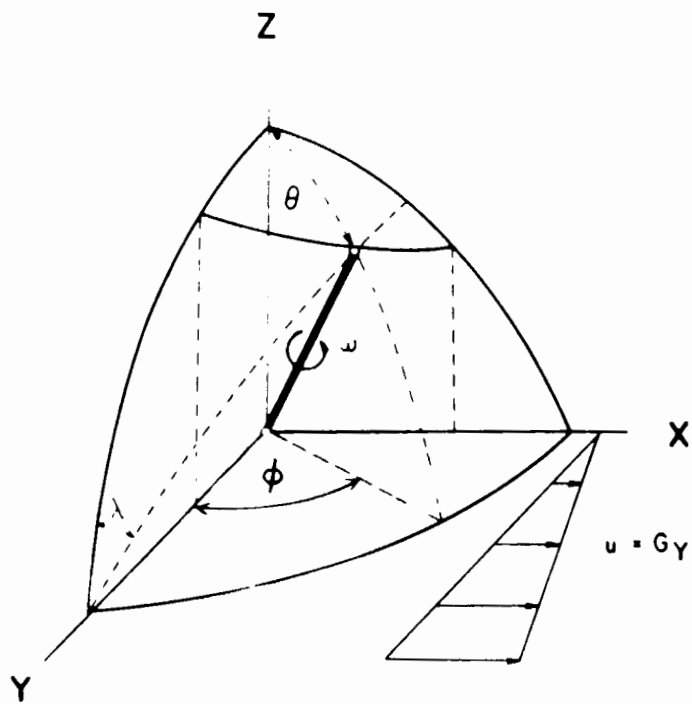
$$T = 2\pi(r_e + \frac{1}{r_e})/G \quad (3)$$

$$= 2\pi r_e/G \quad \text{for } r_e \gg 1$$

In addition, it was predicted that the particle undergoes

FIGURE 1

The spherical elliptical orbit of a rotating cylinder. The co-ordinate system is shown in relation to the shear field (upper diagram). In studying the particle orbits, the angle λ is conveniently measured by viewing along the Y-axis. The lower diagram shows a series of orbits corresponding to various values of the orbit constant C.



spin about its major axis at an angular velocity ω_s given by

$$\omega_s = d\Omega/dt = \frac{G}{2} \cdot \cos \theta \quad (4)$$

where Ω is the angle of rotation (spin) about the main axis.

Various experimental studies (2, 3, 4) of the rotations of straight rigid rods have shown excellent agreement with the details of the orbits defined by Eqs. (1) and (2) provided that the "equivalent ellipsoidal axis ratio" (r_e) calculated from the measured period of rotation using Eq. (3), was used instead of the true axis ratio r in the orbital equations. Observations of the spin of wood-pulp fibres were made which showed qualitatively agreement with Eq. (4), (5).

In earlier studies of the rotations of wood-pulp fibres it was found that under certain conditions the fibres were deformed by the action of the liquid and that this deformation resulted in orbits which were different from those of rigid particles (6), (see Appendix I). In this Part a simple theory of the onset of bending and corroborative experimental data obtained by means of uniform filaments are presented. In addition experiments are described which were designed to provide a quantitative test of the spin predicted from Eq. (4).

B. THEORETICAL

1. The Spin of Rigid Rods

The simplest test of Eq. (4) is to calculate the number of complete axial spins executed in the course of a complete rotation

about the Z-axis, and to compare this with the observed value. This calculation is made below.

The variation of θ with time can be determined by eliminating ϕ from Eqs. (1) and (2) to yield:

$$\cos \theta = \frac{A}{B} \left[\frac{1 + \tan^2 2\pi t/T}{1 + \Gamma^2 \tan^2 2\pi t/T} \right]^{1/2} = F(t) \quad (5)$$

$$\text{where } A^2 = \frac{r_e^2}{r_e^2 - 1}, \quad B^2 = \frac{r_e^2(c^2 + 1)}{r_e^2 - 1} \quad \text{and} \quad \Gamma^2 = \frac{c^2 r_e^2 + 1}{c^2 + 1}$$

The theoretical number of complete spins through $\Omega = 2\pi$ which a particle undergoes in time T is therefore given by integrating Eq. (4)

$$n = \Delta\Omega/2\pi = \frac{G}{2} \int_0^{T/4} F(t) dt$$

By making the substitutions into the above equation:

$$\psi = 2\pi t/T, \quad k = \Gamma^2 - 1 = \frac{c^2(r_e^2 - 1)}{c^2 + 1}$$

it may readily be shown that

$$n = \frac{TG}{2\pi^2} \cdot \frac{A}{B} \cdot f(k) \quad (6a)$$

$$\text{where } f(k) = \int_0^{\pi/2} \frac{d\psi}{(1 + k^2 \sin^2 \psi)^{1/2}} \quad (6b)$$

The function $f(k)$ was evaluated by graphical integration for a series of values of k , with the results shown in Fig. 2. Eq. (6a) was tested by viewing individual particles along the Y-axis, so that the XZ-projection of the particles was observed. The particle rotations may also be described by the variation of the azimuthal angle λ formed by the Z-axis and the projection of the particle on the XZ-plane (Fig. 1). By combining Eqs. (1) and (2) it has been shown (2) that

$$\tan \lambda = Cr_e \sin 2\pi t/T \quad (7a)$$

According to Eq. (7a), the XZ-projection rocks back and forth between $\pm \lambda_{\max}$ given by

$$\tan \lambda_{\max} = Cr_e \quad (7b)$$

from which the orbit constant C , a parameter in Eq. (6a), can be evaluated if λ_{\max} and r_e are known.

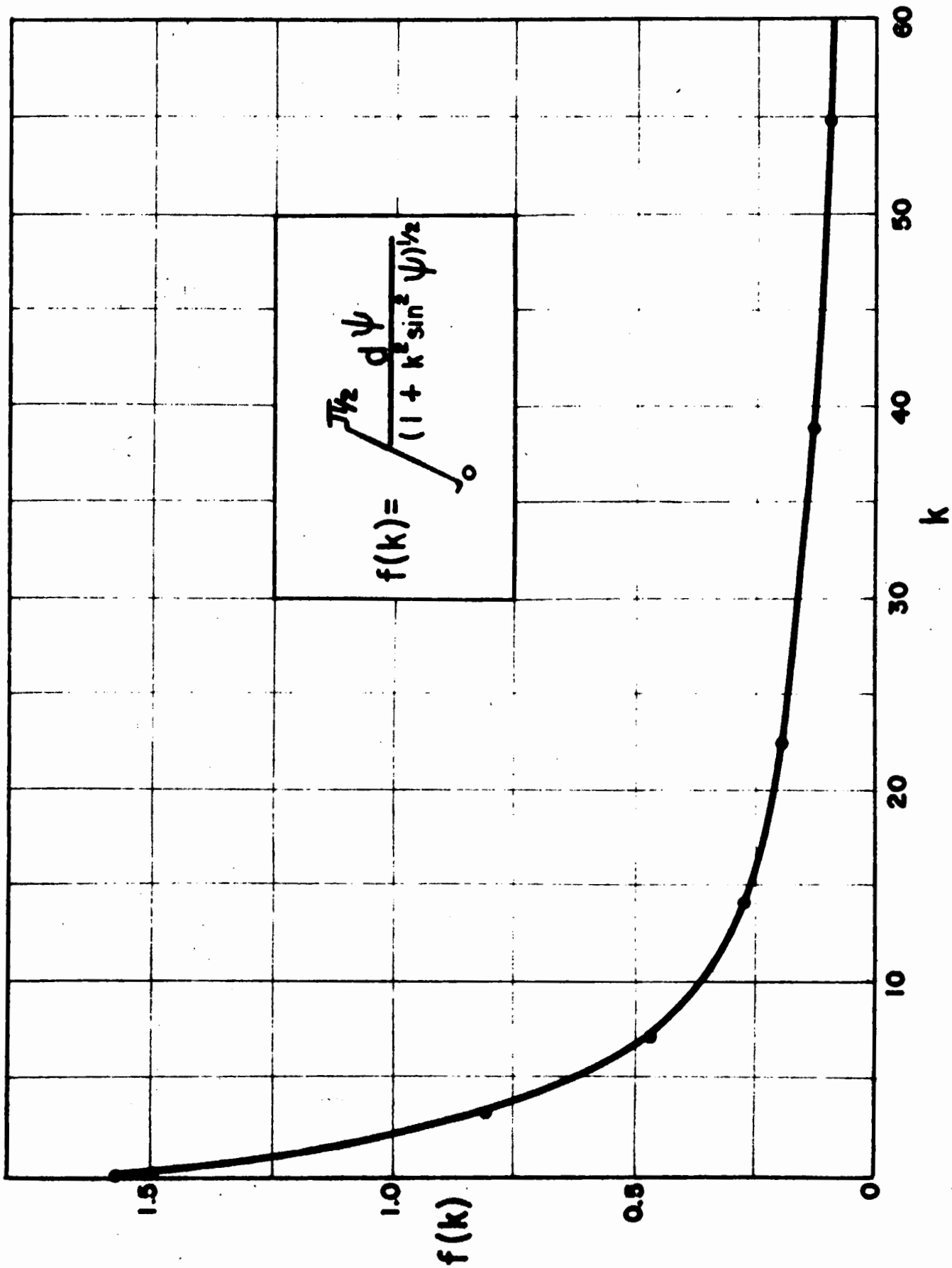
2. The Forces Causing Deformation

(i) Burgers' Theory

In this section we consider briefly an approximate theory of the forces acting on a thin rod in laminar shear, developed by Burgers (7) to explain certain anomalies in the streaming birefringence of macromolecules in solution. The theory assumes the particles to be rigid, non-sedimenting, without Brownian motion and to be so thin that the

FIGURE 2

The variation of $f(k)$ with k . Values of $f(k)$ were obtained by graphical integration of Eq. (6b).



disturbance of the flow pattern of the suspending medium is negligible; inertial effects are neglected and it is assumed that there is no slip at the interface.

Let \underline{l} be the distance from the centre along the rod of total length $2a'$ ^{*}, so that $\underline{l} = 0$ at the origin of the co-ordinate system shown in Fig. 1. We may now write

$$u = G\underline{l} \sin \theta \cos \phi$$

u , the velocity in the X-direction, may be resolved into three perpendicular components. Two of the components act at right angles to the axis of the rod, one tending to increase ϕ and the other θ . Since inertial effects are assumed negligible, these components will cause rotation of the rod about the Z-axis, but will not create stresses along the axis of the rod. The third velocity component given by

$$u' = G\underline{l} \sin^2 \theta \sin \phi \cos \phi = G\underline{l} M \quad (8)$$

acts along the axis of the rod. $M = \sin^2 \theta \sin \phi \cos \phi$ is an orientation factor. To satisfy the condition of no slippage at the rod-fluid interface, u' must set up a system of forces $f(\underline{l}) d\underline{l}$ (= the increment of force over length $d\underline{l}$) to produce a velocity $-G\underline{l} \sin^2 \theta \sin \phi \cos \phi$ at the surface of the rod.

^{*}

In previous publications on this subject from this laboratory \underline{a} and \underline{b} have been used to designate the length and diameter respectively of a rod. In the analysis given here it is convenient to use the semi-length and semi-diameter. To avoid confusion with the earlier symbols, a' and b' are employed in this presentation.

The total axial force F acting on the central cross section of the rod (at $\underline{l} = 0$) is obtained from the integral

$$F = - \int_a^0 f(\underline{l}) d\underline{l}$$

which Burgers has shown to have the approximate form

$$F = \frac{\pi G \eta a'^2 M}{\log_e 2a'/b' - 1.75} \quad (9)$$

where η is the viscosity of the suspending medium. The sign of F depends upon whether ϕ is negative or positive, and determines whether the rod is under compression or tension respectively.

(ii) Effect of Orientation on Axial Forces

Eq. (9) shows that F depends on the dimensions of the particles, the product $G\eta$ and the orientation factor M . To find how F varies with M we write:

$$M = \frac{\tan^2 \theta \sin \phi \cos \phi}{\tan^2 \theta + 1} \quad (10)$$

Substituting for $\tan \theta$ by means of Eq. (1) yields

$$M = \frac{C^2 r_e^2 \sin \phi \cos \phi}{C^2 r_e^2 + r_e^2 \cos^2 \phi + \sin^2 \phi}$$

or

$$2M = \frac{C^2 \sin 2\phi}{C^2 + 1 - \sin^2 \phi} \quad \text{for } r_e^2 \gg 1 \quad (11)$$

Fig. 3 shows $2M$ as a function of ϕ at orbit constants $C = \infty, 1, 0.5$ and 0.1 . It will be seen that when $C = \infty$, the magnitude of $2M$ (and hence F) is a maximum at $\phi = -45^\circ$. As C decreases, the values $2M_{\max}$ (corresponding respectively to maximum compression and tension) decrease and occur at angles ϕ which approach -90° . The values of ϕ corresponding to $2M_{\max}$ may also be obtained by differentiating Eq. (11) with respect to ϕ and equating to zero, whence it may readily be shown that

$$(\phi)_{M_{\max}} = \cos^{-1} \left[\frac{C^2}{2C^2 + 1} \right]^{1/2} \quad (12)$$

Values of $2M_{\max}$ are obtained by substituting $(\phi)_{M_{\max}}$ back into Eq. (11), and are given for a series of orbit constants in Table I. The significance of these calculations will be discussed later.

(iii) Shear Induced Buckling

We now assume that under the system of axial forces predicted from Burgers' theory, a' remains constant, and the rod remains straight until the critical condition for buckling under compression is exceeded. This represents the onset of bending of the particle by the action of the liquid.

From Fig. 3 it may be seen that the greatest stresses are exerted on a particle which rotates wholly in the XY-plane ($C = \infty$), and that compression reaches a maximum when $\phi = -45^\circ$. In this position, Eq. (9) gives

FIGURE 3

Calculated variation with ϕ of the orientation factor $2M$ of the axial force on a thin rod. As C decreases the peak values of $2M$ decrease and approach $\phi = \frac{\pi}{4} 90^\circ$.

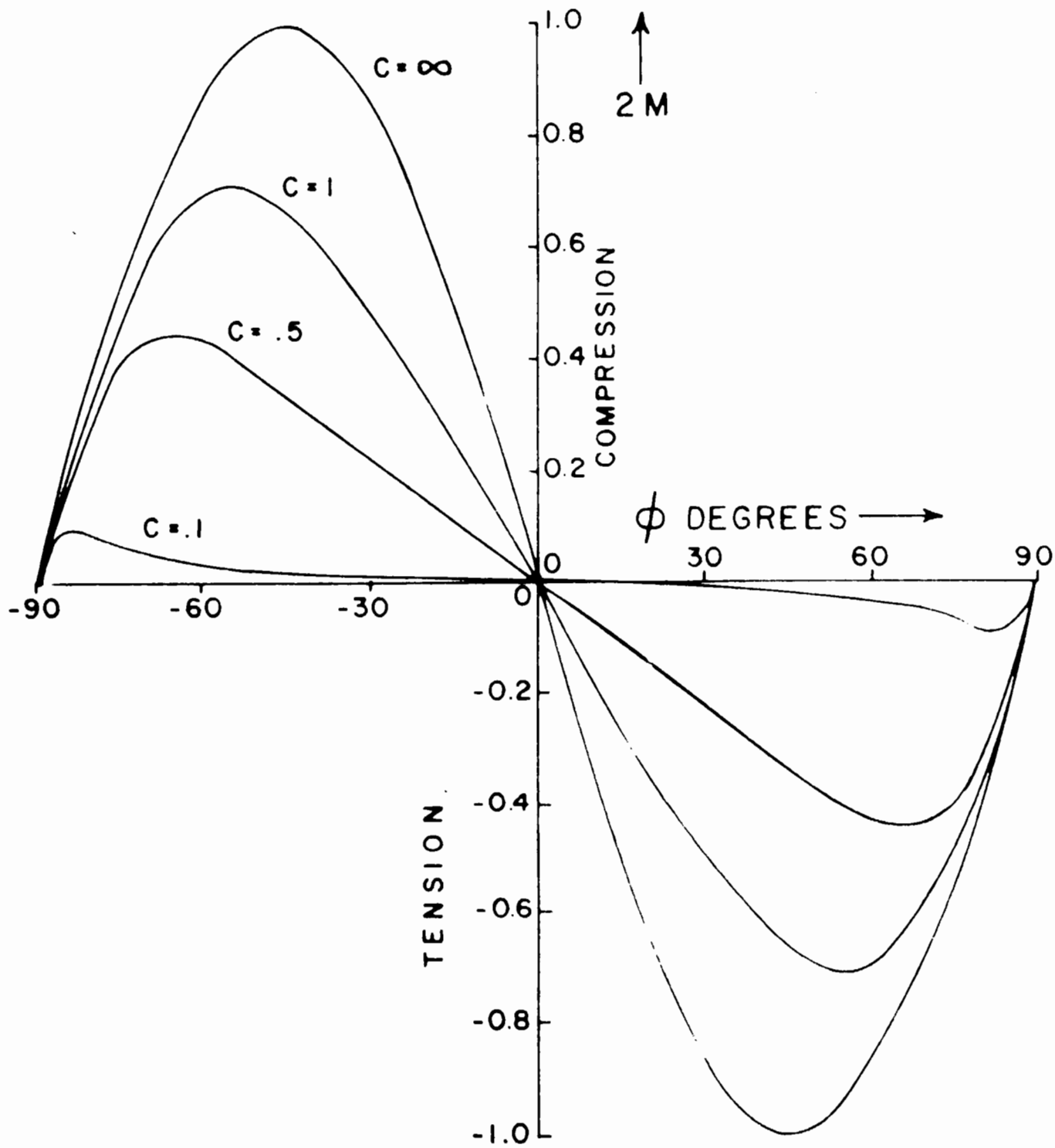


TABLE I $2M_{\max}$ at Different Values of C

C	$\phi_{M_{\max}}^{\circ}$	$2M_{\max}$
∞	45.0	1.000
5	45.2	.982
3	45.5	.950
2	46.4	.894
1	54.8	.707
0.5	64.6	.447
0.3	74.0	.258
0.1	84.3	.099
0	90.0	0

$$F_{\max} = \frac{\pi G \eta a'^2}{2(\log_e 2a'/b' - 1.75)} \quad (13)$$

We wish to calculate the least force required to buckle a rod in the orbit $C = \infty$. To do this we require to know the distribution of compressive forces along the axis of the rod.

Let us assume that the increment of axial force per unit length along the rod is proportional to the axial component of fluid velocity u' given by Eq. (8), i.e.

$$f(\underline{l}) = p\underline{l}$$

where p is a proportionality constant which depends on the particle orientation and on $G\eta$. Corresponding to the position of maximum compression ($\phi = -45^\circ$, $\theta = 0$) we have

$$F_{\max} = - \int_{a'}^0 p_{\max} \underline{l} d\underline{l} = p_{\max} a'^2/2 \quad (14)$$

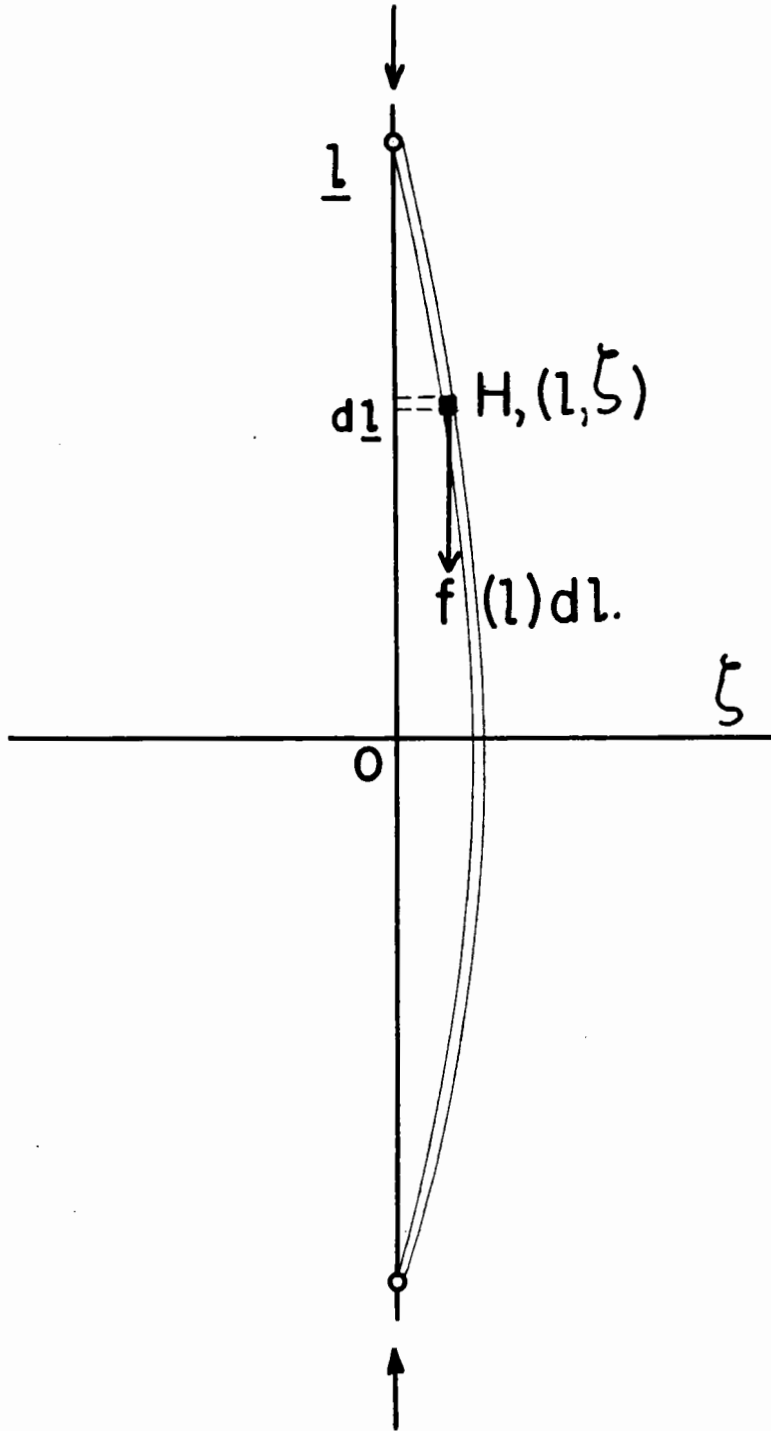
Eliminating F_{\max} from Eqs. (13) and (14), we obtain

$$p_{\max} = \frac{\pi G \eta}{\log_e 2a'/b' - 1.75} \quad (15)$$

Let us consider the rod to be hinged at the ends, as shown in Fig. 4, and to be subjected to a system of axial forces given by $p\underline{l} d\underline{l}$ acting on an element $d\underline{l}$. The total compressive force at any point H with co-ordinates (ζ, \underline{l}) acting on a cross-section of the rod

FIGURE 4

A rod, hinged at both ends, used as a model in the theory of shear-induced buckling. Euler's equation, (Eq. 17), for critical buckling, is derived by assuming that the rod is slightly bent under axial compression.



is given by

$$F_H = - \int_{\underline{l}}^{a'} p \underline{l} d\underline{l} = 1/2 \cdot p(a'^2 - \underline{l}^2) \quad (16)$$

The equation for the shape of the rod suffering small deformations under compressive forces (8) is given by Euler's classical equation

$$E_b I \cdot \frac{d^2 \zeta}{d\underline{l}^2} = -F_H \zeta \quad (17)$$

where E_b is the bending modulus of the rod, I is the moment of inertia of the smallest cross section and ζ is the displacement of the rod at \underline{l} (Fig. 4). By eliminating F_H from Eqs. (16) and (17) we have

$$\frac{d^2 \zeta}{d\underline{l}^2} + c(a'^2 - \underline{l}^2)\zeta = 0 \quad (18)$$

where $c = p/2EI$. We require the solution to Eq. (18) for the least permissible value of c .

Substituting $z = c^{1/4} \underline{l}$ into Eq. (18) yields

$$\frac{d^2 \zeta}{dz^2} + (c^{1/2} a'^2 - z^2)\zeta = 0 \quad (19)$$

By making the further substitution $\zeta = e^{-z^2/2} y$, Eq. (19) becomes

$$\frac{d^2 y}{dz^2} - 2z \frac{dy}{dz} + (c^{1/2} a'^2 - 1)y = 0 \quad (20)$$

Provided that $c^{1/2}a'^2$ is of the form $2n + 1$, Eq. (20) has the solution $y = He_n(\mathbf{z})$ where He_n denotes the Hermite function of order n , (9).

The smallest even value of n is zero, and corresponds to the first mode of buckling of the rod, so that

$$ca'^4 = 1$$

$$\text{or } P_{\max} = 2E_b I / a'^4 \quad (21)$$

By combining Eqs. (15) and (21) for the position of maximum compression,

$$(G\eta)_{\text{crit}} = \frac{E_b (\log_e 2r - 1.75)}{2r^4} \quad (22)$$

where $(G\eta)_{\text{crit}}$ is the minimum value at which rod-like particles of axis ratio $r = a'/b'$ may be expected to buckle under shear-induced compression. It follows that for any given value of $G\eta$ and E_b there also exists a critical value $r = r_{\text{crit}}$ which will satisfy Eq. (22). It should be noted that Eq. (22) depends solely on r , and not on the absolute dimensions of the particle.

In the experiments described below, the validity of Eq. (22) was tested.

C. EXPERIMENTAL METHODS

The experiments were conducted by means of two Couette devices (2, 4) in which the suspension was placed between two concentric cylinders which were rotated in opposite direction. In one of these (Apparatus No. 1) particles were observed through a microscope aligned along the Y-axis (Fig. 1) and in the other apparatus (No. 2) observations were made along the Z-axis. A full description of the apparatus

is given in Appendix II.

The following materials were used:

1. Rayon continuous filament, highly stretched, of circular cross section 3.5μ dia. supplied by the Research Department, American Viscose Corporation, Marcus Hook, Pa.
2. Nylon continuous filament, of circular cross section 12.2μ supplied by the Textile Fibres Division, Du Pont of Canada Limited, Kingston, Ontario.
3. Dacron continuous filament, of circular cross section 7.8μ dia. from the Pioneering Research Laboratory, Experimental Station, E.I. du Pont de Nemours and Co., Wilmington, Del.

Particles of known length were prepared from the filaments by mounting the strands in embedding wax and cutting them in a sliding microtome. Details of the method of sectioning are given in Appendix II.

Most of the work was conducted in a medium of household corn syrup (made by the Canada Starch Co.) of viscosity 91.2 poises at 20°C ., having an equilibrium relative water-vapour pressure of 70%. Castor oil (No. 300 Oil, Baker Castor Oil Co., New York) of viscosity 40.5 poises at 20°C . was used to provide a non-swelling medium in the experiments with rayon. Both liquids exhibited Newtonian flow properties up to velocity gradients of 100 sec.^{-1} as determined by viscosity measurements in a Couette type viscometer. Since the viscosities of these liquids were highly temperature-dependent, the experiments were conducted in a room conditioned to $20 \pm 1^{\circ}\text{C}$.

The temperature of the suspension was measured after each experiment and the viscosity of the medium read to $\pm .5$ poises from previously determined viscosity-temperature calibration curves.

Particle concentrations of about $10^{-4}\%$ by weight were used. At these low concentrations interaction effects were negligible.

The Young's (tensile) modulus of elasticity E of each material was determined from the linear portion of the tensile load-extension curve of samples of thread. The curves were obtained using an Instron Tensile Testing Instrument, Model TT-B, operating at a low constant rate of strain in a room conditioned to 50% relative humidity and 22.8°C. In calculating E from the curves, the stress was calculated from the total load and the total cross sectional area calculated from the mean optically-measured cross-sectional area per filament and the number of filaments per strand. The cross sectional area agreed well with the value calculated from the density and the measured denier per strand.

D. RESULTS AND DISCUSSION

1. The Spin of Rigid Rods

In the experiments to test the validity of Eq. (6a) for axial spin, Nylon filaments cut to lengths between 100 and 150 μ were suspended in corn syrup and the suspension was sheared in Apparatus No. 1.

The following measurements were made for each of twelve

particles:

- (i) The angle λ_{\max} by means of a goniometric ocular.
- (ii) The average period of rotation T in the spherical elliptical orbit over ten successive rotations.
- (iii) The average number of spins per rotation over the same ten rotations as for (ii) above.
- (iv) The shear-rate G from the speeds and diameters of the cylinders (2).

The r_e of each particle was calculated from Eq. (3) using measured values of T and G , and the orbit constant C from Eq. (7) using the measured λ_{\max} . The $f(k)$ for the appropriate value of k was found from Fig. 2. The theoretical numbers of spins n calculated from Eq. (5) are compared with observed values in Table II.

The observed values were generally low. Possible reasons for this difference were the deviation of the shapes of the particles from those of prolate spheroids, and the errors introduced by counting n_{obs} only to the nearest $1/2$ and in measuring the λ_{\max} of curved particles. In view of these sources of error, the agreement between theory and experiment is considered to be good.

2. The Onset of Bending

The validity of Eq. (22) was tested by measuring $(G\eta)_{\text{crit}}$ at various values of η and r , and using materials of different elastic constants. The experiments were performed in Apparatus No. 2, using filaments with orbits in the XY-plane ($C = \infty$) and without visible permanent deformations.

T A B L E II

Predicted and Observed Axial Spin for Slightly Curved Nylon Filaments

Mean T sec.	G sec. ⁻¹	r _e	λ_{\max}°	f(k)	Calculated n	Observed n	n _{obs.} /n _{calc.}
145.0	1.65	38.1	12.0	1.45	17.6	18.0	1.02
113.0	1.80	32.4	52.0	1.24	12.8	11.5	0.90
135.4	1.60	34.5	57.5	1.11	12.2	10.0	0.78
145.0	1.34	30.9	49.0	1.23	12.1	11.5	0.94
410.0	0.37	24.5	28.0	1.38	10.8	11.5	1.06
120.0	1.69	31.5	60.0	1.07	10.7	8.0	0.75
86.0	1.49	25.8	57.0	1.13	9.3	9.0	0.97
92.4	1.82	28.6	69.5	0.92	8.3	7.0	0.84
126.0	1.42	20.4	45.5	1.25	8.1	6.5	0.80
105.0	1.11	19.2	43.0	1.19	7.3	6.5	0.80
82.0	1.85	24.1	69.0	0.90	6.9	5.5	0.80
62.0	1.83	18.0	80.0	0.59	3.4	2.5	0.74
Mean n _{obs.} /n _{calc.} = 0.87							

(i) Variation of η

Samples of Dacron filament of $r = 310$, suspended in corn syrup diluted with water to yield viscosities ranging from 11.5 to 91.2 poises were used. The critical values of G at which bending during rotation was just detectable were measured for ten filaments at each viscosity.

The results given in Table III support the theory which predicts that G_{crit} varies inversely with η .

The high standard deviations from the mean in G_{crit} may be caused by small variations in r which can have a profound effect since, according to Eq. (22), G_{crit} is roughly proportional to r^{-4} . Small permanent deformation in the XZ-plane of some of the particles which are not apparent in the XY-projection seen in Apparatus No. 2 could be an additional cause. Such a deformation might be expected to cause a particle to bend at a lower G_{crit} than if its unstressed shape were perfectly straight.

(ii) Variation of r

These experiments were performed with Dacron particles having axis ratios ranging from 180 to 310 using undiluted corn syrup as the medium. The mean values of $(G\eta)_{\text{crit}}$ are summarized in Table IV. The Table includes the product $(G\eta)_{\text{crit}} \cdot F(r)$ where

$$F(r) = \frac{2r^4}{(\log_e 2r - 1.75)} \quad (23)$$

T A B L E III

The Effect of Viscosity on Critical Bending

Dacron Filament, (r = 310) in Corn Syrup		
η poises	G_{crit} sec. ⁻¹	$(G\eta)_{crit}$ gm.cm. ⁻¹ sec. ⁻¹
11.5	7.24 (2.15)	83.7
17.9	3.95 (.70)	70.6
41.8	2.10 (.50)	88.5
91.2	0.72 (.30)	65.8
Mean $(G\eta)_{crit} = 77.1$		
$(G\eta)_{crit} \cdot F(r) = 29.2 \times 10^{10}$ dynes.cm. ⁻²		

Values in brackets are standard deviations of associated means of 10 samples

T A B L E IV

Comparison of E_p at Various Axis Ratios with E for Dacron, Rayon and Nylon Filaments

Material	Medium	r	Mean G_{crit} sec. ⁻¹ (10 specimens)	Mean $(G\eta)_{crit}$ gm.cm. ⁻¹ sec. ⁻²	$F(r)$ $\times 10^{-8}$	$(G\eta)_{crit} \cdot F(r) = E_p$ $\times 10^{-10}$ dynes.cm. ⁻²	Tensile Modulus $E \times 10^{-10}$ dynes.cm. ⁻²
DACRON	Corn syrup	180	6.93 (1.54)	632	5.08	32.2	7.26
		228	3.12 (.57)	260	12.2	31.8	
		268	1.32 (.26)	112	22.6	25.4	
		310	0.72 (.30)	66	39.6	26.2	
RAYON	Corn syrup	190	2.67 (.55)	248	6.28	15.6	26.4
		281	0.38 (.11)	34.7	26.8	9.32	
	Castor oil	241	10.30 (2.35)	386	15.26	59.2	
NYLON	Corn syrup	170	3.84 (1.02)	350	4.48	15.6	6.30
		194	2.32 (.75)	209	6.90	14.4	

Bracketed values are standard deviations of associated means

If Eq. (22) applies, the product should be constant for a given series of particles; for the Dacron particles it was constant within 30%, yielding a mean value of 28.9×10^{10} dynes/cm². This value agreed well with the mean value of 29.2×10^{10} dynes/cm² calculated from the data of Table II.

Similar results for less extensive experiments using rayon and Nylon were obtained and are included in Table IV.

(iii) The Elastic Constants

According to Eq. (22),

$$(G\eta)_{\text{crit}} \cdot F(r) = E_b \quad (24)$$

Values of the tensile modulus E are included in Table IV and are compared with corresponding values of E_b calculated from Eq. (24). Since Dacron does not absorb appreciable quantities of water and hence is not plasticized by contact with water, the comparison would appear to be most valid for this material; in this case $E_b/E = 4$ approx.

Closer agreement was obtained for Nylon. However, it has been shown (10) that the (dynamic) tensile modulus of Nylon increases by about 20% for a decrease in relative humidity from 70% to 50%. If the value of E_b for Nylon shown in Table IV is increased by 20% for direct comparison with E , the ratio E_b/E corrected to 50% relative humidity is approximately 3.2.

With Rayon, the decrease in E_b between castor oil and corn syrup clearly shows the plasticizing effect due to water absorbed from the corn syrup.

It will be noted that with each material, the values of E_b obtained tended to decrease slightly with increasing r . This deviation from Eq. (22) may have been due to the approximations made in developing the theory. It could also have resulted from a greater incidence of slight permanent deformations in the longer samples.

While values of E_b obtained were of the same order of magnitude as the corresponding values of E , they were nevertheless 2 to 4 times greater. It should be noted that $E_b = E$ only if the filaments are homogeneous, but that the two moduli frequently differ due to "skin" effects (11). It is improbable that skin effects can account entirely for the differences between E_b and E in the above results. However, in view of the assumptions and approximations made in Burgers' treatment and in the present extension of the theory, precise numerical agreement could hardly be expected.

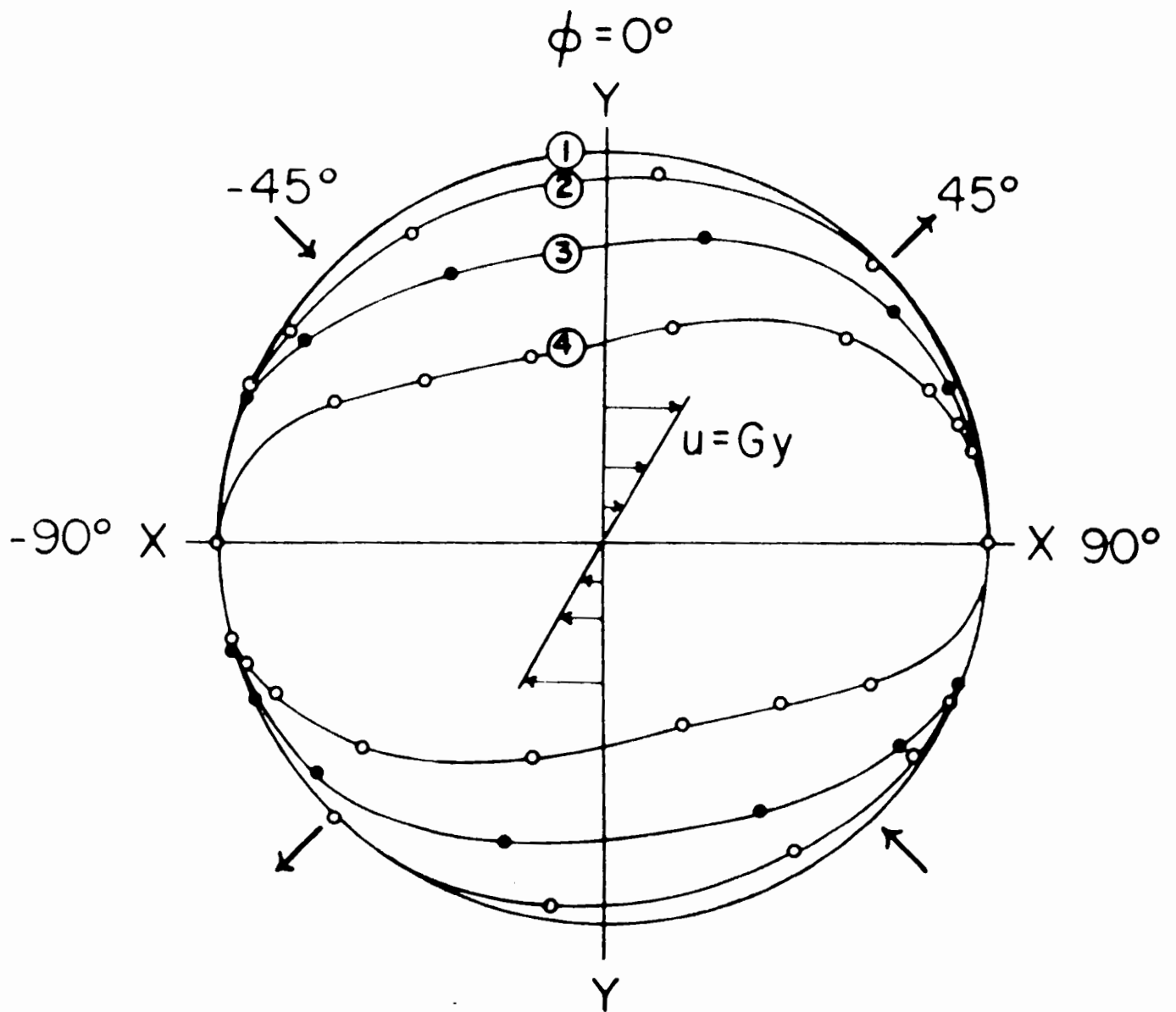
It has been shown that the experimentally determined relationships between G , η and r were in general agreement with those predicted by Eq. (22). The results may therefore be taken as good confirmation of the theory of deformation presented above.

(iv) Orbits of Bent Particles

Attempts were also made to determine if critical bending of a particle rotating in the XY-plane ($C = \infty$) commences at $\phi = -45^\circ$, as implied in Eq. (13). The experiments proved difficult to perform.

FIGURE 5

Polar plot of the loci of the ends of a Nylon filament ($r = 170$) during rotation in the XY-plane. Curve 1 represents rigid rotation at $G < G_{crit}$. Curves 2, 3 and 4, for which G_{crit} has been exceeded, correspond to $G = 3.20, 3.54$ and 4.25 sec.^{-1} respectively. The theory predicts that as G approaches G_{crit} , deviation from curve 1 will commence at $\phi = -45^\circ$.



Photomicrographs were taken at short time intervals during the rotations of Nylon filaments close to G_{crit} , again using Apparatus No. 2. The loci of the ends of the filament images were plotted as a function of ϕ . Fig. 5 clearly shows the assymetry of the loci about the Y-axis due to the compression and tension forces. It also shows the increase in deformation occurring above G_{crit} ; this will be discussed further in Part III (12). The results suggest but do not definitely show that initial bending occurred at $\phi = -45^\circ$. The main experimental difficulty is to obtain a particle which not only appears free from permanent deformation, but also rotates wholly in the XY-plane, since even slight displacements from $C = \infty$ would result in foreshortening of the XY-projection due to the spherical elliptical orbit.

It should be noted that the above theory of bending as the result of axial forces does not apply once the particles are deformed. Evidence will be presented in Part III that the disturbance to the flow field caused by curved particles is much greater than that due to straight ones: this indicates that the system of forces acting on a curved particle is more complicated and cannot be analysed even approximately by a treatment which assumes the disturbance to the flow field to be negligible.

The phenomena considered here are of interest in connection with the viscosity (13) and other flow properties of suspensions of thread-like particles and will be discussed further in Parts III and IV. In addition they form an important background to the study of the more complex orbits of flexible particles discussed in Part III.

E. SUMMARY

The axial spin of slightly curved but rigid cylindrical particles rotating in a velocity gradient have been shown to be in good accord with Jeffery's theoretical equation for ellipsoids of revolution provided that the equivalent ellipsoidal axis ratio is substituted for the true axis ratio in the equation.

A theory of deformation of cylindrical particles rotating in a velocity gradient is presented. Equations are developed to calculate the critical value of (gradient x viscosity) at which the shear-induced axial compression causes the particle to buckle. Experiments conducted with Dacron, Nylon and rayon filaments cut to various axis ratios and dispersed in various liquid media showed reasonably good agreement with the theory. Some observations of the increase of particle deformation beyond the critical gradient for bending are presented.

REFERENCES

1. Jeffery, G.B., Proc. Royal Soc. (London) A 102:161 (1922).
2. Trevelyan, B.J. and Mason, S.G., J. Colloid Sci. 6:354 (1951).
3. Mason, S.G. and Manley, R.St.J., Proc. Royal Soc. (London) A 238:117 (1956).
4. Bartok, W. and Mason, S.G., J. Colloid Sci. 12, No. 3:243 (1957).
5. Mason, S.G., Tappi 37, No. 11:494 (1954).
6. Arlov, A.P., Forgacs, O.L. and Mason, S.G., Svensk Papperstidn. 61, No. 3:61 (1958). A reprint of this publication is attached as Appendix I.
7. Burgers, J.M., Second Report on Viscosity and Plasticity, North Holland Publishing Co., Amsterdam (1938) Ch. III, 19 and 10.
8. Prescott, J., Applied Elasticity, Dover Publications, N.Y. (1946) Ch. IV, 76.
9. Margenau, H. and Murphy, G.M., The Mathematics of Physics and Chemistry, D. Van Nostrand Co., Inc., N.Y. (1943) Ch. 3, 10.
10. Quistwater, J.M.R. and Dunell, B.A., J. Polym. Sci. 28:309 (1958).
11. Meredith, R., The Mechanical Properties of Textile Fibres, North Holland Publishing Co., Amsterdam (1956) Ch. IV, 8.
12. Part III of this Thesis.
13. Nawab, M.A. and Mason, S.G., J. Phys. Chem., forthcoming publication.

PART III

THREAD-LIKE PARTICLES: FLEXIBLE ORBITS

A. INTRODUCTION

Particles in liquid suspensions subjected to velocity gradients undergo rotational and translational motions. In addition, the shear field exerts stresses on the particles which under certain conditions are capable of causing deformation. In Part II of this thesis (1), the forces exerted in a field of laminar shear on cylindrical particles were considered, and it was shown that there exist critical conditions beyond which a particle will bend in the course of rotation. In this Part, the effects of shear-induced deformation on the rotational motions of thread-like particles are described.

Previous work in this laboratory has dealt with the rotations, orientations and interactions of simple particles such as rigid spheres (2, 3, 4) fluid drops (5, 6) and smooth rigid rods (2, 4, 7). Most of the phenomena observed could be explained theoretically. There exists, however, no comparable theory for the phenomena described in the present work.

A recent paper (8), attached as Appendix I, described the motions of wood-pulp fibres. It was found that rigid fibres executed the same types of rotation as rigid cylinders. If the fibres were flexible, their orbits and periods of rotation differed appreciably from those of rigid cylinders. However, a quantitative study using pulp fibres was limited in scope by the irregularity in shape of the individual particles.

In the present investigation, a more systematic study was possible with uniform particles prepared from synthetic filaments.

Rigid rods in suspensions subjected to laminar shear rotate in spherical elliptical orbits (2, 4) and spin about their major axes (Part II) according to the predicted equations of motion for prolate spheroids (9), provided the "equivalent ellipsoidal axis ratio" r_e is used in place of the true axis ratio r of the particles. The r_e is calculated from Jeffery's equation, (9)

$$TG = 2\pi\left(r_e + \frac{1}{r_e}\right) \quad (1)$$

$$\dot{=} 2\pi r_e \quad \text{for } r_e \gg 1$$

T is the measured periodic time of rotation of the particle axis through $\phi = 360^\circ$ where ϕ is the azimuthal polar co-ordinate ($Z =$ polar axis) as shown in Fig. 1 of Part II, and G is the velocity gradient.

It follows from Eq. (1) that for a particle which has two perpendicular axes of symmetry (so that its shape relative to the field of flow will remain unchanged by axial spin), e.g. prolate spheroids and straight cylindrical rods, the product TG will depend solely on the particle shape and will be independent of G .

If, however, a particle undergoes shear-induced deformation, its shape and hence the flow pattern around it at any instant will depend on the deforming forces. Since these were shown in Part II to be a function of the product $G\eta$, where η is the viscosity of the suspending

medium, we may expect that for deformable particles, Eq. (1) will take the form

$$TG = S(G\eta) \quad (2)$$

where $S(G\eta)$ is a particle shape factor which varies with $G\eta$. If η is constant we should expect that if a particle is deformable, $\Delta TG/\Delta G$ will be related to the deformation undergone by the particle as the result of an increment ΔG . Experiments with deformable pulp fibres (Appendix I) have shown that TG increases with G. Similarly, measurements of the period of circulation T of the interface of a deformed fluid drop (6) have shown that TG increases with G. The product TG therefore becomes a useful parameter in studying the effects of deformation on particle rotations.

The experimental results of the present investigation are presented in two sections. The first describes the motions of deformable thread-like particles over a wide range of flexibility; the second deals principally with the effects of deformation on the product TG.

B. EXPERIMENTAL PART

1. Apparatus and Materials

The technique using the two twin cylinder Couette devices for viewing along the Y- and Z-axes respectively was similar to that outlined in Part II and described in detail in Appendix II.

In addition to the 3.5μ dia. rayon and 7.8μ Dacron filaments

previously used (Part II) and which were microtomed to required lengths (Appendix II), the following materials were also used:

(i) Spruce sulphite-pulp fibres, screened to yield a mean length of 1.6 mm. with a standard deviation from the mean of about 20%. These were used in preliminary experiments.

(ii) Elastomer continuous filament, of undisclosed composition, approximately elliptical in cross-section, width of largest cross-section = 12μ , supplied by the Pioneering Research Laboratory, E.I. du Pont de Nemours and Company, Wilmington, Delaware. This material was highly flexible by comparison with the other materials. Because of its extensibility, it could not be embedded and microtomed; instead, single filaments were cut to lengths ranging from one to 20 mm., using a sharp razor.

The suspending media used were household corn syrup and castor oil (No. 300 oil, Baker Castor Oil Co., New York). The castor oil, which was also used in associated studies of the viscosity of suspensions (12), provided a non-swelling medium for rayon.

Concentrations by weight of about $10^{-4}\%$ were used in experiments with pulp fibres, rayon and Dacron, since at these low concentrations individual particles could be studied in the absence of interactions over extended periods of time. With the elastomer, observations were made of filaments which were introduced into the medium individually by means of a fine needle.

Observations were made visually or with the aid of photomicrography.

2. Method of Varying Particle Flexibility

The ability of a thread-like particle to bend could be increased by swelling the material, by increasing the deforming forces exerted by the shear field, or by increasing the particle length (Part II).

Since swelling tended to be non-uniform along the length of a filament, this method of increasing flexibility was rejected. The deforming forces could be increased in a particular suspending medium by increasing $G\eta$. However, G was limited to a maximum of 10 sec.^{-1} . Furthermore, experiments at high gradients were complicated by the rapid movement of the particles and difficulty of maintaining particles in the stationary layer (Appendix II). The viscosity η could be varied by diluting the suspending medium, but the range of η that could be used was limited, since at low viscosities sedimentation effects became significant. Flexibility was therefore varied principally by varying the particle length, while small changes in the particle orbits were studied by varying G and η .

The orbits of rayon filaments were studied up to axis ratios of 780, corresponding to a length of over 3 mm. At greater lengths, these thin filaments could no longer be resolved in the microscope at the low magnifications required to obtain a sufficiently wide field. Studies of very long and flexible filaments were therefore made using the thicker but much more flexible elastomer.

C. RESULTS AND DISCUSSION

1. The Orbits of Deformable Threads

In this section are described the motions of thread-like particles under conditions at which the values of $(G\eta)_{\text{crit}}$ or $(r)_{\text{crit}}$ (defined in Part II) for the onset of deformation were exceeded.

(i) Springy and Snake Orbits

The orbits of filaments when the critical conditions for bending were only slightly exceeded were termed "springy". This type of rotation is illustrated by the Dacron filament rotating in the XY-plane in Fig. 1. The particle in frame (1) was aligned in the X-direction. Frames (2) to (7) were taken at intervals during a rotation through 180° (from $\phi = -90^\circ$ to $\phi = +90^\circ$). As the particle approached $\phi = -45^\circ$, it bent like a leaf-spring, and then flicked straight as it rotated into the quadrant $0 < \phi < 90^\circ$.

The loci of the ends of a filament undergoing springy orbits in the XY-plane are shown in Fig. 5 of Part II: curves 2, 3 and 4 show that as G was increased, deformation became more pronounced, and the onset of bending during rotation tended towards $\phi = -90^\circ$.

When the flexibility of a filament was increased further, by increasing either $G\eta$ or r , a stage was reached at which the two ends of the filament appeared capable of independent movement; however, the particle continued to straighten in the positions $\phi = \mp 90^\circ$. This type of orbit was termed "snake-turn" (Appendix I) and is identical with the

orbit designated as "flexible rotation" in papers dealing with the flexibility of pulp fibres (Part IV) (10), (11). It is illustrated by photomicrographs of an elastomer filament in Fig. 2. The filament was aligned in the X-direction in frame (1). After an interval during which little motion could be observed, one end bent abruptly in the XY-plane. The bend ran along the particle until it once again lay in the X-direction, but pointing the opposite way, frame (5). After another interval during which little motion was apparent, the process was repeated, the particle, thereby completing a rotation through $\theta = 360^\circ$. By comparing the two series of pictures in Fig. 2 it may be seen that the extent of deformation of the particle during rotation was again increased by increasing G.

The period of rotation was found to be constant for successive rotations of the particle at constant G; the abrupt bending of one end occurred at definite and reproducible time-intervals in the course of each rotation.

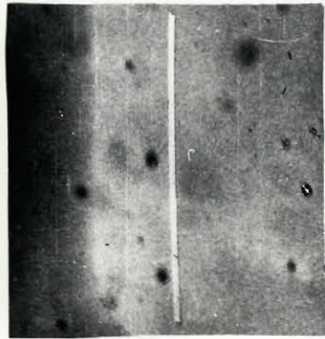
When the particles were highly symmetrical, that is, entirely free of any permanent deformations, both ends bent simultaneously in opposite directions, so that the particles formed an S-shape and then straightened again. This orbit proved to be the exception rather than the rule with the filaments used in this work.

Particles undergoing snake-turns showed a preference for orbits lying close to the XY-plane. Previous work on rigid rods (5)

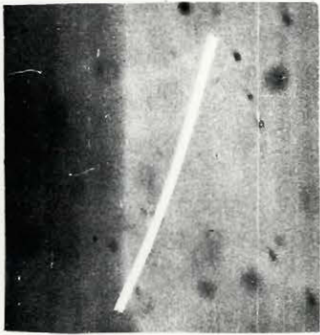
FIGURE 1

Springy Rotation. Photomicrographs of a 7.8μ dia. Dacron filament rotating in the XY-plane. In frame 1, the filament is aligned along the direction of flow. In the first quadrant ($-90^\circ < \phi < 0^\circ$), frames 1 to 4, the filament bends under compression. In the second quadrant, ($0 < \phi < 90^\circ$), frames 4 to 7, it relaxes rapidly under tension.

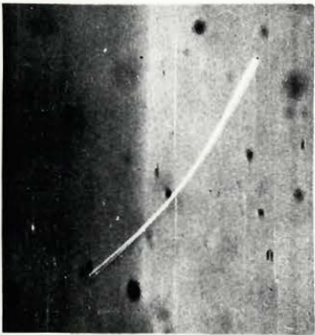
$$\begin{aligned}\text{Axis Ratio} &= 180 \\ G\eta &= 640 \text{ gm.cm.}^{-1}\text{sec.}^{-2}\end{aligned}$$



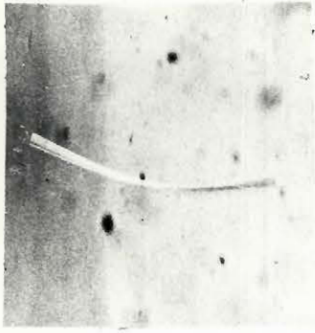
1



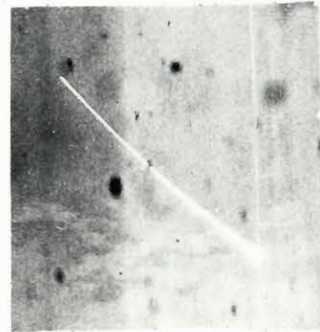
2



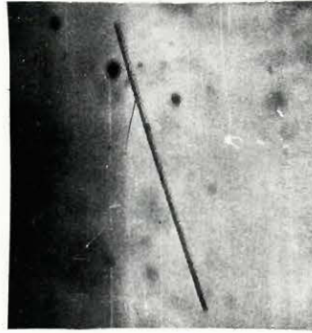
3



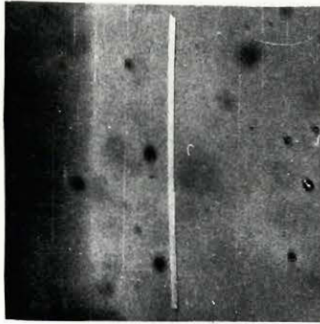
4



5



6



7

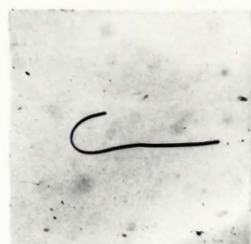
SPRINGY ROTATION
VIEWED ALONG THE Z-AXIS

FIGURE 2

Snake Rotation. Photomicrographs of an Elastomer filament undergoing snake-turns through $\phi = 180^\circ$, at $G = 0.94 \text{ sec.}^{-1}$ (upper series) and $G = 2.57 \text{ sec.}^{-1}$ (lower series). By comparing corresponding pictures of the two series it will be seen that deformation increases as G increases.



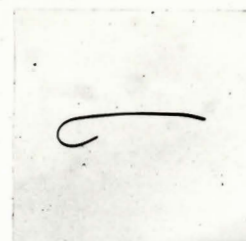
1



2



3



4



5

$G = 0.94 \text{ sec.}^{-1}$



1



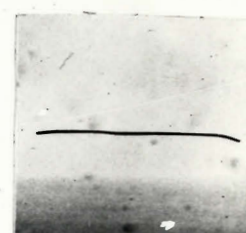
2



3

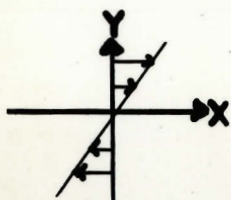


4



5

$G = 2.57 \text{ sec.}^{-1}$



1 mm.

**SNAKE - TURNS
VIEWED ALONG THE Z-AXIS**

failed to establish any definite drift in the orbital constant C (Part II) with time. However, it was observed that flexible pulp fibres either drifted so that they rotated in the XY -plane or so that their axes were aligned in the Z -direction (Appendix I). When the filaments used in the present work underwent sufficient deformation to describe snake-turns, they invariably drifted so as to rotate wholly in or very close to the XY -plane. The drift occurred in the course of two or three half-rotations whatever the orientation of the filaments was at the onset of shear. Further work on this phenomenon is required before an explanation of it can be attempted.

The orbits of rayon filaments and Dacron filaments of various axis ratios in corn syrup and at constant G are given in Fig. 6 and Table III. These results indicated that the snake-orbits commenced at values of r roughly equal to $1.5(r_{\text{crit}})$.

(ii) Coiled Orbits Without Entanglement

Experiments with rayon filaments showed that at values of $r > 3(r_{\text{crit}})$ approximately, the filaments no longer straightened between half-rotations but assumed coiled configurations. A particle which was initially orientated at random relative to the Couette cylinders became fully extended close to the X -direction on setting the apparatus in motion. After a time, one end started to bend as described for snake-turns. The bend ran along the length of the filament, but before it had reached the tail end, the head began a second bend so that the particle never straightened completely. This type of orbit was also observed in corn syrup at

$G > 3 \text{ sec.}^{-1}$ with long, highly delignified pulp fibres, as will be shown in Part IV, and elastomer filaments over 2.5 mm. in length.

If sufficiently long and flexible, filaments rotated so that the XY-projection of their configurations appeared as closed loops, as illustrated with an elastomer filament in Fig. 3. The leading end was usually displaced slightly in the Z-direction, presumably as the result of hydrodynamic interaction with the tail, so that the filament rotated about the Z-axis in a helix. The greatest cross-section of the XY-projection of the orbit was inclined at an angle to the direction of flow as the result of the compressive and tensile forces of the kind described in Part II. Fig. 3 also shows that as G was increased, this angle of inclination approached the X-direction ($\phi = 90^\circ$) in a manner similar to that observed with fluid drops (6). As with springy and snake orbits, deformation was increased by increasing G . At $G = 0.30$ and 0.53 sec.^{-1} the filament in Fig. 3 had two bends along its length. At $G = 2.04 \text{ sec.}^{-1}$, three bends were present during certain stages of the orbit: this indicates that the number of "turns" of the helix tended to increase with increasing flexibility. Further evidence of this is given below.

Elastomer filaments between 3 and 10 mm. in length frequently assumed these helical configurations, although with the longer samples, the orbits passed through a number of intermediate phases. Once the helix was formed, however, a filament rotated like a corkscrew about the Z-axis

FIGURE 3

Helix rotation viewed along the Z-axis. Photomicrographs of an Elastomer filament. As G increases, the amount of deformation increases and the major axis of the configuration tends towards the direction of flow (the X-axis).



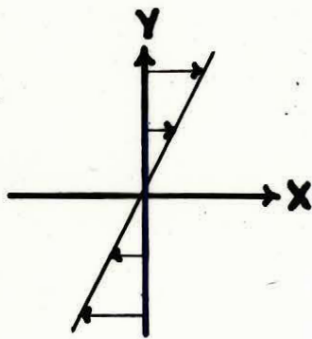
$G = 0.30 \text{ sec.}^{-1}$



$G = 0.53 \text{ sec.}^{-1}$



$G = 2.04 \text{ sec.}^{-1}$

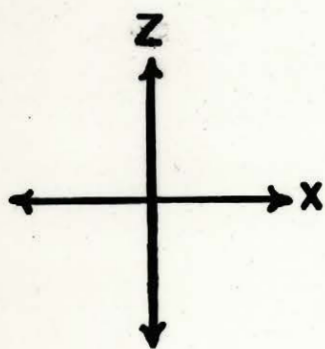
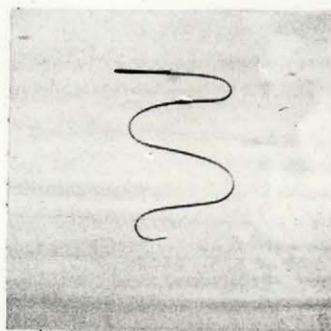
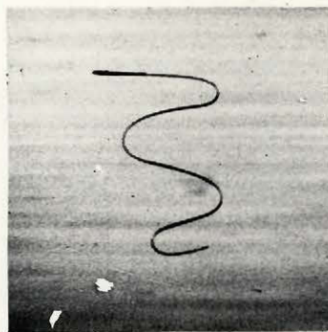


1 mm.

**HELIX ROTATION
VIEWED ALONG THE Z-AXIS**

FIGURE 4

Helix rotation viewed along the Y-axis. Photomicrographs of an Elastomer filament. The filament rotates about the Z-axis like a corkscrew unless disturbed by another particle.



HELIX ROTATION
VIEWED ALONG THE Y-AXIS

T A B L E I

Helix Formation of Elastomer Filaments

$$G = 3 \pm 1 \text{ sec.}^{-1}$$

Particle no.	Length of extended fil. mm.	Time observed min.	Time to form stable helix min.	No. of turns in helix
1	3.25	30	2	1 1/2
2	4.00	55	18	2 1/2
3 ^x	4.50	40	--	--
4 ^x	4.50	38	5 [*]	3
5	5.00	50	24	3
6	5.75	45	32	3 1/2
7	6.50	72	70	4
8	7.00	60	--	--

^x Permanently deformed.

^{*} Unstable helix formed at intervals.

for many hundreds of rotations, unless disturbed by another particle. It will be seen from Table I that of eight samples observed, six formed helices. The time to form the helix increased with the filament length. The width of the helices in the X-direction varied little with the filament length, and in each case was between 1 and 2 mm.; the number of turns of the coil, however, increased with the filament length. Fig. 4 shows photomicrographs taken along the Y-axis of a helix of 3 turns, similar to that formed by particle No. 5 (Table I). Particles No. 3 and 4 did not form stable helices: it was noticed that both these filaments had permanent deformations which appeared to inhibit their rotation in a smooth spiral.

A tentative reason for the stability of the helical configuration is that it is the only way in which a long filament can rotate without axial spin, and thus without setting up torsional stresses along its axis.

The mode of formation and the stability of these configurations require further investigation

(iii) Coiled Orbits With Entanglement

Elastomer filaments over 10 mm. in length were never observed to form helices. It appeared that the complicated entanglement during initial coiling prevented the formation of the spiral configuration, even after prolonged shearing. The coiling of a very long filament may be considered in five consecutive stages, illustrated in Fig. 5. These may be described as follows:

a) Whatever its initial orientation, the filament always aligned itself close to the X-axis on the commencement of shear, either fully extended or, occasionally, folded double.

b) After a time in the extended position, the ends started to bend as though commencing independent snake orbits.

c) After the ends had travelled towards each other for some distance, they once more turned to form closed loops. After travelling away from each other, the ends eventually turned again, until coils of two or three loops had formed at the extremities of the otherwise extended filament.

d) As the coils at the ends grew, they began to rotate bodily and to move towards each other, slowly winding up the extended part of the filament.

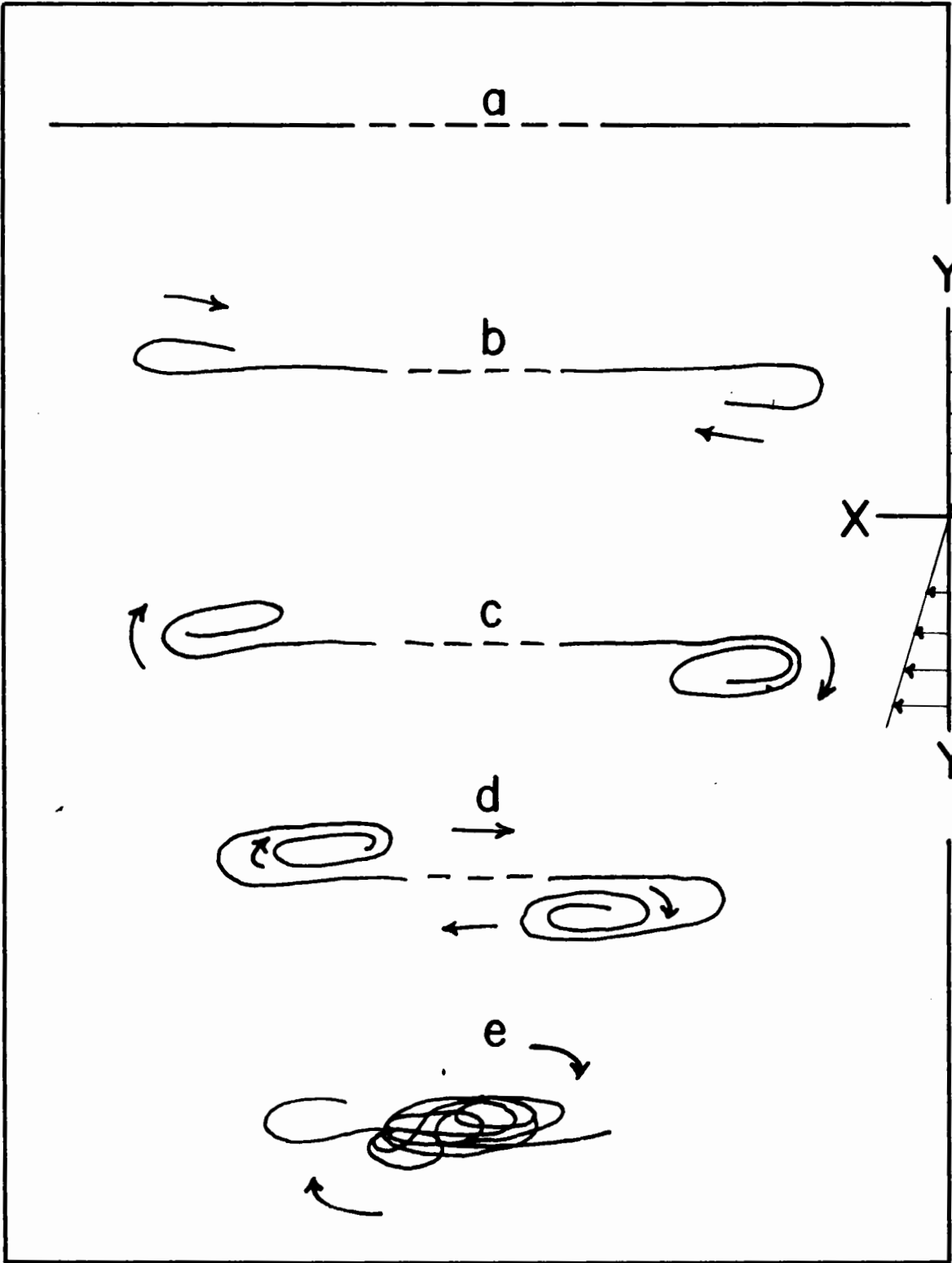
e) After passing each other a few times, the coiled ends, which were continuously growing in complexity, entangled with one another to form a complex writhing bundle. Sometimes the ends worked themselves free and moved away from the main coil, only to bend again and re-enter the coil, thereby adding to the entanglement.

These stages represent a simplification of the process. Often the two ends did not reach the first four stages simultaneously. Sometimes one end had coiled considerably before the other had even started to bend.

The projection on the XY-plane of the coiled bundle was always longer in the X-direction than in the Y-direction. As with the helical configurations, this asymmetry was increased by increasing G.

FIGURE 5

Coil formation. Schematic diagram showing the stages of coiling of a very long flexible filament.



The projection on the XZ-plane of a coil was usually longer in the Z-direction than in the X-direction. The bundle usually rotated about the Z-axis at a more or less constant angular velocity, though the individual elements continued to move relative to each other.

2. The Effect of Deformation on TG

To avoid the complicating effect of axial spin mentioned in the introduction, measurements of the periods of rotation T of filaments were made exclusively in or very close to the XY-plane, where it has been shown (Part II) that there is no axial spin.

(i) Preliminary

Preliminary experiments were conducted in the Couette Apparatus No. 1 (viewing along the Y-axis), using pulp-fibres, 1.6 mm. in length, suspended in corn syrup. The periods of rotation of 100 fibres were measured at $G = 3 \pm 1 \text{ sec.}^{-1}$. The results (Table II) show that the mean TG was lower for fibres describing springy orbits than for those that were rigid, and lower still for fibres describing snake orbits.

Fig. 6 shows the variation of TG with r for rayon filaments (dia. in corn syrup = 4.5μ). Each point represents the mean TG of about five filaments at each axis ratio. Over the rigid range, the results were in good agreement with those of Trevelyan and Mason (2) and Manley and Mason (5). The sharp fall in TG, which coincided with the beginning of the snake-orbit region, was first considered to be a characteristic of the orbit resulting from flexibility (11). This conclusion was, however, based on the incomplete information obtained by viewing the particles

T A B L E IIThe Effect of Flexibility on TG of Pulp Fibres

Orbit	No. of Fibres	Mean TG
Rigid	19	124.0 (32.8)
Springy	20	92.8 (21.0)
Snake	61	45.4 (12.7)

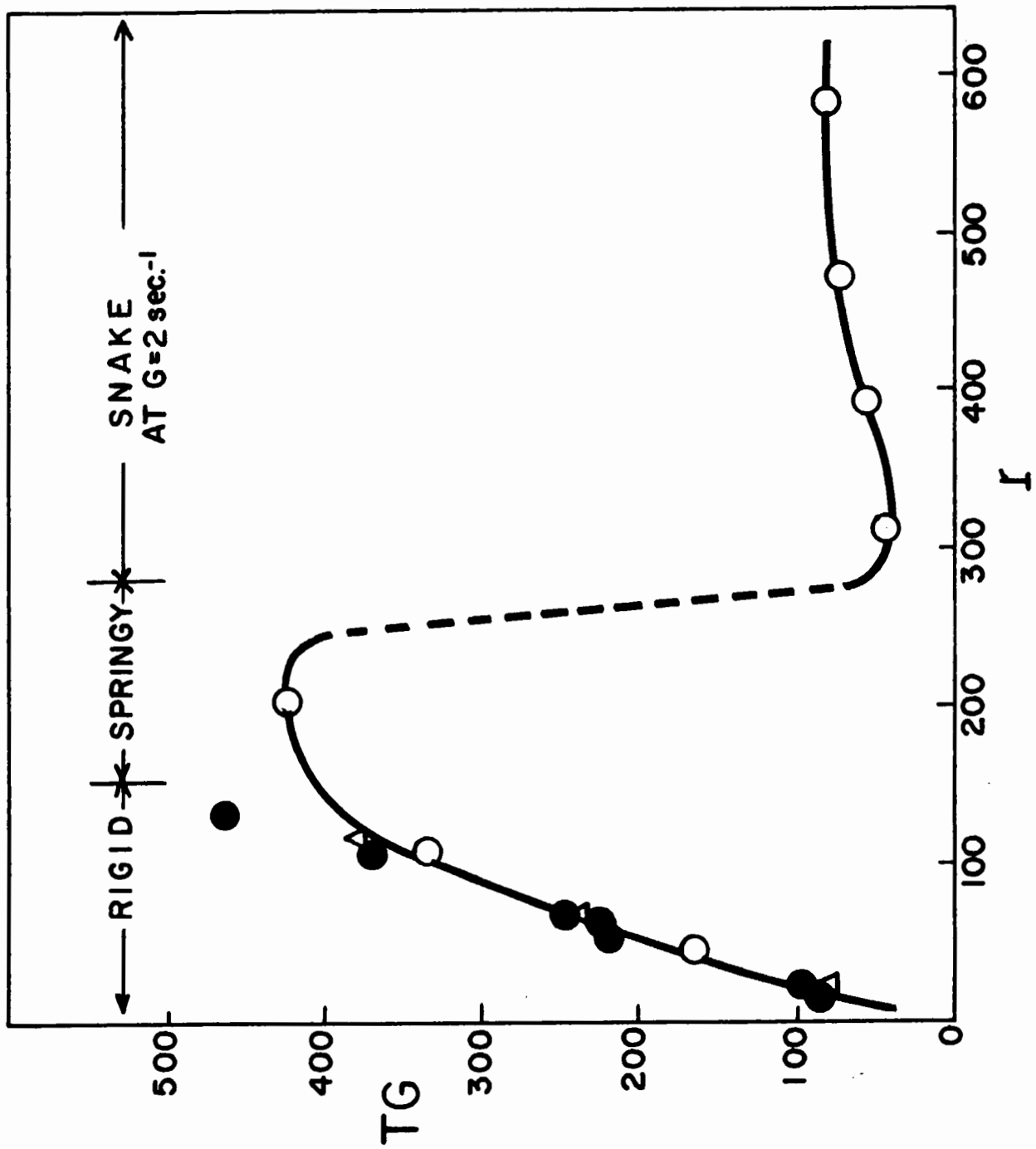
Bracketed values are standard deviations of associated means.

Mean length of fibres = 1.6 mm.

FIGURE 6

TG vs. r - preliminary results. Open circles: 4.5 μ dia. Rayon filaments in Corn Syrup. Closed circles: 9.5 μ dia. glass fibre (Trevelyan and Mason). Triangles: 12.4 μ Dacron filaments (Manley and Mason).

TG decreases appreciably at the axis ratio corresponding to the onset of snake-rotations. Subsequent experiments showed this effect to be the result of permanent deformation.



along the Y-axis. Experiments with pulp fibres and rayon filaments in the Apparatus No. 2 (viewing along the Z-axis) revealed that after shearing for prolonged periods, the particles frequently remained curved in the XY-plane when motion was stopped. In the experiments, summarized in Fig. 6, the suspensions had been sheared for two hours before making observations to ensure good dispersion. This caused the particles to have permanent deformations which could not be seen by viewing along the Y-axis.

It was therefore considered to be important to study as a next step the effect of permanent deformations on the period of rotation.

(ii) The Effect of Permanent Deformation

A sample of 3.5μ dia. rayon filaments which had been cut to an axis ratio of 173 was suspended in Castor Oil and sheared in a "Drage" rotating viscometer at $G = 96 \text{ sec.}^{-1}$ for 30 minutes. These filaments were also used conjunctively for the viscosity measurements reported by Nawab and Mason (12). Microscopic examination of the sheared filaments showed that most of them had been permanently bent into circular arcs.

The sheared suspension was diluted and placed in the Apparatus No. 2. The periods of rotation of 24 filaments whose XY-projections showed various degrees of permanent deformation were timed at known shear-rates between 9 and 10 sec.^{-1} . The particles described rigid rotations. After the period of rotation of each particle had been measured, the apparatus was stopped and a photograph of the corresponding filament was taken through the microscope aligned along the Z-axis.

The negatives were projected on a screen and the angle α subtended by the tangents at the ends of each filament image (see inset Fig. 7) was measured. This angle served as an inverse measure of the extent of permanent curvature of the filaments in the XY-plane.

The r_e for each particle was calculated from measured values of T and G using the exact version of Eq. (1).

The experimental points in Fig. 7 show that r_e (or more correctly TG) was extremely sensitive to small deformations. As α fell from 180° for a straight particle to 160° for a bent one, r_e decreased by a factor of about 9.

For comparison, the axis ratio r_v of the figure formed by rotating the XY-projection of each filament about the chord joining its ends was calculated from the equation

$$r_v = \frac{\cos\alpha/2}{1 - \sin\alpha/2} \quad (3)$$

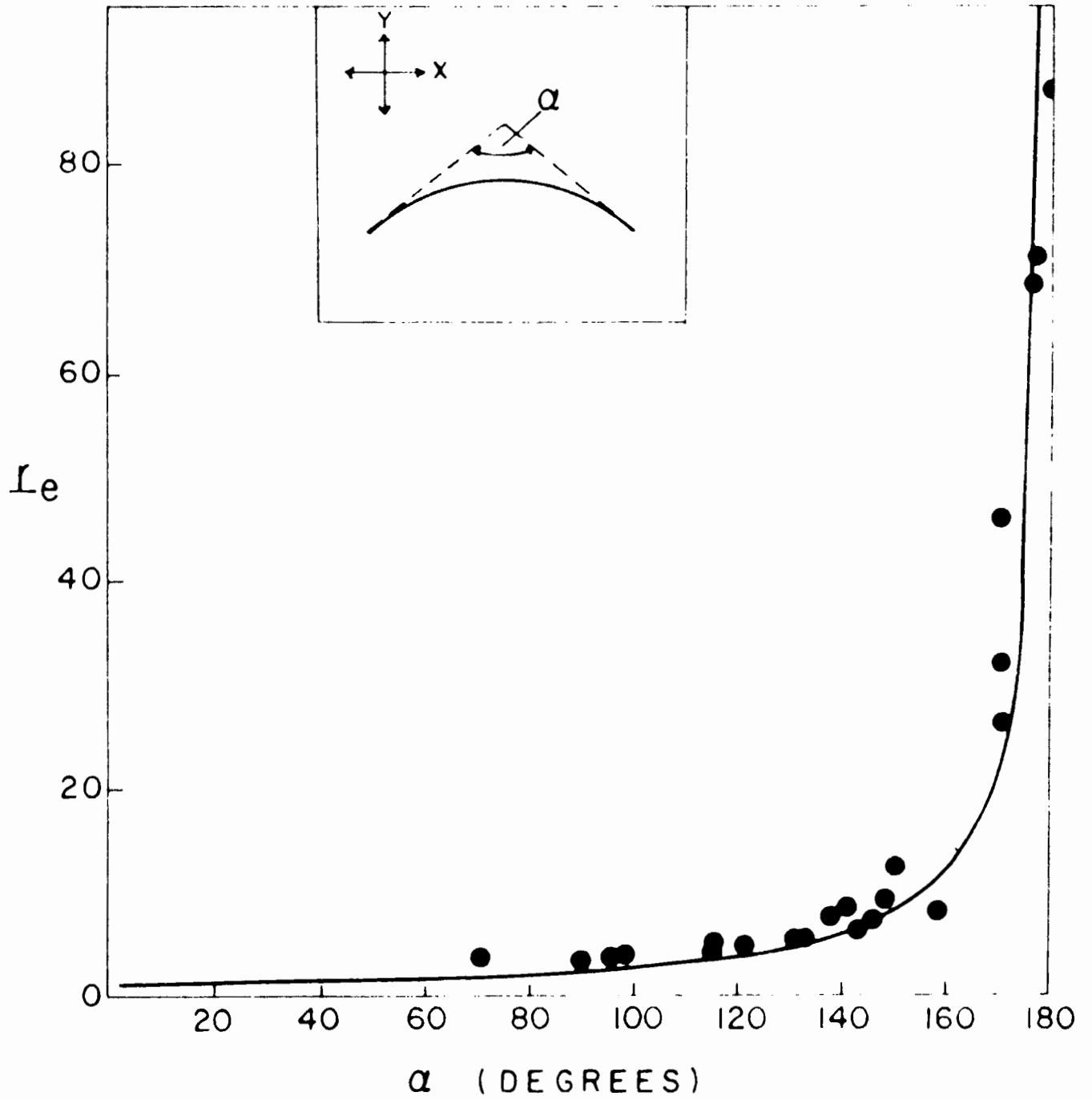
which is based on the approximation that the configurations formed arcs of a circle.

The change in r_v with α is shown as the solid line in Fig. 7. The trends of r_e and r_v with α showed remarkable agreement except at $\alpha = 180^\circ$, where r_v tends to infinity since Eq. (3) neglects the finite thickness of the particles.

The above experiment demonstrated the sensitivity of TG to small deformations. The fall in TG found previously (Fig. 6) in the region of r where pronounced shear-induced bending of the particles

FIGURE 7

The effect of permanent deformation on r_e for rigid rotations in the XY-plane. The angle α (inset) is an inverse measure of the curvature of a particle in the XY-plane. The experimental points show that r_e is highly sensitive to small deformations. The solid line represents calculated values of the axis ratio r_v , of the solids formed by revolution of the XY projections of the filaments about the chords joining their ends.



occurred was therefore explainable as the result of permanent deformation of the particles in the XY-plane. To determine the variation of TG with r up to values of r at which the particles described springy and snake orbits, it was therefore necessary to use particles which were free of permanent deformations. Such experiments are described below.

The significance of the above results on permanent deformation, in connection with theory of the viscosity of suspensions, has been discussed elsewhere (12) and will be considered further in Part V.

(iii) The Variation of TG with r

Experiments on TG vs. r were repeated, using the Apparatus No. 2, taking great care to use only those particles which were initially straight.

Rayon and Dacron filaments were each cut to a series of lengths corresponding to axis ratios from 50 to 400. The Dacron samples were suspended in corn syrup and the rayon in castor oil. The periods of rotation of ten filaments of each length and material were timed at known shear-rates.

Table III and Fig. 8 show that the results for rayon and Dacron were in good agreement despite the high standard deviations from the mean in TG. With the precautions taken in these experiments TG increased with r over the entire range of r , even at values at which springy and snake orbits were observed. As r increased, the value of TG

T A B L E III
Variation of TG with r

Material and Suspending Medium	r	No. in Sample	Mean $G\eta$ $\frac{\text{gm}}{\text{cm. sec.}^2}$	Mean TG	Orbit
3.5 μ Rayon Filament in Castor Oil $\eta = 40.5$ poises	43	10	319	172.0(13.4)	Rigid
	100	10	249	347.5(23.1)	Rigid
	173	10	338	513.4(40.1)	Rigid
	241	10	311	549.2(47.9)	Springy
	357	10	308	622.3(50.6)	Springy-Snake
7.8 μ Dacron Filament in Corn Syrup $\eta = 91.2$ poises	102	12	541	320.7(36.4)	Rigid
	139	10	542	397.2(43.6)	Rigid
	180	10	469	477.2(59.5)	Rigid
	228	10	544	580.0(58.0)	Just Springy
	310	10	445	631.0(42.6)	Springy
	414	5	440	648.0(52.9)	Snake
7.8 μ Dacron Filament in Diluted Corn Syrup $\eta = 11.4$ poises	228	10	44.7	537.5(64.9)	Rigid
	310	10	54.3	610.2(68.0)	Rigid
	414	5	54.3	616.4(78.5)	Just Springy

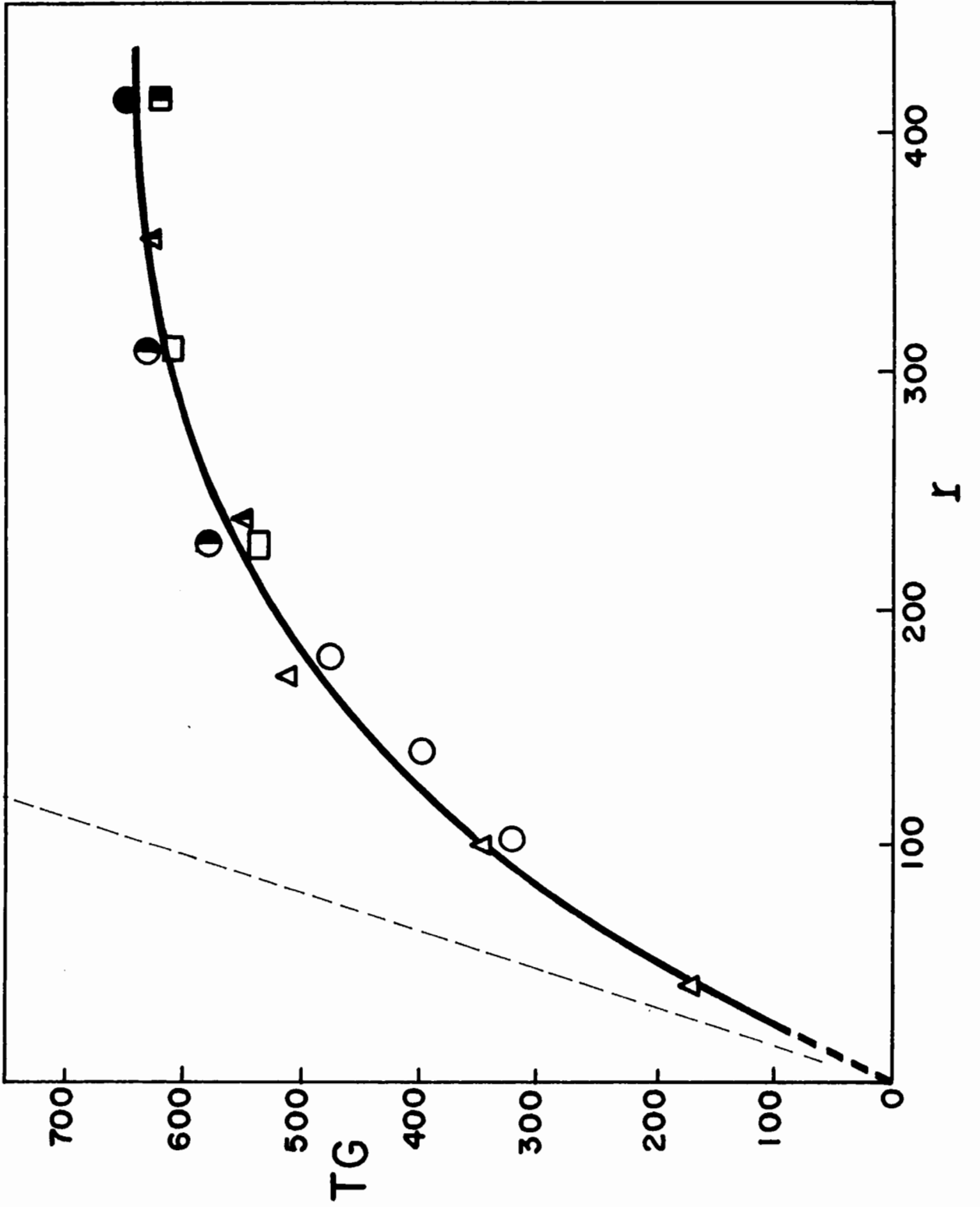
Bracketed values are standard deviations of associated means.

FIGURE 8

TG vs. r . Triangles: 3.5μ dia. rayon in Castor Oil, $\eta = 40.5$ poises. Circles: 7.8μ dia. Dacron in Corn Syrup, $\eta = 91.2$ poises. Squares: 7.8μ dia. Dacron in Corn Syrup, $\eta = 11.4$ poises. Open points: rigid rotations. Half-closed points: springy rotations. Closed points: snake rotations.

The broken line represents the relationship for prolate spheroids as calculated from Eq. (1).

TG increases with increasing r over the entire range of r .



deviated at an increasing rate from the predicted value for rigid prolate spheroids of corresponding axis ratios.

It was shown in Part II that the deforming forces exerted by the shear field and hence the extent of shear-induced deformation were a function of $G\eta$. It was therefore of interest to repeat the experiments with Dacron samples of $r = 228, 310$ and 414 at similar shear-rates, this time in corn syrup diluted with water to reduce the viscosity (and therefore $G\eta$) by a factor of about 10. In the diluted medium, the $r = 228$ and 310 samples described rigid orbits (compared to springy in the undiluted medium) and the $r = 414$ sample appeared springy (compared to snake orbits). It seemed that a small drop in TG resulted from the reduced flexibility, as is evident in Table III; however, the scatter in TG for the individual specimens in each sample was too high to draw quantitative conclusions from this set of experiments. The results nevertheless indicated that with filaments of high r which are straight when at rest, any change in TG resulting from changes in flexibility is small when compared to the changes caused by permanent deformation.

In this work, the relationship between TG and r was determined up to values of r at which snake orbits occurred. A further extension to filament lengths at which coiled orbits occur would be of interest.

(iv) The Variation of TG with G

The change in TG with G was investigated for a series of rayon filaments undergoing flexible orbits. Slightly curved particles were used, since the lower periods of rotation (compared with straight particles)

greatly facilitated accurate timing, without altering the nature of the experiments.

Fig. 9 shows the TG vs. G curves for filaments of axis ratios 311, 386, 491 and 583. Each curve represents the average of separate measurements on three single filaments of the same r. TG increased with G, following the same pattern as for pulp fibres (Appendix I). The rate of increase $d(TG)/dG$ was greater the longer the filaments, though no further change between the two samples of highest r was apparent. Since the ability of filaments to deform under given shear stresses increases with r, the results support the previous evidence (Appendix I) that $\Delta(TG)/\Delta G$ is determined by the amount of shear-induced deformation.

It is probable that the change in TG with G would be less pronounced for filaments which are perfectly straight when relaxed, since permanently curved particles not only bend under compression, but also straighten visibly in the quadrants of the rotation during which the filaments are under tension, thereby enhancing the overall shear-induced deformation.

The increase of TG with G is not confined to thread-like particles. Several bundles of rayon filament ($r = 311$) were prepared by joining about 20 filaments at their centres by means of droplets of wax, and their periods of rotation over a range of G were measured. The periods of rotation of elastomer helices at various velocity gradients were also measured, as were the periods of circulation of deformed cyclohexanol phthalate drops ($\eta = 238$ poises at $20^\circ\text{C}.$), using small particles of dust

FIGURE 9

TG vs. G for rayon filaments undergoing snake rotations. Curve 1: $r = 311$. Curve 2: $r = 386$. Curve 3 (open points): $r = 491$. Curve 4 (closed points): $r = 583$.

The increase of TG with G is more pronounced, the longer (and hence more flexible) the filaments.

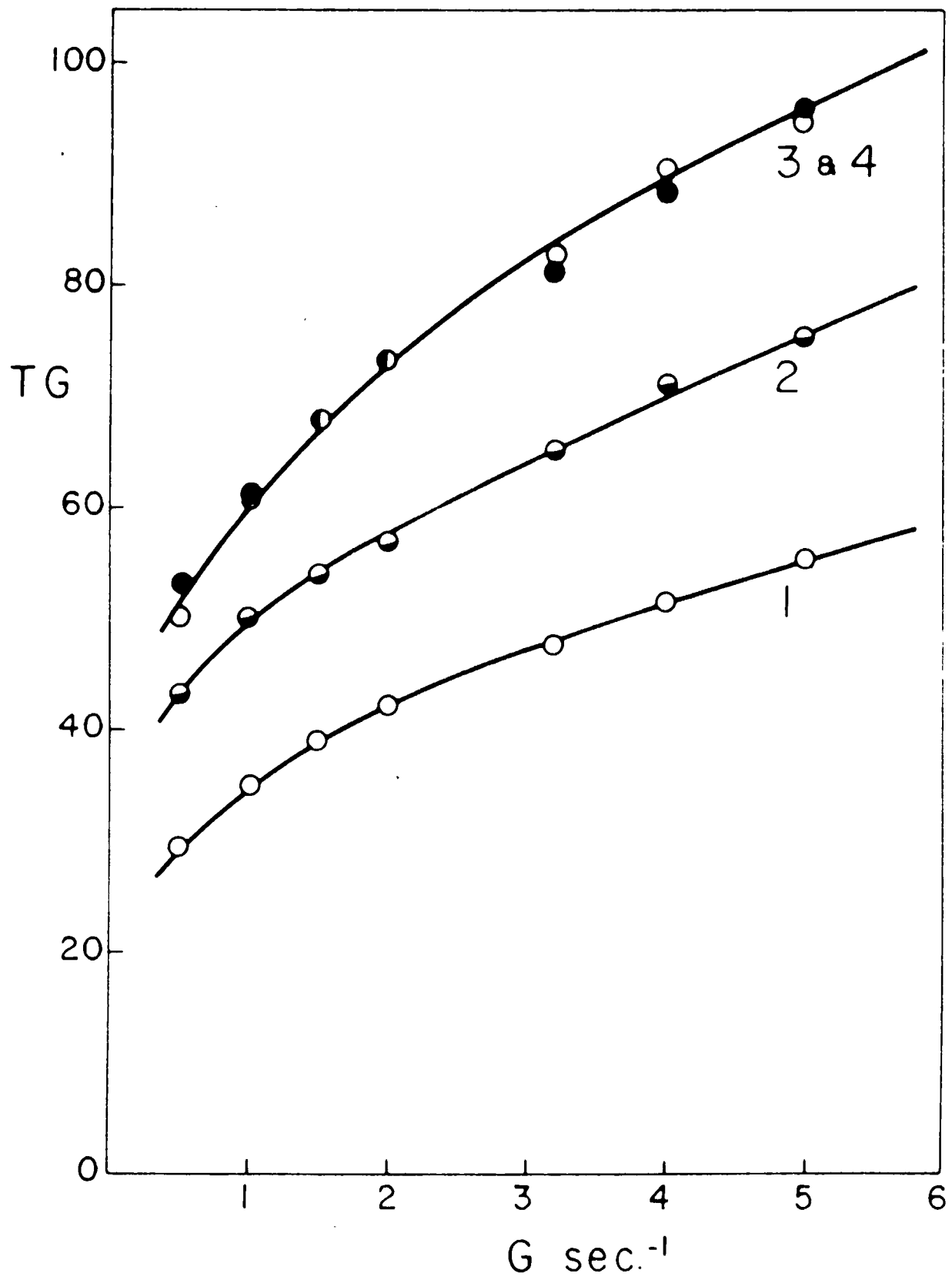
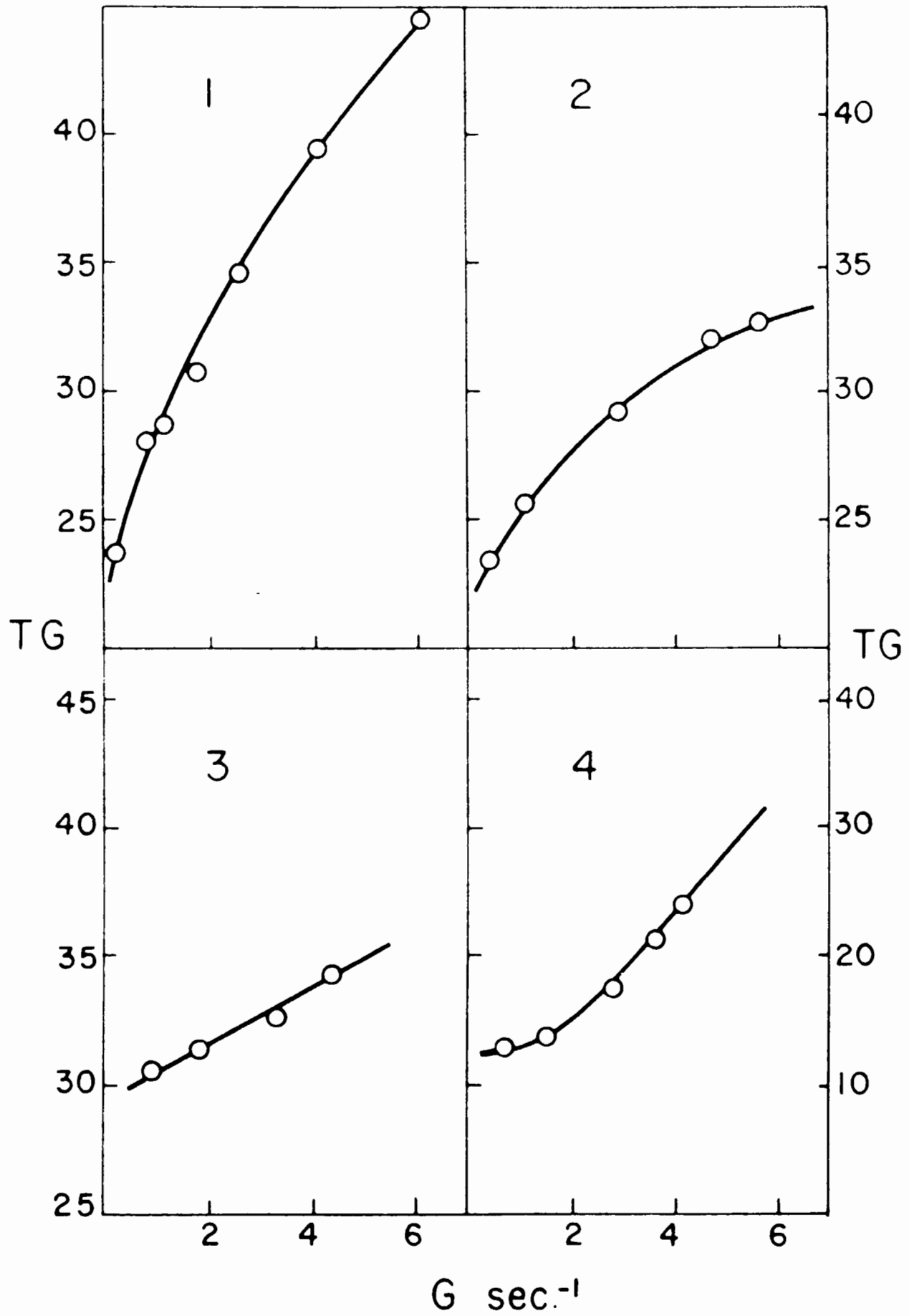


FIGURE 10

TG vs. G for various deformable particles. 1. Rayon filament (snake rotation), $r = 311$. 2. Rayon "bundle". 3, Elastomer helix. 4. CHP drop. In each case, TG increases with G.



at the drop interface as markers. Fig. 10 shows the TG vs. G curves for a flexible rayon filament, a bundle, a helix and a drop, all of which underwent increasing deformation with increasing G. In each case, TG increased with G, in contrast with rigid particles such as rods and spheres (2) where TG was independent of G. These results generally confirm the hypothesis presented in the introduction.

D. SUMMARY

The behaviour of deformable thread-like particles in suspensions subjected to velocity gradients has been studied.

For a given value of (shear rate) \times (viscosity of suspending medium), there exists a critical length at which thread-like particles in suspension will bend during rotation under the stresses imposed by the shear field. Over a limited range of particle lengths above the critical length, the deformation increased as the length was increased. However, the particles straightened twice during each rotation, during that part of the orbit in which they lay parallel to the planes of shear. When the particle length was increased further, the particles formed helices or coils which rotated at a more or less constant angular velocity. As the shear-rate was increased, the change in shape of the projection of the coils on the plane parallel to the velocity gradients resembled the change in shape of fluid drops under similar conditions.

The periods of rotation of permanently bent particles were

shown to be appreciably lower than those of straight particles. Whereas the product (period of rotation) \times (velocity gradient) was constant for rigid spheres, ellipsoids and rods, it increased with deformable particles at a rate which was related to the amount of deformation.

The work is of interest in connection with the viscosity and other flow properties of suspensions, and the streaming birefringence of solutions of macromolecules. Further discussion of the significance of the results is presented in Part V.

REFERENCES

1. Part II of this Thesis.
2. Trevelyan, B.J. and Mason, S.G., *J. Colloid Sci.* 6, No. 4:354 (1951).
3. Manley, R.St.J. and Mason, S.G., *J. Colloid Sci.* 7, No. 4:354 (1952).
4. Bartok, W. and Mason, S.G., *J. Colloid Sci.* 12, No. 3:243 (1957).
5. Manley, R.St.J. and Mason, S.G., *Can. J. Chem.* 33:763 (1955).
6. Bartok, W. and Mason, S.G., Forthcoming publication.
7. Mason, S.G. and Manley, R.St.J., *Proc. Royal Soc. (London) A* 238:117 (1956).
8. Arlov, A.P., Forgacs, O.L. and Mason, S.G., *Svensk Papperstidn.* 61, No. 3:61 (1958). Also Appendix I of this Thesis.
9. Jeffery, G.B., *Proc. Royal Soc. (London) A* 102:117 (1922).
10. Part IV of this Thesis.
11. Forgacs, O.L., Robertson, A.A. and Mason, S.G., *Pulp Paper Mag. Can.* 59, No. 5:117 (1958).
12. Nawab, M.A. and Mason, S.G., *J. Phys. Chem.* In Press.

PART IV

THE FLEXIBILITY OF WOOD PULP FIBRES

A. INTRODUCTION

In this Part we consider the application of the phenomena of particle deformation in a velocity gradient to the study of flexibility of wood-pulp fibres. Fibre flexibility is recognized as an important factor in the flow properties of paper-making pulp suspensions (1), in the formation of the paper sheet, and in the changes imparted to fibres on beating (2, 3). Rheological measurements of textile fibres, which are usually long and of uniform cross-section, are well developed. Several effective methods of measuring the flexibility of textile yarns and filaments have been reported, and were reviewed by Meredith (4). Unfortunately the application of these techniques to wood fibres is not practicable, because of their shortness and the wide spectrum in flexibility in any sample resulting from variations in wall thickness and other factors.

A method for measuring the flexural rigidity of ramie fibres based on the vibration technique used by Steenberg to study the flexibility of sheets (5) was reported by Nethercut (6), but this method also appears unsuited to short fibres. Seborg and Simmons (7) have described a method for single wood fibres in which the fibres were clamped to form cantilevers, and the deformation caused by small loads applied to the free ends was measured. However, since the wide distribution of flexibility in any sample of natural fibres required measurements on a large number of specimens, the method was too time-consuming for wide application.

The method which will be described below is based on the characteristic rotational orbits described by fibres when they are suspended in a liquid undergoing laminar shear and are thereby subjected to deforming stresses as discussed in Parts II and III. The technique has been used to study the effect of fibre length, pulp yield, beating and drying on fibre-flexibility. Some of the results, especially those on the effects of beating and of drying, are of a preliminary nature and are presented primarily to illustrate the scope of the method.

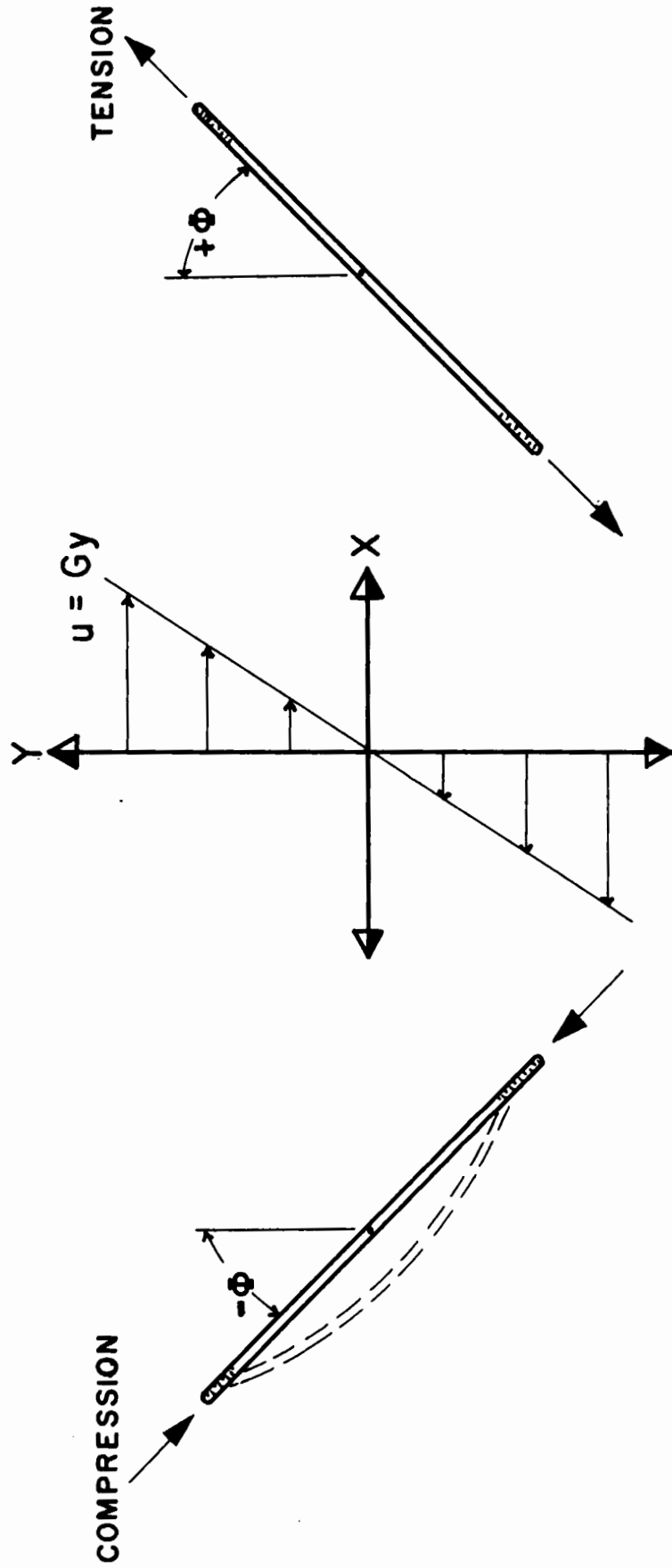
B. PRINCIPLES OF THE METHOD

1. General

Earlier studies of sheared suspensions have dealt with the rotational orbits and orientation of rigid cylindrical particles (8, 9) and of wood fibres (Appendix I). It was found that rigid pulp fibres underwent the same types of rotation as cylindrical rods. The orbits of flexible fibres, however, differed in a number of respects. Whereas rigid rods and fibres seemed to assume preferred orbits only after prolonged shearing, and presumably as the result of hydrodynamic interactions and collisions (9), flexible fibres rapidly aligned themselves either with their major axes close to the Z-axis or more frequently described orbits with their axes in or close to the XY-plane (Appendix I) of the co-ordinate system shown in Fig. 1.

FIGURE 1

The co-ordinate system in relation to the shear field. The Z-axis (not shown) is normal to the plane of the figure. During the first quadrant of rotation a rod-like particle is subjected to compression while during the second quadrant it is under tension.



The work presented in Parts II and III, on the rotational orbits of model filaments close to the XY-plane revealed that there were four major types of orbit: one rigid and three corresponding to different degrees of bending. Similar orbits were also described by pulp fibres, though an additional type of rotation was described by fibres which had sustained localized damage.

2. Orbit Types

The following are the descriptions of the five types of orbit. These are illustrated schematically in Fig. 2.

Type I. Rigid rotation. The fibre rotates in the manner predicted by Jeffery (10) and remains rigid (Fig. 2a).

Type II. Springy rotation. When aligned in the direction of flow, the fibre starts a rigid rotation; during the first quadrant of the rotation it bends like a leaf-spring and then flicks straight as it moves into the second quadrant, completing the half rotation as though rigid (Fig. 2b).

Type III. Flexible rotation. This orbit is exhibited by fibres which are more flexible than those yielding Type II. The fibre is initially aligned in the direction of flow (along the X-axis). One end (the head) starts to bend into a different shear (XZ-) plane with the bend passing as an undulation along the fibre from the head to the trailing end (the tail), until the particle has rotated through 180° and is aligned along the X-axis but pointing in the opposite direction (Fig. 2c). This was previously called a snake-turn (11). A less common

variation is an S-turn in which each end forms a head so that the fibre bends into an S-shape (Fig. 2d). Occasionally irregularities in shape cause the bend to start in the middle of the fibre so that it bends into an S-shape, but with the ends trailing the rotation. It should be noted that the transition from a springy to a flexible rotation is not sharply defined. Ambiguity was avoided by classifying only those fibres as Type III whose ends appeared capable of moving independently of each other. This distinction, although somewhat arbitrary, provided acceptable reproducibility, as will be shown later.

Pulp fibres are not always uniformly flexible. In some cases, there are regions in the fibre which can be seen to be more flexible than others. Low yield (<50%) sulphite and kraft pulps contained fibres which had constrictions or nodes at strikingly regular intervals along their lengths. With such fibres the greater bending took place at the nodes as shown in the photomicrographs (Fig. 3), so that the shape of the bending fibre was comparable to that of a railway train turning a curve. This type of bending was especially characteristic of low-yield sulphite pulps; in these

nearly every fibre showed a tendency to bend in segments¹.

Type IV. Complex Orbit. This type of orbit was termed "simple coil" rotation in Part III. When a fibre is sufficiently flexible, it can undergo a rotation in which the leading end starts a second half rotation before the tail has had time to complete the first, so that it never becomes straight during the rotation as shown in Fig. 2e. If still more flexible, a closed loop may form. The orbits of the category are easily distinguished from Type III because the fibre never straightens. However, fibres which have been subjected to drastic drying or mechanical treatment sometimes have permanent deformations and though flexible, are incapable of straightening even in the absence of liquid shear. For this reason Type IV orbits can be considered distinctive only in virgin pulps i.e. pulps which have never been dried. In experiments on dried and beaten samples, Types III and IV were therefore combined in analysing the data.

¹ These nodes appeared to be similar to those described by Emerton (3). His photomicrographs also show the regularity of the spacings between the nodes and suggested that they were gatherings of the outer secondary wall (S_1 layer) possibly caused by incipient balloon swelling which had occurred in the course of pulping. Though this hypothesis would explain why the nodes are only observed in low yield pulps it would also imply greater rigidity at the nodes, which is contrary to the observations reported above. In a recent private communication, Mr. Emerton stated that in certain cases where fibres were attached side by side at one end but separated at the other and where cross-field pitting corresponded along their lengths, the constrictions also occurred at corresponding positions, probably arising while the fibres were still associated as chips. This suggests that the nodes occur at points where the fibre wall is weakened by the presence of pits, and may explain the present results that the fibres bend more readily at these points.

FIGURE 2

Schematic diagram of the rotational orbits of fibres in the XY-plane.
The orbit types are represented in order of increasing fibre flexibility.

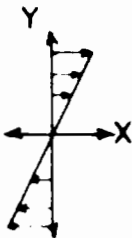
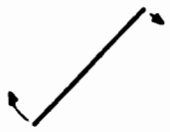
	ORBIT CLASS	HALF ROTATION					
	I RIGID	1 	2 	3 	4 	5 	a
	II SPRINGY						b
	III 'SNAKE TURN'						c
	'S-TURN'						d
	IV COMPLEX						e

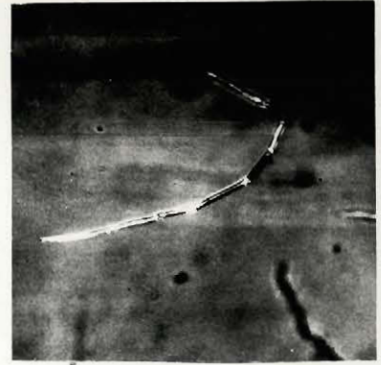
FIGURE 3

Segmental bending: Photomicrographs of spruce sulphite fibres in polarized light.

Plate I: segmental bending of a fibre during flexible rotation.

Plate II: photomicrograph of a fibre during relaxation after stopping the shear.

It is shown that bending occurs primarily at the nodes.



—|—
1 mm.

SEGMENTAL BENDING

SPRUCE SULPHITE FIBRE

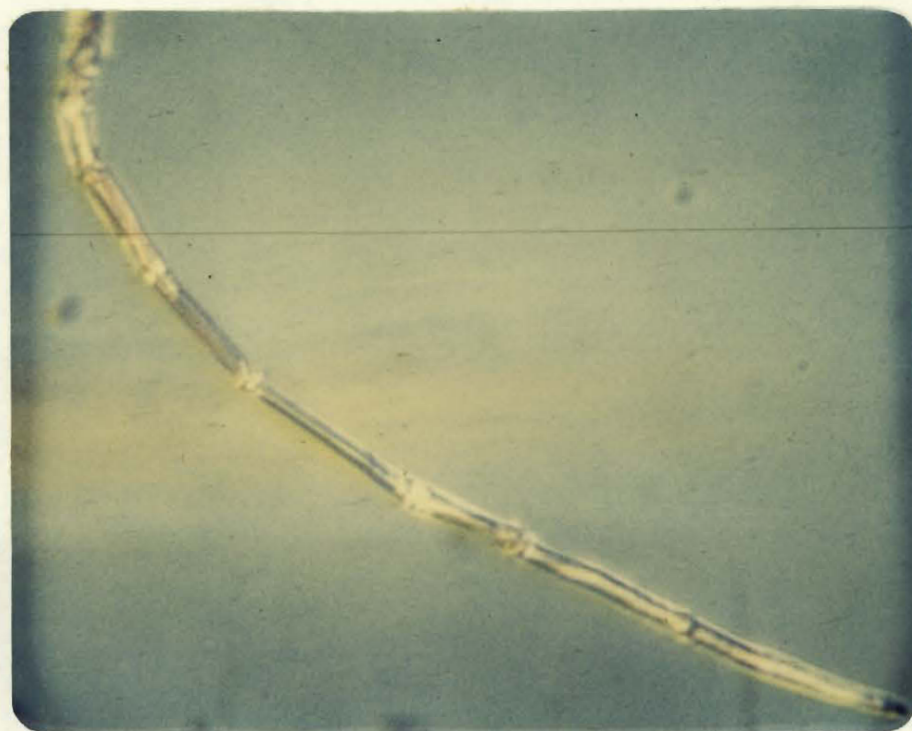


PLATE II

Magnification x212

Type V. Jointed fibre orbits. Sometimes bending occurs at one or more highly flexible joints presumably caused by localized fracture of the cell wall. Often these are "knee-joints", i.e. bending can occur in one direction and not the other. Pulps which had not been subjected to severe mechanical treatment contained a low fraction of fibres with hinges (usually less than 10%) and such fibres were therefore rejected in the sampling. However, in the beating experiments the high incidence of damaged fibres led to the inclusion of fibres (moving in Type III and IV orbits) with joints in a separate category which is designated as Type V.

3. Theoretical Considerations

The theory of deformation of the fibres is considered to be identical with that discussed in Part II and is outlined briefly as follows. When a rigid cylinder rotates in the XY-plane, it is acted on by an axial stress F generated by the sheared liquid which Burgers (12) has shown to be given approximately by the equation

$$F = \frac{\pi n a^2 G}{2(\log_e 2r - 1.75)} \cos 2\phi \quad (1)$$

where $2a'$ and r are the length and axis ratio of the particle, G is the gradient and η the viscosity of the liquid.

During the first quadrant of rotation (between $\phi = -90^\circ$ and 0°) the force is a compression which tends to deform the fibre, and

during the second quadrant a tension tending to pull it straight, Fig. 1. If the compressive force, which reaches a maximum at $\phi = -45^\circ$, exceeds a critical value the particle will buckle.

It has been shown in Part II that the critical value of the quantity $G\eta$ is given approximately by

$$(G\eta)_{\text{crit}} \sim \frac{E}{F(r)} \quad (2)$$

where E is the bending modulus (= Young's modulus when the particle has ideal isotropic elasticity), and $F(r)$ is a function of r alone and is approximately proportional to r^4 .

It follows from Eq. (2) that as $(G\eta)$ is increased past the critical value, the orbit of the particle will change from rigid (Type I) to springy (Type II). Similarly if G , η and E are fixed Eq. (2) predicts that particles will describe rigid orbits below a critical value of r . This theory of bending has been confirmed by means of experiments on model filaments as described in Part II.

Although no theory exists for Type III and IV orbits, it is reasonable to predict, by analogy, that critical values of the same variables exist for the higher orbit transitions.

This is illustrated by the orbit types observed at constant $G\eta$ for rayon particles cut to a series of lengths listed in Table I. The orbit was transformed from Type I to IV between $r = 120$ to $r = 600$. Table I also shows that the transitions can be made to occur at lower axis ratios by increasing G .

T A B L E IRotational Orbits of Rayon Filament in Corn SyrupFilament diameter = 5.4 μ

AXIS RATIO	TYPE OF ORBIT	
	G = 0.5 Sec. ⁻¹	G = 4.0 Sec. ⁻¹
45	I	I
105	I	I
204	I	II
311	II	III
386	III	III
491	III	III
583	III	III + IV
780	IV	IV

Eq. (2) was derived for ideal cylinders and although it may not be directly applicable to pulp fibres, the same general mechanism of deformation is undoubtedly involved. The theory outlined above does, however, serve to illustrate the importance of controlling the variables G , η and fibre length in order to obtain reproducible orbit distributions. The methods of control are discussed below.

C. EXPERIMENTAL PART

1. Apparatus

The measurements were made in the Couette device (Apparatus No. 2) used previously and described in Appendix II, in which two coaxial cylinders were rotated in opposite directions by driving mechanisms which enabled the speed of either cylinder to be varied continuously and independently. The dilute suspension was placed in the annulus between the cylinders. Single fibres were selected for viewing in the stationary layer ($y = 0$) between the cylinders through a microscope with its axis directed along the planes of shear, i.e. perpendicular to the plane of Fig. 1. The velocity gradient G was computed from the diameters and speeds of rotation of the two cylinders (8).

2. Materials

Three series of pulps (two sulphite and one kraft) were prepared to provide fibres having a wide range in flexibility. The

T A B L E II
Pulping Condition

Series	Liquor	Yield %	pH	Max.T °C	Time at Max.T Min.
1 Douglas Fir	<u>Sulphite</u> Soda-base	83.1	5.5	160	30
		76.9	5.5	160	120
		68.0	4.0	160	150
		62.5	3.0	160	150
		48.5	2.0	160	150
2 Black Spruce	<u>Sulphite</u> Soda-base	89.9	4.0	150	0
		73.8	4.0	160	30
		67.8	4.0	160	90
		63.3	4.0	160	120
		58.9	1.5	140	60
		47.9	1.5	140	255
3 Black Spruce	<u>Kraft:</u> 17% effective alkali	84.5		95	0
		76.7		130	0
		66.5		155	16
		58.5		165	14
		46.3		165	183

pulping conditions and yields are given in Table II. The same batch of Black Spruce chips was used for series 2 and 3. In the experiments to study the effect of fibre-length, yield and beating on these samples, virgin pulps were used exclusively.

Most of the experiments were made with suspensions in household corn-syrup with a viscosity of 67 poises at 22.5°C. and a relative water-vapour pressure of 70%. A few measurements were made with dried fibres in oxidized castor oil (No. 300 Castor oil, Baker Castor Oil Co., New York) with a viscosity of 33 poises at 22.5°C.

3. Procedure

Small bundles of the fibres were removed from a concentrated water suspension by means of a teasing needle, and were gently pressed between two clean blotters.

The concentration of the suspension had to be low enough to allow observations of orbits to be made over several fibre rotations without interference from other fibres in the suspension, yet sufficiently high to permit rapid sampling; w/v concentrations of about 2×10^{-3} percent proved to be satisfactory and made it possible to observe the orbits of about 100 fibres in a period of 1.0 to 1.5 hours.

The selection of fibres in the apparatus was made through the microscope which was adjusted so that the stationary layer crossed the center of the field of view. The orbit class of each fibre drifting into the microscope field was recorded, provided that the following condi-

tions were fulfilled:

1. The fibre rotated with the principal axis close to the XY-plane. This was easy to judge from the constancy of focus during the fibre rotation.

2. The length of each fibre fell between fixed limits. Most of the experiments were conducted using fibres close to 2 mm. long, since this was close to the maximum in the length distribution curves of the pulps used.

The pulps were fractionated in a Bauer-McNett classifier. It was found that a fraction with a mean fibre length of about 2 mm. was obtained between the 20 and 28 mesh screens, while the SD in length was reduced from about 50 to 25 percent. Fractions 1 and 3 mm. long were also prepared using 30/48 and 14/20 mesh screen combinations respectively. Subsequent selection of fibre according to length was made in the microscope field by means of a calibrated graticule in the eyepiece; this reduced the SD to about 10 percent. To achieve this, fibres under 1.6 mm. and over 2.4 were rejected for the 2 mm. fraction, and similar limits were imposed on the sampling for the 1 and 3 mm. fractions. The lengths of the selected fibres were recorded and used to calculate the mean fibre length of each sample.

To avoid observing the same fibre more than once, the depth of the annulus under observation was changed periodically by raising or lowering the microscope. In addition, the relative speeds of the Couette cylinders were changed after every two or three

T A B L E IIIReproducibility Experiment

68% Yield Spruce Sulphite Pulp
Sampling based on 100 fibres

Observer	Mean Length mm.	Orbit Distributions, %			
		I	II	III	IV
A	2.05	39	39	21	1
B	2.02	39	34	26	1

observations, thereby changing the location of the stationary layer.

The velocity gradient was standardized as a matter of convenience at $4 \pm 0.5 \text{ sec.}^{-1}$. The viscosity was controlled by regulating the room temperature to $22.5 \pm 1^\circ\text{C.}$; this corresponded to viscosity limits of 67 ± 6 poises for the corn syrup and 33 ± 2.5 poises for the castor oil. Orbit distributions were determined from observations on 100 fibres except in the early experiments on some of the pulps in series 1 when only 50 fibres were selected.

The effectiveness of these arbitrary limits must be judged from the reproducibility. Table III gives the results of two observers on the same pulp and for this case shows agreement within $\pm 5\%$ for each type of orbit.

D. RESULTS

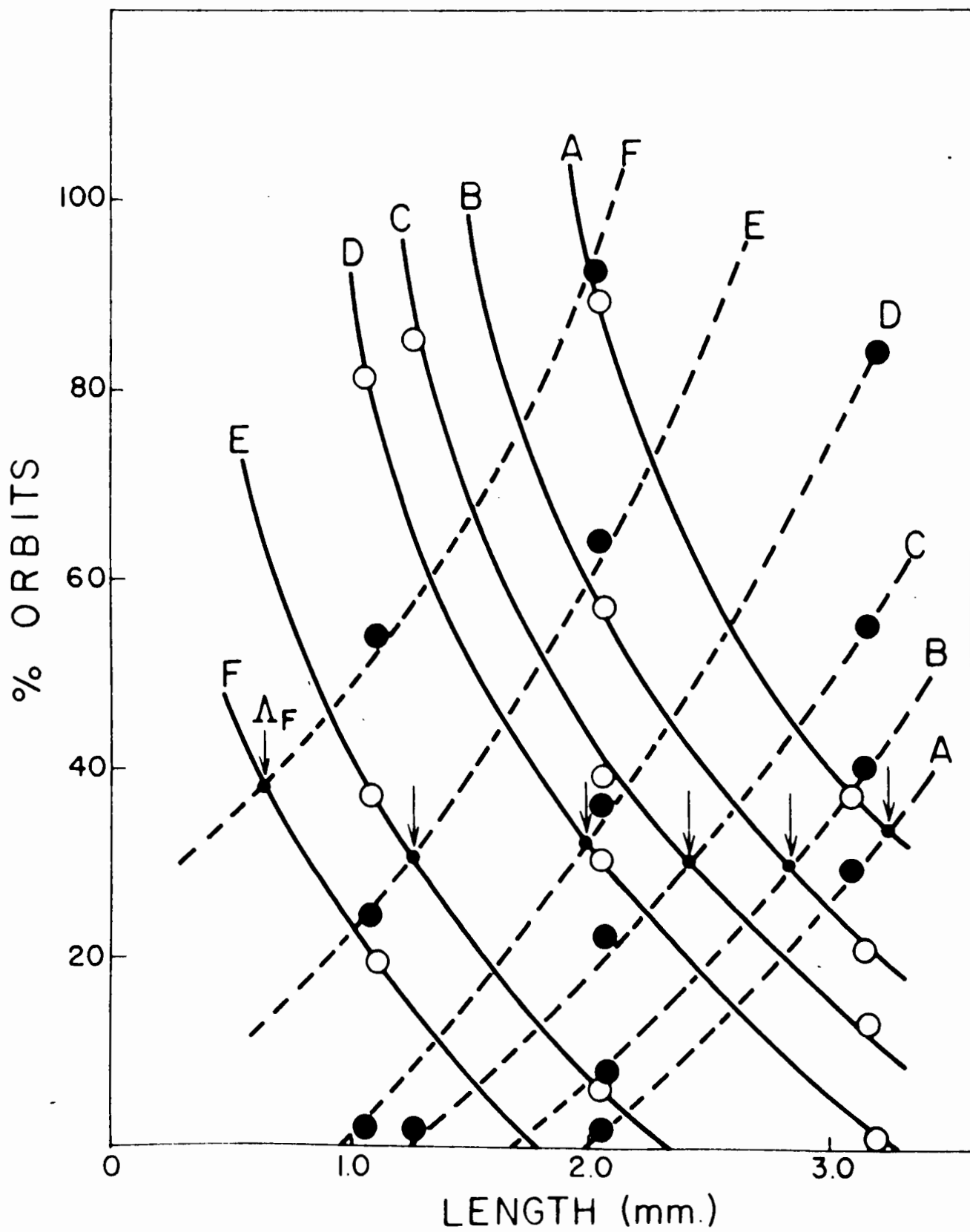
1. The Effect of Fibre Length

As was found with model filaments, the flexibility of wood fibres in a given sample increased with fibre length. This was shown by comparing the orbit distributions for different length fractions of the same pulps.

Fig. 4 shows the distribution of rigid (Type I) orbits and flexible (Types III + IV) orbits as a function of the fibre length for six spruce sulphite pulps. For simplicity, the transitional 'springy' (Type II) orbits have been omitted and III and IV have been combined. It

FIGURE 4

The effect of fibre length on the orbit distributions for six sulphite pulps, designated A to F as in Table IV. The continuous lines represent Type I orbits, the broken lines Types (III + IV) orbits. The arrows indicate Λ , the length at which the occurrence of Type I orbits equals that of Types (III + IV) for each pulp.



is seen from the curves that in all cases the fraction of rigid fibres decreased and the fraction of flexible fibres increased as the length was increased.

The significance of the intersection between the curves representing Type I and Types (III + IV) will be discussed later. The high slopes show that the orbit distributions are highly sensitive to changes in fibre-length (as would be expected from Eq. (2)) and demonstrate the importance of standardizing the fibre-length when comparing different pulps.

2. The Effect of Pulping Conditions

The flexibility of pulp fibres increased continuously as the pulp yield diminished.

The distributions of the four types of rotational orbits in the 2 mm. fractions of undried Douglas Fir and Black Spruce sulphite pulps are shown in Tables IV and V and Figures 5 and 6. The development of flexibility with decrease in yield was similar in both series. As the yields decreased from about 90 to 45 percent, the fraction of rigid (Type I) orbits decreased from a high value to practically zero, the fraction of springy (Type II) orbits increased to a maximum near 68 percent yield and then diminished, and both fractions of flexible (Types III and IV) orbits increased.

Table V includes the orbit distributions for a spruce sulphite pulp which had been bleached by a commercial three-stage process,

dried and rewetted. The high flexibility of the fibres in this sample was reflected by the complete absence of orbits of Types I and II. The high incidence of Type IV orbits may have been partly due to permanent deformation caused by drying and not entirely to a genuine increase in flexibility.

Table VI and Fig. 7 show the orbit distributions of the 2 mm. fractions for the series of Black Spruce kraft pulps which were prepared from the same chips as the spruce sulphite series. Although the general trends were similar to those of the sulphite series, there were several striking differences. A comparison of Fig. 6 and 7 yields qualitative information on the development of flexibility in the two series. Firstly, the maximum in Type II orbits occurred at 77 percent yield in the kraft series and at 68 percent yield in the sulphite series. This indicated that the kraft pulps became flexible at a considerably earlier stage in cooking than the sulphite pulps. Secondly, the increase in flexibility below 60 percent yield was more gradual in the kraft series. This was shown by the persistence of a considerable fraction of Type I fibres, slow growth of Type IV fibres, and especially by the comparatively small slopes of the distribution curves, over the lower range of yields.

Another important difference is reflected by the variation of rigid fibres with lignin content shown in Fig. 8. The Klason (sulphuric acid) lignin was determined according to the Tappi Standard Method (T222M) and calculated as a percentage of the original wood. For the

spruce sulphite series the fraction of rigid fibres diminished at a rate which increased with the removal of lignin. In the kraft series, however, a drop of over 40 percent in the fraction of rigid fibres took place for removal of less than 1 percent lignin between the two mildest cooks (see Table II). On the other hand, the removal of lignin below 14 percent lignin content was accompanied by a relatively small decrease in the fraction of rigid fibres. Fig. 8 shows that below about 7 percent lignin the kraft pulps contained more rigid fibres than the corresponding sulphite pulps. While the data are too limited to permit generalization, it is interesting to note that a similar result was obtained at low lignin contents by Seborg and Simmons (7).

Pentosan estimations of the two spruce series were made, but no correlation between flexibility development and the pentosan content was apparent.

Standard handsheets were also prepared for these two series of pulps. In each series, bulk decreased with decreasing yields and increasing flexibility. At corresponding yields, the kraft pulps were always bulkier than the sulphite.

Some qualitative observations were made with poplar, birch and oak pulps. The fibres were generally more rigid than those of softwood pulps of corresponding yields. However, low yield and bleached hardwood fibres exhibited orbit types I, II and III. It therefore appears that the method can be used to study fibre flexibility in hardwood pulps.

T A B L E IV

Orbit Distributions of Douglas Fir Sulphite Pulps

Yield %	Mean Fibre Length mm.	Orbit Distributions, %			
		I	II	III	IV
83.0	1.94	90	10	0	0
76.9	1.99	82	16	2	0
68.0	2.01	42	46	12	0
62.5	1.98	24	28	46	2
48.5	1.99	2	16	70	12

TABLE V

Orbit Distributions for Black Spruce Sulphite Pulps

Sample	Yield %	Klason Lignin ¹ %	Mean Fibre- Length, mm.	Orbit Distributions							
				Measured				Calculated ²			
				I	II	III	IV	I	II	III	IV
A	89.9	22.4	2.04	89	9	2	0	87	10	2	0
B	73.8	13.6	2.06	57	36	7	1	60	29	10	0
C	67.8	11.3	2.05	39	39	21	1	38	38	24	0
D	63.3	8.7	2.04	30	34	35	1	26	38	35	1
E	58.9	7.2	2.04	6	30	59	5	6	31	61	2
F	47.9	0.9	2.02	0	8	80	12	1	7	85	7
Bleached			2.10	0	0	67	33				

1. Calculated as percentage of original wood.

2. See Discussion.

T A B L E VI

Orbit Distributions of Black Spruce Kraft Pulps

Yield %	Klason Lignin % ¹	Mean Fibre- Length, mm.	Orbit Distributions %			
			I	II	III	IV
84.5	23.0	2.10	80	17	3	0
76.7	22.3	2.09	37	39	24	0
68.0	14.5	2.08	17	29	53	1
58.5	10.1	2.06	12	25	62	1
46.0	1.6	2.01	8	14	75	3

1. Calculated as percentage of original wood.

FIGURE 5

Orbit distributions at various yields for the 2 mm. fractions of the Douglas Fir sulphite series.

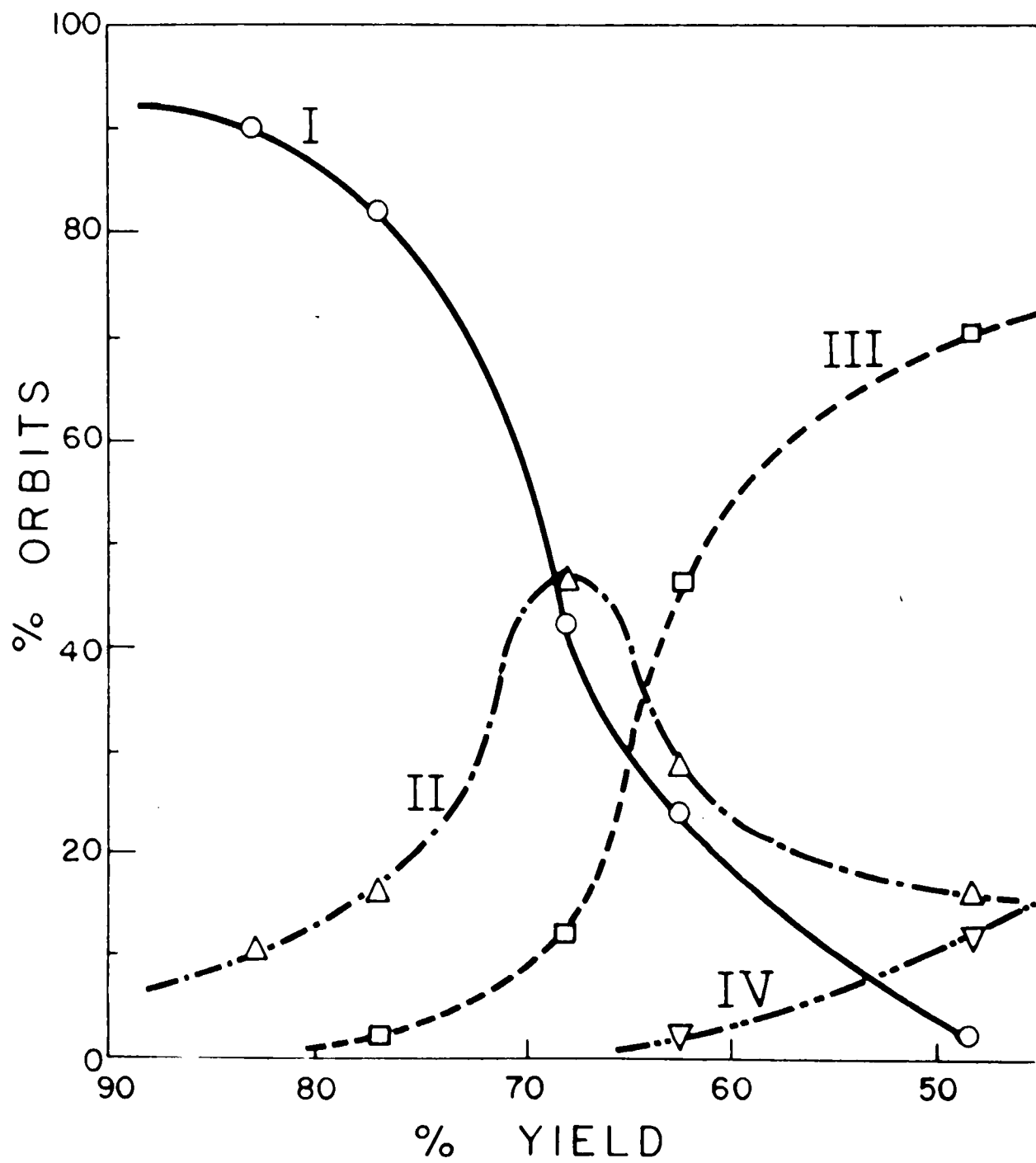


FIGURE 6

Orbit distribution versus yield: Black spruce sulphite series,
2 mm. fraction.

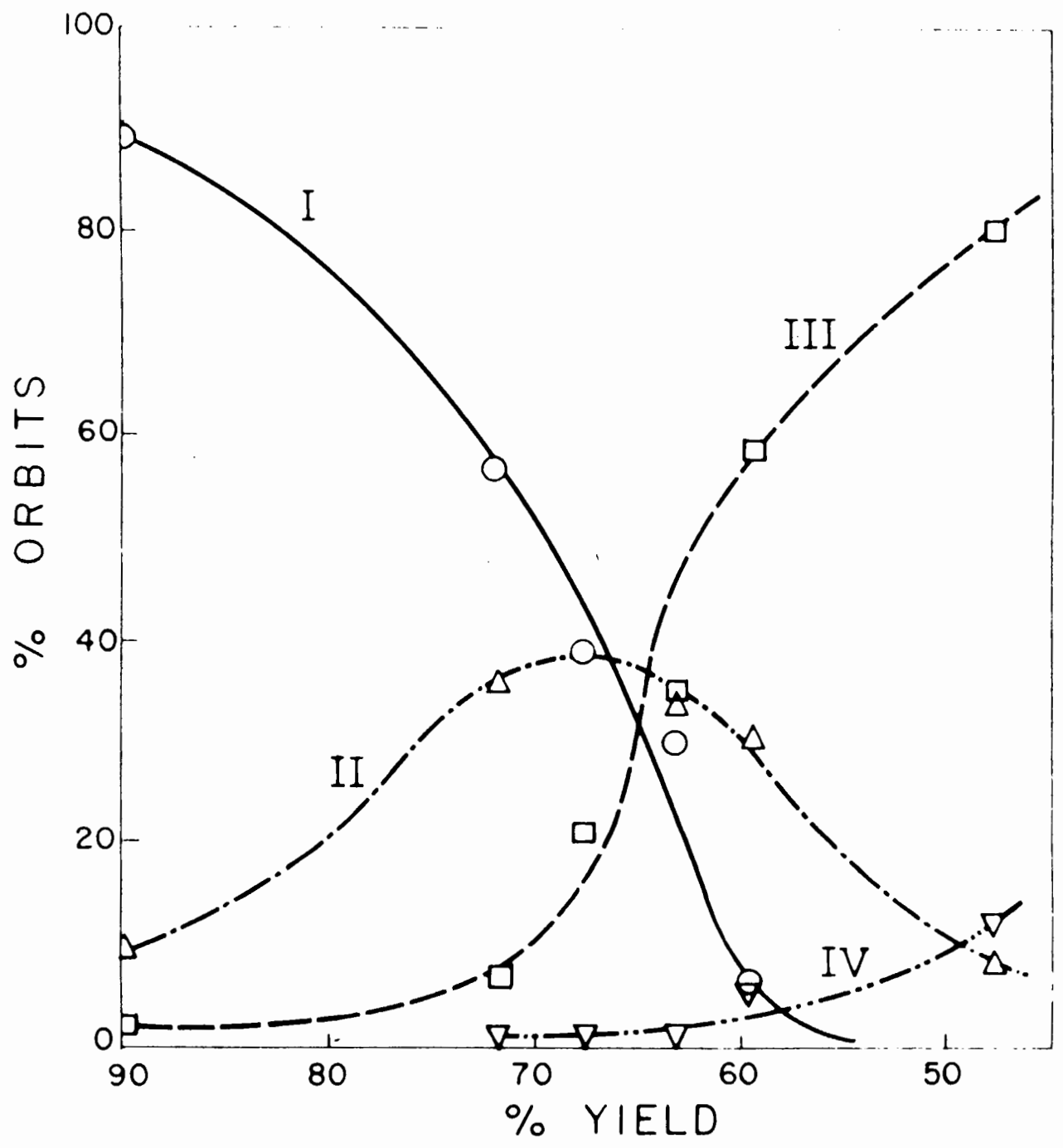


FIGURE 7

Orbit distributions versus yield: Black spruce kraft series,
2 mm. fraction.

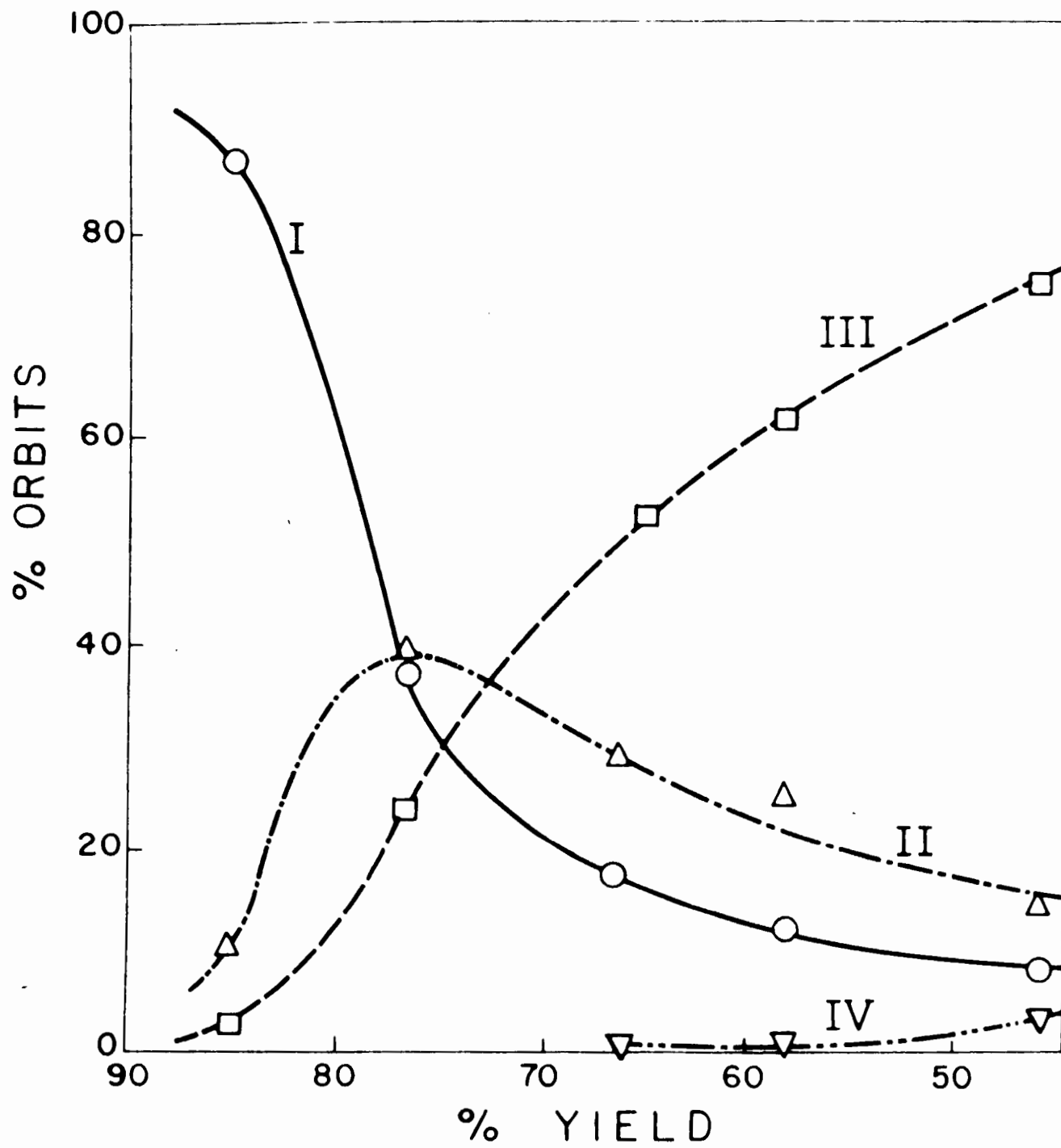
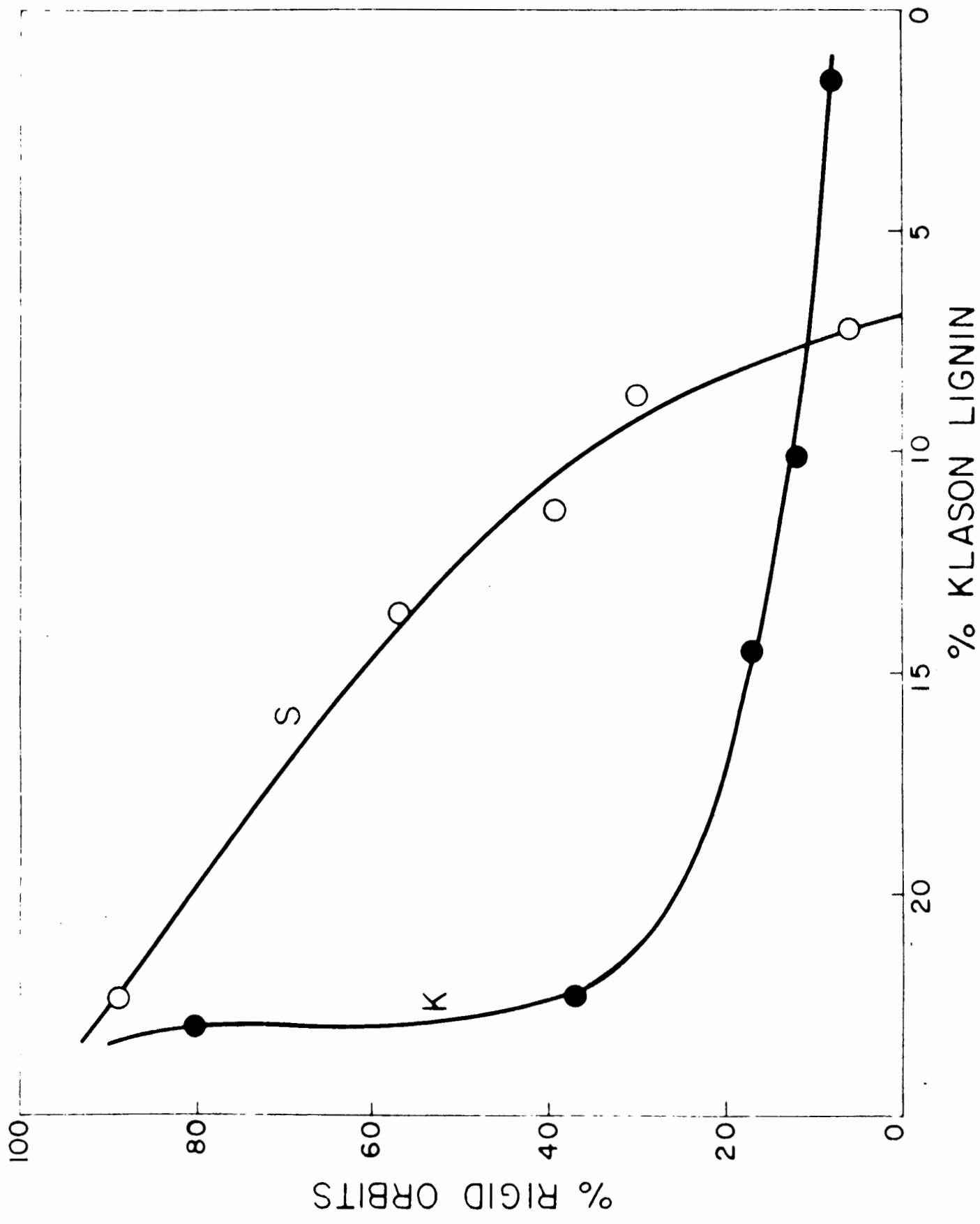


FIGURE 8

Percent rigid orbits versus Klason lignin content for spruce sulphite (Curve S) and kraft (Curve K) pulps. The lignin content was calculated as a percentage of the original wood.



3. The Effect of Beating

The data available on the effect of beating are limited and require amplification. However, the results obtained serve to demonstrate that the orbit distribution method may be used to study the effects of treatment involving mechanical damage, as well as physical and chemical changes in the structure of the fibres.

The experiments were made on a sample of 68 percent yield spruce sulphite pulp. This sample was selected because of the spread in rotational orbits of the fibres in the unbeaten state. No claim is made that the development of flexibility on beating of this sample is necessarily characteristic of the behaviour of other, and especially lower yield pulps, although it is likely that other pulps would follow the same general trends.

The pulp was beaten in a 1 1/2 lb.-Valley beater at a consistency of 1.55 percent. The weight on the bedplate was 1 kg. instead of the usual 5.5 kg. in order to reduce the amount of damage to fibres by cutting and crushing. 30 gm. samples of pulp were removed from the beater at intervals and flexibility determinations were conducted on the 2 mm. fractions.

In assessing the orbit distributions in unbeaten pulps, fibres having hinge-joints, i.e. exhibiting localized rather than continuous bending throughout the lengths of the fibres, were omitted in the sampling. Since the occurrence of fibres with one or more hinge-joints greatly increased with beating, the omission of fibres

with joints in the beater experiments was no longer practical nor, indeed, justified. Fibres which exhibited localized bending were therefore included in the sampling and recorded as a separate class, i.e. Type V orbits.

It was mentioned previously that a distinction between Types III and IV orbits was of doubtful significance in samples containing many damaged or deformed fibres. These two classes were therefore combined in the analysis of data on beating.

Table VII shows the orbit distributions for two beater runs made under the same conditions except that the beater bars were sharper in Run 2. Both runs showed similar variation of flexibility with freeness (Fig. 9) though both flexibility and freeness changed more rapidly in Run 2.

As beating proceeded:

- i. The fraction of Types I and II orbits decreased to a small fraction.
- ii. Types (III + IV) increased initially. We may attribute this effect to what is termed "internal fibrillation", that is, the disruption of the internal structure of the fibres due to swelling and the repeated deformation caused by the high shear-rates between the beater bars and the bedplate. It is probable that this type of softening of the fibres continued throughout the beater run. The decrease in the frequency of Types III and IV during the latter half of each beater run merely means that a greater number of these fibres have been reclassified as Type V on developing hinge-joints.

iii. The proportion of Type V fibres increased steadily throughout the beater runs.

Fig. 10 shows Types (III + IV) and V plotted against beating time for run 1. The sum of Types (III + IV + V) orbits is also shown for reasons discussed below.

Standard handsheet properties were determined on the samples of run 1. The view has frequently been expressed that the development of burst and tensile strength and the decrease in bulk on beating are partly the result of increasing fibre flexibility. The more the fibres are capable of deforming under the surface tension forces acting during drying of the web, the more intimate will be the contact between fibres affording a greater area for interfibre bonding.

In forming a sheet, Type V fibres may be assumed to contribute in much the same way as Types III and IV, since all these fibres are assumed capable of deformation under stresses generated by capillary forces. Fig. 11 also shows the summed orbits of Types (III + IV + V) together with tensile strength and bulk, as a function of beating time. The similarity in shape between the flexibility, bulk, and tensile strength curves may be taken as evidence for a relationship between the ability of fibres to deform and the extent of bonding. However, the surface properties of the fibres, which also change during beating (3, 14) and on which bonding ultimately depends, must also be considered as a contributing factor in the correlation. It is worth noting that the

T A B L E VII

Orbit Distributions In Beaten Pulps

	Beating Time min.	C.S.F.	Orbit Distributions %					
			I	II	III	IV	V	III+IV+V
RUN I	0	735	38	25	25	1	11	37
	234	643	13	18	47	2	20	69
	390	558	3	5	50	6	36	92
	480	403	5	4	44	4	43	91
	528	262	4	6	30	3	57	90
RUN 2	0	735	38	25	25	1	11	37
	135	622	21	9	34	2	34	70
	240	539	6	10	40	3	41	84
	291	440	2	8	36	6	48	90
	320	318	3	3	27	11	56	94

FIGURE 9

The development of flexible orbits (including damaged fibres) as a function of Canadian Standard Freeness for two beater runs on 68% yield spruce sulphite pulp.

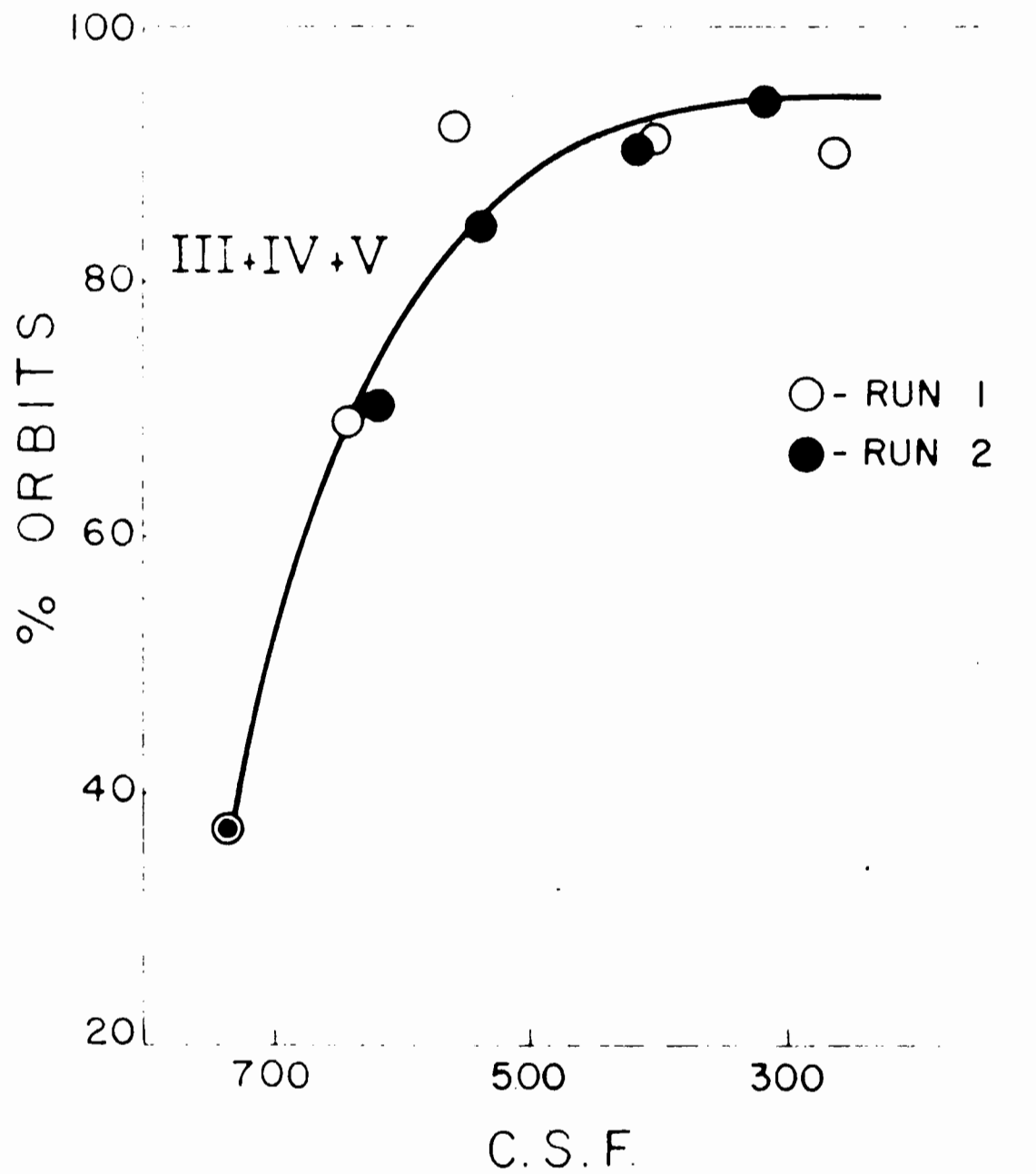


FIGURE 10

The frequency of flexible fibres (Types (III + IV) orbits) and jointed fibres (Types V orbits) versus beating time (Run 1, Table VII). The curve marked (III + IV + V) represents the development of flexible orbits, including the damaged (jointed) fibres.

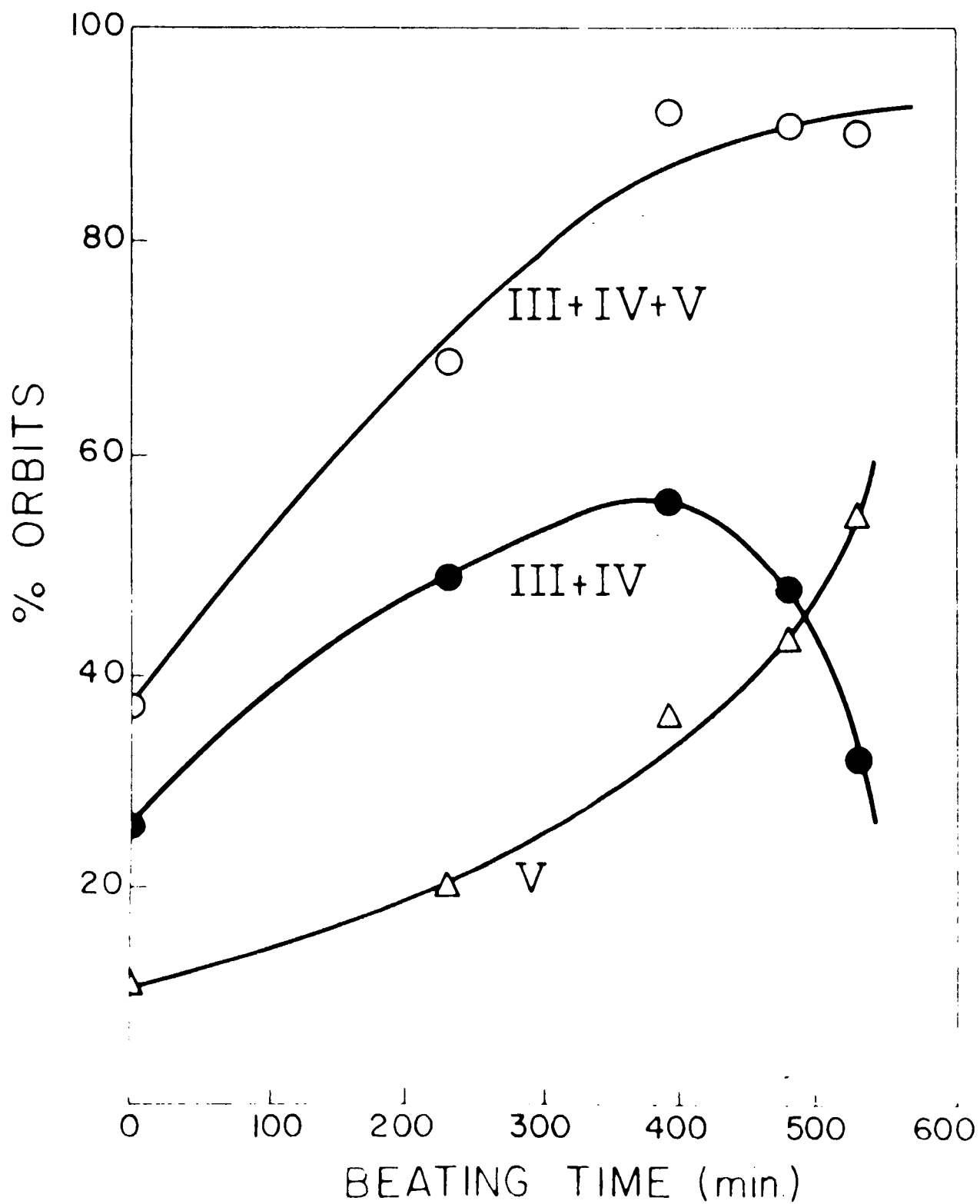
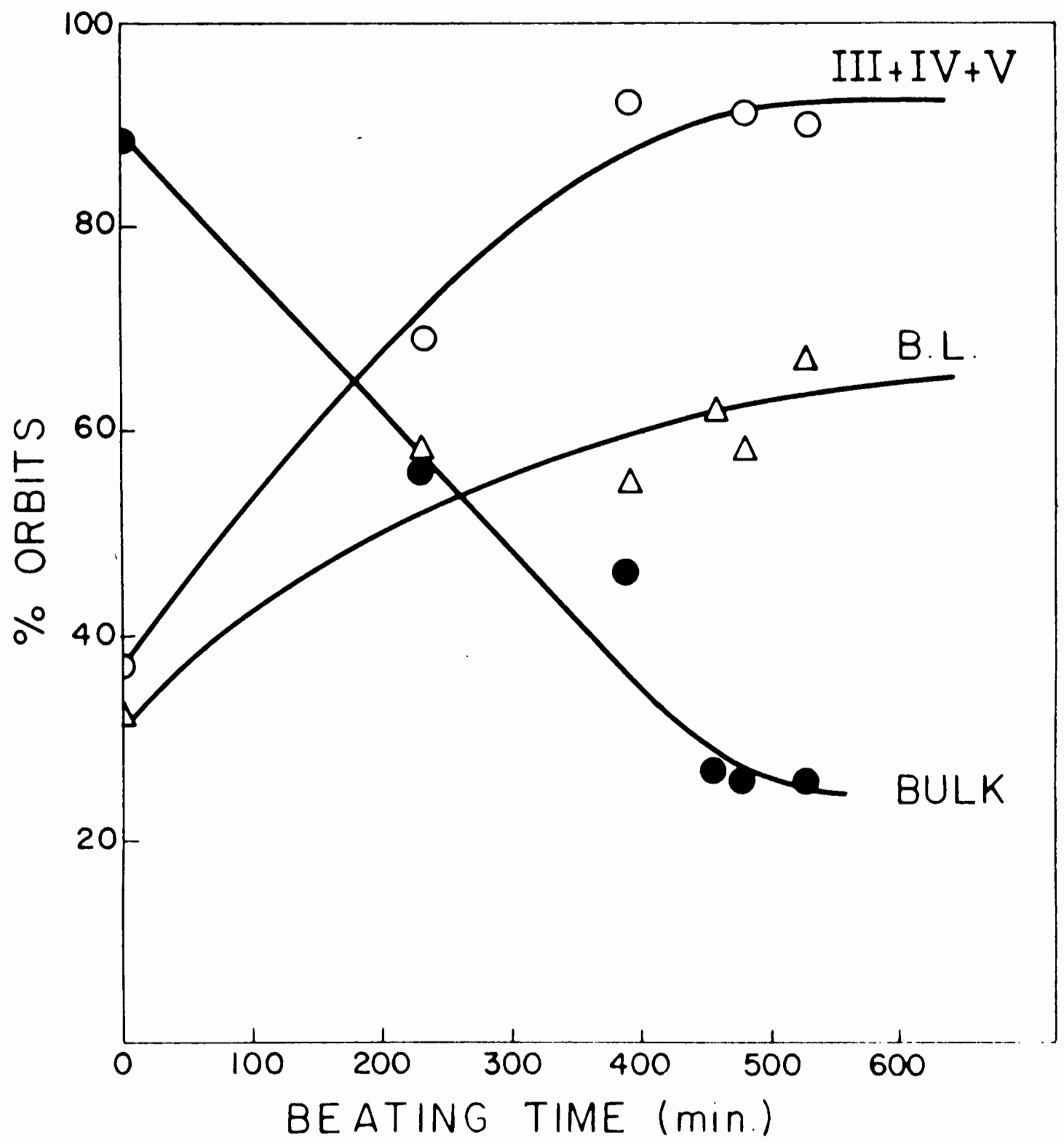


FIGURE 11

Combined flexible orbits (III + IV + V) together with breaking-length and bulk of standard handsheets as a function of beating time (Run 1).



growth of the hydrodynamic specific volume of pulp fibres with beating (16, 17) and the removal of outer secondary wall (14) follow trends similar to the development of flexibility.

An interesting observation in the beater experiments was that the development of joints in thin-walled (early-wood) fibres was more rapid than in thick-walled (late-wood) fibres. Further work is required before speculating on the significance of this and other observations on jointed and uniformly flexible fibres.

4. The Effect of Moisture

Since water acts as a plasticizer for cellulose it was of interest to carry out a few experiments on the effect of drying on flexibility. Three of these are summarized below.

1. A moist sample of the 2 mm. length fraction of 48 per cent yield fibres from the spruce sulphite series was suspended in the castor oil. It was observed that the fibres stiffened appreciably in the course of a few minutes. For example, a fibre which initially described a Type IV orbit lapsed into a Type III orbit within about 2 min., and after a further 2 min. into a Type I orbit. At the same time the lumen collapsed in places causing the fibre to become permanently bent and twisted. This stiffening undoubtedly resulted from dehydration of the fibre by the medium.

2. One sample of the same fibres used in the preceding experiment was oven-dried and another was freeze-dried, to constant weight. Both samples were suspended in castor oil and the orbit distri-

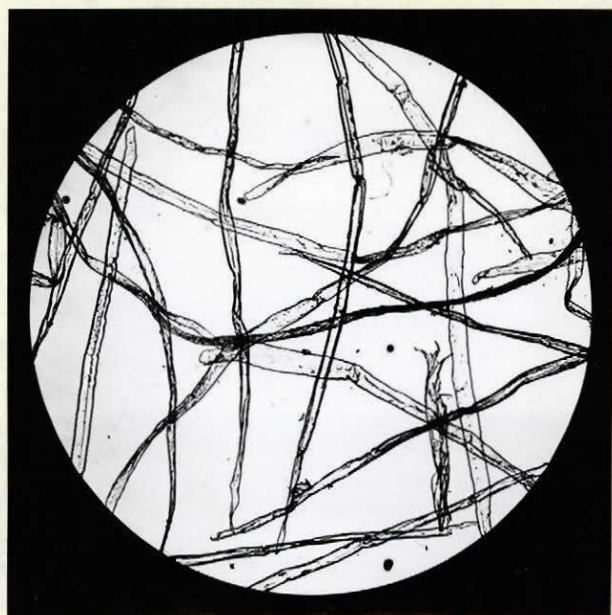
T A B L E VIII

Effect of Drying48% Yield Spruce Sulphite

	SAMPLE	SUSPENDING MEDIUM	Orbit Distributions %			
			I	II	III	IV
a	Freeze dried	Castor oil	74	21	5	0
	Oven dried	Castor oil	43	36	21	0
b	Freeze dried and rewetted	Corn Syrup	1	10	77	12
	Oven dried and rewetted	Corn Syrup	0	2	83	15
	Undried	Corn Syrup	0	8	80	12

FIGURE 12

Photomicrographs, 48% yield spruce sulphite fibres: a) virgin, b) oven dried, c) freeze dried. The collapsed structure of oven dried fibres is reflected in their greater flexibility when observed in castor oil.



3



2



1

butions were determined. Table VIIIa indicates the greater flexibility of the oven-dried fibres compared to those that had been freeze-dried. It was observed that the oven-dried fibres were twisted, deformed and collapsed, whereas the others generally retained their swollen form, as illustrated by the photomicrographs shown in Fig. 12. It is not surprising that the collapsed, ribbon-like structure was less resistant to bending than the open, tubular one. On the basis of previous work (17) it was expected that the freeze-dried fibres would be stiffer.

3. Two further samples which had been dried as above were rewetted and immersed in corn-syrup, which it will be recalled had a relative water vapour pressure of 70 percent and thus acted as a mild swelling agent. The fibres which had been freeze-dried were indistinguishable in appearance from the virgin sample, whereas the fibres which had been oven-dried retained much of their twisted and collapsed appearance. Somewhat surprisingly, the orbit distribution in corn-syrup of both the rewetted samples, however, turned out to be the same as for the virgin sample, within the experimental error (Table VIIIb).

E. DISCUSSION

It is apparent from the results presented above that the method can only be used to advantage when more than one type of orbit is observed in each sample. This can, in principle, be arranged by suitably fixing G , η , the type of suspending medium (so as to control

content of water and other plasticizers) and fibre length. The method therefore appears to be versatile.

In presenting the experimental data in the preceding section the distributions among single orbits or combinations of orbits have been used to compare the mean flexibilities of pulp samples. Other methods of processing the data have been considered, two of these will be described here since they may have further application.

Fig. 12 shows a single differential distribution curve which was constructed to describe the experimental data obtained on the six spruce sulphite pulps cooked to various yields (Table V). In this plot, f is an empirical scale of flexibility which together with the curve was set up in relation to the different orbit types by trial and error so that the area under the curve between any two limits of f yielded the corresponding integral distribution. In this way it was found possible to describe the distribution of each sample in the series by shifting the same distribution curve along the f axis so that the maximum of the curve coincides with the positions indicated for the various samples designated A to F. These correspond to the various yields listed in Table V. The orbit distributions calculated from the area under the curve in the various positions are included in Table V and show good agreement with the directly measured values. This method of representation indicates both the spread in flexibility and a mean value in a given sample, and has advantages which are self-evident. It remains to be seen

how applicable it is to other cases.

The second method is based on measurements using different fibre lengths. Analysis of the curves shown in Fig. 3 has suggested the use of Λ , the fibre length at the point of intersection of the Type I and Types (III + IV) curves for a given pulp (i.e. the length at which there are equal numbers of rigid and flexible fibres) as a statistical parameter describing flexibility. Clearly, the smaller is Λ , the greater is the mean flexibility. Fig. 14 shows the variation of Λ and of Klason lignin content with percent yield for the whole series of spruce sulphite pulps. These curves show clearly the increase in flexibility attending the removal of lignin. Though the determination of Λ involves orbit distributions of at least two length fractions of each sample, Λ is representative of a whole pulp. In comparing the development of fibre flexibility with, say, different pulping methods, the advantages of a single parameter to characterize a sample may outweigh the additional labour involved in its determination.

It has been shown how the orbit distribution method can be applied to compare fibre flexibility in wood pulps, both in the absence and presence of localized damage to the fibres. Though the method yields comparative rather than absolute measurements of fibre flexibility, it has the advantages that:

1. It is easily applicable over the range of lengths corresponding to most wood fibres.

2. Sampling can be carried out rapidly and reproducibly.
3. No tedious manipulation of the individual fibres is required.

Future application of the method to studies of the effect of removing different chemical components from the fibres and of different pulping, drying and beating procedures should provide a deeper insight into the mechanisms of development of fibre-flexibility and of its significance in papermaking.

FIGURE 13

The differential distribution of flexibility $D(f)$ versus flexibility f for spruce sulphite pulps (Table V). As the mean flexibility increases, the curve moves to the right. The arrows indicate the locations of the maximum of the curve for each of the corresponding samples.

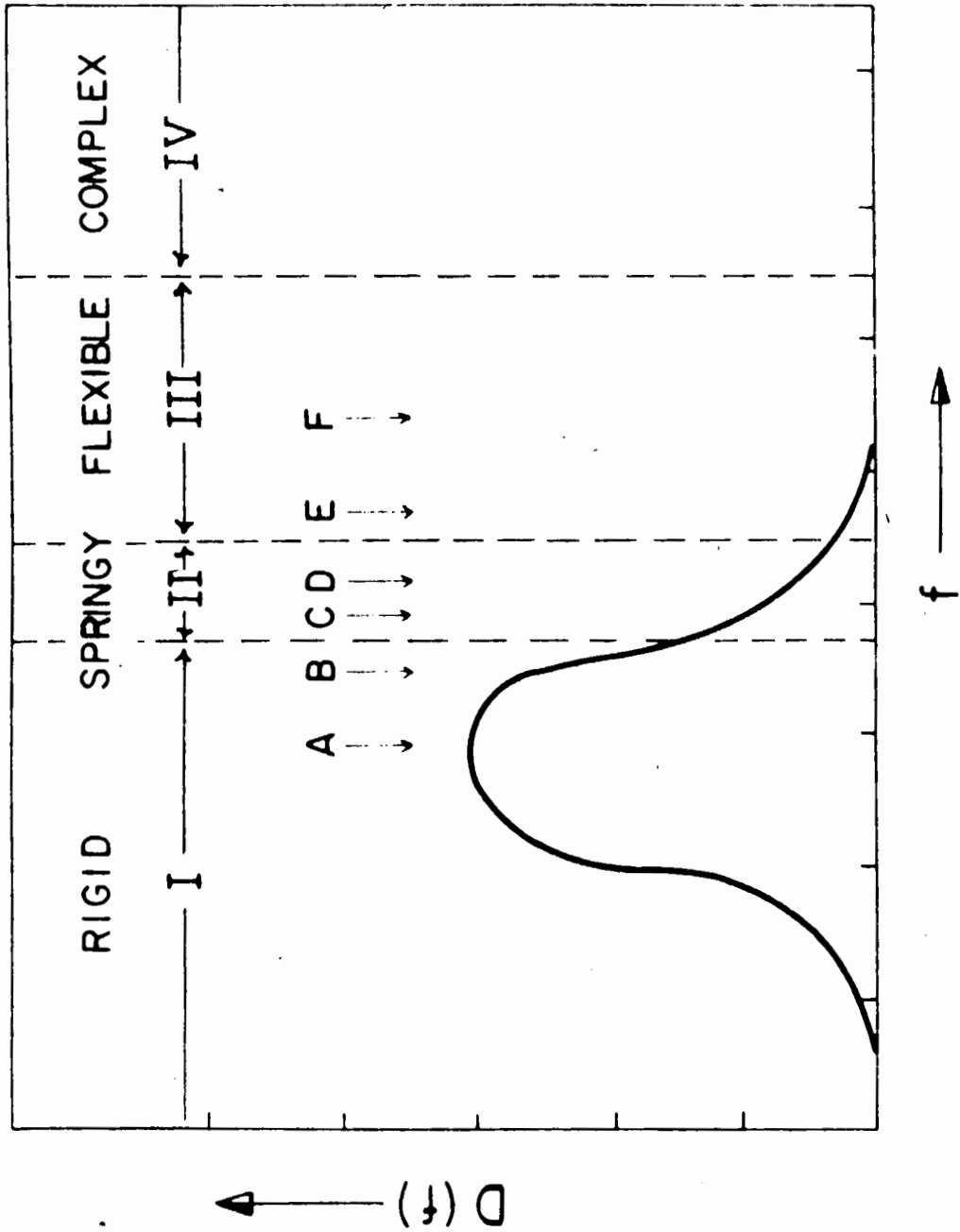
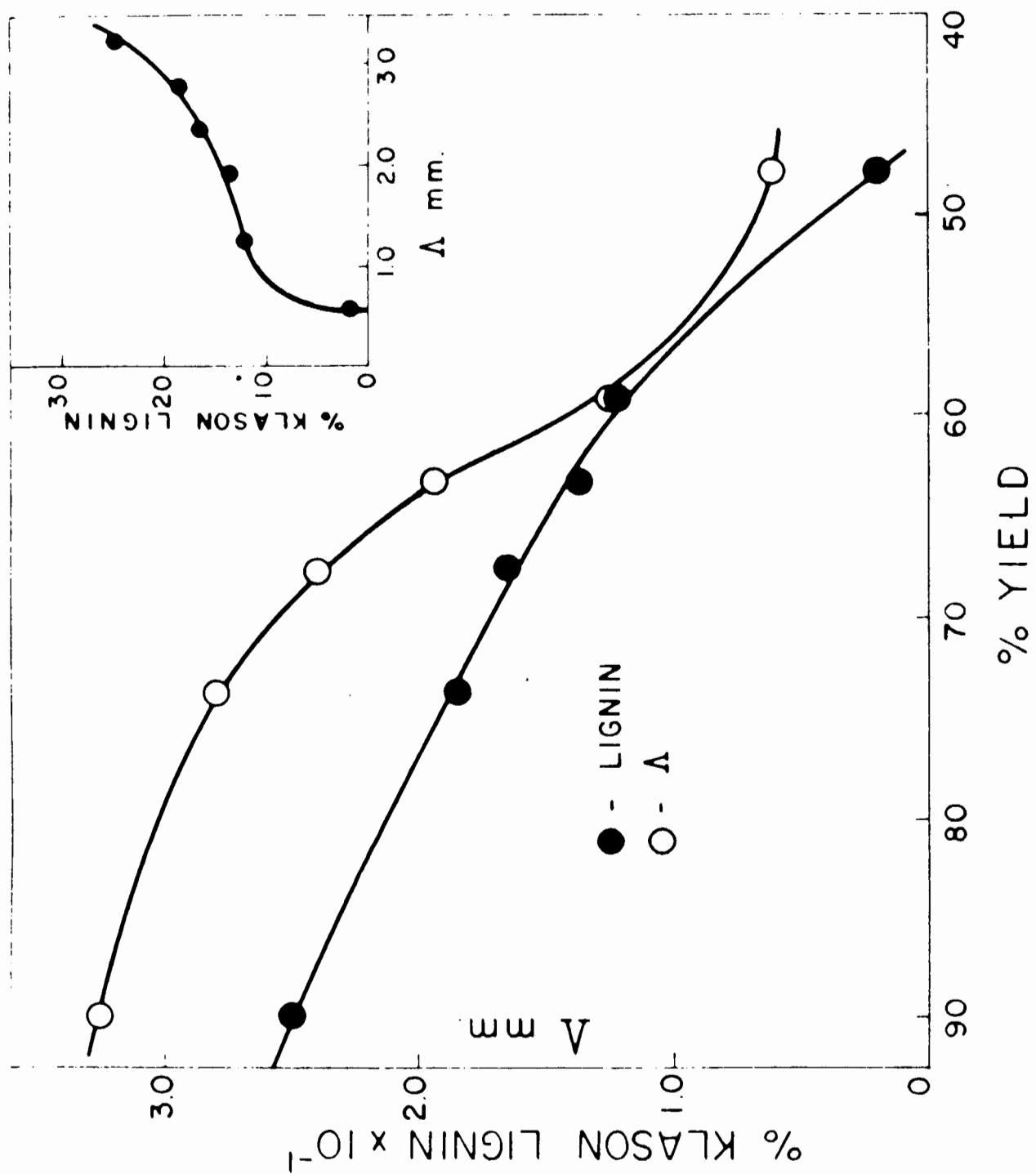


FIGURE 14

Δ and Klason lignin content versus yield for the spruce sulphite series. The development of flexibility attending delignification is also shown by plotting lignin content versus Δ (inset).



F. SUMMARY

When a dilute pulp suspension is subjected to laminar shear, the orbits of rotation described by the individual fibres are related to the ability of the fibres to deform under the stresses generated by the liquid. It was shown that by measuring the distributions among various types of rotational orbit for statistical samples of individual fibres, the fibre flexibility spectra of different pulps may be compared.

A number of pulps were fractionated according to fibre length, and the fibre orbits were observed in a Couette-type apparatus under standardized conditions. The ability of fibres to bend was studied as a function of fibre length and the conditions of pulping and of beating. It was shown that fibre-flexibility increased continuously with decreasing yield for both sulphite and kraft pulps. Whereas the fibres of Sulphite pulps became more flexible on the removal of lignin, it was evident that lignin content was not the dominant factor influencing the flexibility of kraft fibres. Beating increased the ability of fibres to bend, by both softening them and producing localized weak points or hinges.

Some preliminary experiments on the effect of drying are described.

Alternative methods of processing the data which may prove useful in the future are described.

REFERENCES

1. Forgacs, O.L., Robertson, A.A. and Mason, S.G., Pulp Paper Mag. Can. 59, No. 5:117 (1958).
2. Steenberg, B., "Fundamentals of Papermaking Fibres", Tech. Section, B.P. and B.M.A., Kenley, England (1958) p. 239.
3. Emerton, H.W., "Fundamentals of the Beating Process", B.P. and B.I.R.A., Kenley, England (1957).
4. Meredith, R., "The Mechanical Properties of Textile Fibres", North Holland Publishing Co., Amsterdam (1946).
5. Steenberg, B., Finnish Paper Timber J. 29, No. 7A:64 (1947).
6. Nethercut, P.E., Tappi 40, No. 1:39 (1957).
7. Seborg, O. and Simmons, F.A., Paper Trade J. 113, No. 17:49 (1941).
8. Trevelyan, B.J. and Mason, S.G. J. Colloid Sci. 6:354 (1951).
9. Mason, S.G. and Manley, R.St.J., Proc. Royal Soc. (London) A 238:177 (1956).
10. Jeffery, G.B., Proc. Royal Soc. (London) A 102:161 (1922).
11. Mason, S.G., Tappi 37, No. 11:494 (1954).
12. Burgers, J.M., "Second Report on Viscosity and Plasticity", North Holland Publishing Co., Amsterdam (1938).
13. Bartok, W. and Mason, S.G., J. Colloid Sci. 6:354 (1957).
14. Giertz, H.W., "Fundamentals of Papermaking Fibres", Tech. Section, B.P. and B.M.A., Kenley, England (1958) p. 389.
15. Robertson, A.A. and Mason, S.G., Pulp Paper Mag. Can. 50, No. 13:103 (1949).
16. Mason, S.G., Tappi 33, No. 8:403 (1950).
17. Marchessault, R.H., Lodge, W.C. and Mason, S.G., Svensk Papperstidn. 59, No. 24:859 (1956).

Appendix I has been published as: Arlov, A.P., Forgacs, O.L. and Mason, S.G., Svensk Papperstidn, 61, No. 3:61 (1958).

PART V

GENERAL DISCUSSION AND RECOMMENDATIONS FOR FURTHER WORK

It remains to discuss briefly several implications of the findings described in Parts II, III and IV. These are of interest chiefly in connection with the flow properties of suspensions. Finally, recommendations for future studies are made.

A. PREFERRED ORIENTATIONS OF FLEXIBLE PARTICLES

It was observed (Part III) that, provided the deforming forces exerted on a particle by the shear field were sufficient to cause snake rotation, the particle always moved in the course of the first one or two rotations, so that it rotated in or very close to the XY-plane. It should, however, be recalled that according to the theory of bending presented in Part II, the deforming forces acting on a particle decrease with the orbit constant associated with the spherical elliptical orbit on which the particle lies at the onset of shear, as shown in Fig. 3 and Table I, Part II. We should therefore expect, that in a suspension of identical thread-like particles which are initially oriented at random, there will exist over a certain range of shear rates a critical value of the orbit constant C above which the particles move into the XY-plane; below this value they more or less rotate in their original spherical elliptical orbits. We assume here that the dilution is so great that no particle interactions occur. Quantitative experiments to test this prediction would provide an additional test for Burgers' calculation of the axial forces acting on a particle (Part II).

B. THE VISCOSITY OF SUSPENSIONS

It has already been stated in Part I that one of the purposes of studying individual particles in suspensions is to achieve an understanding of the macroscopic behaviour of suspensions. An investigation of the viscosity of suspensions of thread-like particles conducted by Nawab and Mason (1) in conjunction with the present work is therefore of direct interest to this thesis.

Nawab and Mason used suspensions 3.5 μ dia. rayon in castor oil; both the filaments and the suspending medium were identical with those used in the experiments on individual particles described in Section C.2.iii of Part III. Viscosity measurements were made at various particle axis ratios and concentrations, using a "Drage" rotating cylinder viscometer at gradients between 9 and 100 sec.^{-1} . Before the results of this work are discussed, a brief summary of the relevant viscosity theory must be given.

The theory of the viscosity of suspensions of rigid elongated particles has been developed for prolate spheroids by Jeffery (2) and extended by Guth (3, 4), who obtained the relationship for the intrinsic viscosity.

$$\alpha_0 = (\eta_{sp}/c)_{c=0} = \frac{r}{(2 \log_e 2r - 3)} + 2 \quad (1)$$

for $r \gg 1$ and $C = \infty$ for all particles. Burgers (5) simplified the problem by considering cylindrical particles of negligible thickness. Burgers first calculated the viscosity contribution α_0 of a single thin rod at a given

orientation θ, ϕ , relative to the shear field

$$\alpha_0 = m \cdot f(r) \quad r \gg 1 \quad (2)$$

where $f(r) = \frac{r^2}{6(\log_e 2r - 1.8)}$ is the particle shape factor and

$m = \sin^4 \theta \sin^2 2\phi$ is the particle orientation factor. The resemblance between Eq. (2) and Eq. (9) of Part II for the force F acting on the central cross-section of a rod should be noted.

The time average value \bar{m} for a particle obeying the equations of motion of a prolate spheroid (see Eq. 1 and 2 of Part II) at constant C is given approximately by

$$\bar{m}(C) = \frac{2C}{r(C^2 + 1)^{1/2}} \quad (3)$$

which has its maximum value when $C = \infty$ and minimum value when $C = 0$. To calculate α_0 for the suspension, the distribution of C must be known. Thus on the basis of Eisenschitz's hypothesis (6) mentioned in Part IB, calculation of \bar{m} over all orbits yields

$$\alpha_0 = \frac{4 f(r)}{\pi r} \quad (4)$$

If all the particles assume orbits $C = \infty$

$$\alpha_0 = \frac{2 f(r)}{r} \quad (5)$$

However, it has been shown in Part III and elsewhere (7, 8, 9) that the "equivalent ellipsoidal axis ratio" r_e of a cylindrical particle calculated from the experimentally determined period of rotation T and gradient G by means of Jeffery's equation

$$TG = 2\pi r_e \quad \text{for } r \gg 1 \quad (6)$$

was always lower than the true r of the particle.

The variation of the angle ϕ with time for a particle moving in a spherical elliptical orbit is given by

$$d\phi/dt = \frac{G}{r_e^2 + 1} (r_e^2 \cos^2 \phi + \sin^2 \phi) \quad (7)$$

It follows from Eq. (7) that a cylindrical particle spends less time, than does a prolate spheroid of the same axis ratio, in the neighbourhood of $\phi = \pm 90^\circ$ which corresponds to the position in which the instantaneous contribution to viscosity is a minimum, as shown by inspection of Eq. (2).

Nawab and Mason (1) therefore suggested that $\bar{m}(C)$ should be greater by a factor $\beta = r/r_e$ than given by Eq. (3).

Correction of Eq. (4) and (5) therefore yields

$$\alpha_0 = \frac{4\beta f(r)}{\pi r} \quad , \quad (\text{Eisenschitz distribution}) \quad (8)$$

and

$$\alpha_0 = \frac{2\beta f(r)}{r} \quad , \quad (C = \infty) \quad (9)$$

The experimentally determined values of α_0 obtained by Nawab and Mason are compared with values predicted from Eq. (1), (4), (8) and (9) in Fig. 1. The values of β used in Eq. (8) and (9) were calculated from the experimentally determined TG values given in Table III of Part III.

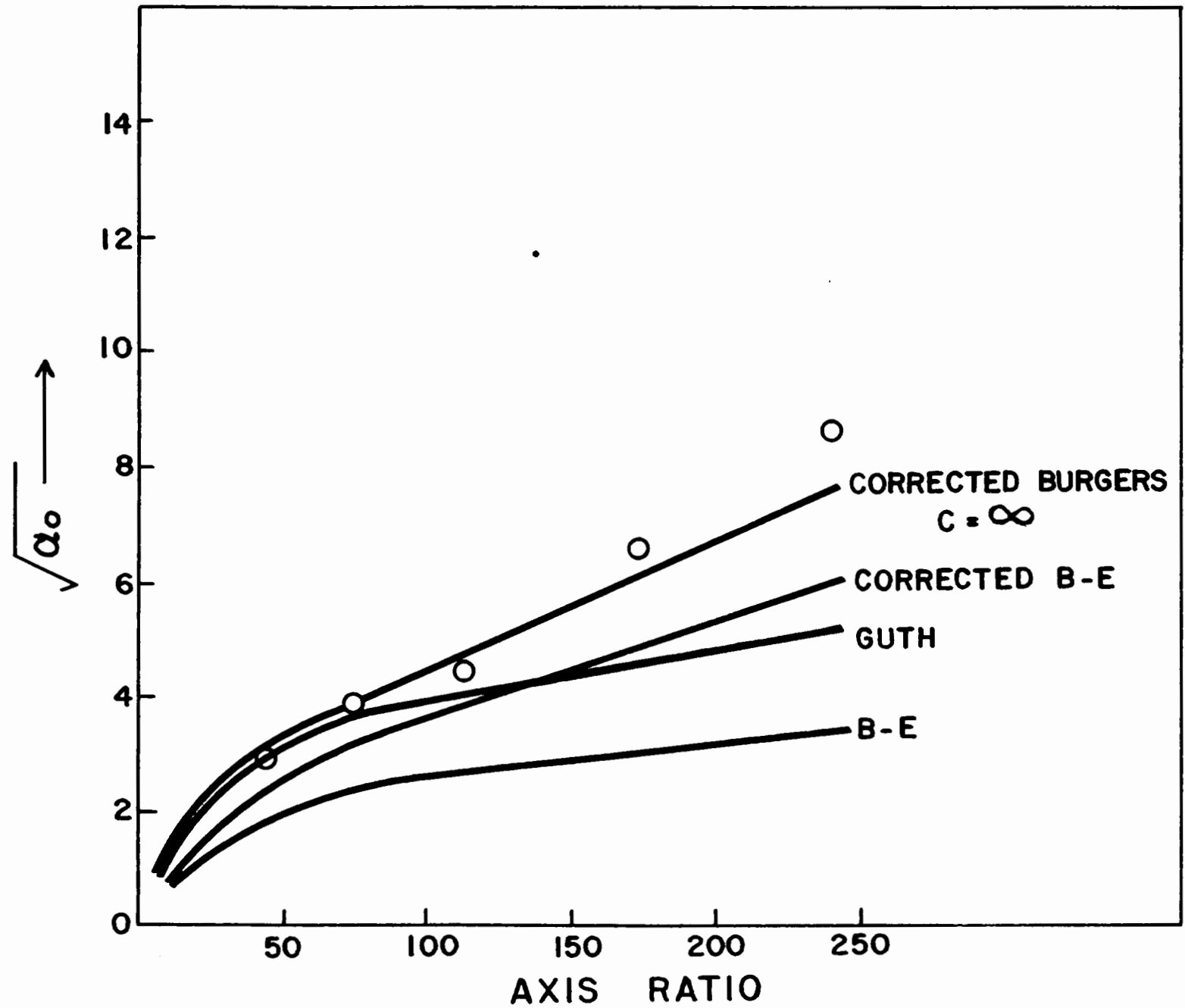
Clearly, the best agreement was provided by Eq. (9) which assumes $C = \infty$. Fig. 1 also shows that at high axis ratios, the predicted values of α_0 were still too low, but it must be noted that the TG values used to calculate β were determined for particles which were straight when at rest. Since many of the particles used by Nawab and Mason had permanent deformations (10) and since it has been shown that such deformations greatly decrease TG, and hence β (Section C.2.ii of Part III), it is certain that the values of β chosen to correct Eq. (9) were too low.

An irreversible increase in the absolute viscosity observed during the early stages of shearing of the suspensions of the particles of higher axis ratio was almost certainly the result of permanent deformation, and strengthens the case for the use of β .

Other discrepancies could be caused by a deviation of curved particles and flexible particles from the equations of motion of prolate spheroids. However, the agreement between the predicted and observed axial spin of curved particles shown in Part II provides indirect evidence that such particles move in the predicted spherical elliptical orbit. That the motions of flexible particles deviate from the motions of ellipsoids was

FIGURE 1

Graph of $(\alpha_0)^{1/2}$ vs. r . The points represent the experimentally determined values of Nawab and Mason (1). The curves represent Eq. (1) - Guth; Eq. (4) - Burgers (Eisenschitz); Eq. (8) - Corrected Burgers (Eisenschitz); Eq. (9) - Corrected Burgers ($C = \infty$).



clearly shown in Part III, but it was also shown that the change in the product TG was small compared to that caused by deformation. It therefore seems unlikely that the results in Fig. 1 were greatly influenced by flexibility of the particles. Also it was shown by Nawab and Mason that α_0 appeared to be independent of G even for suspensions of particles of axis ratio at which they were undoubtedly flexible on shearing in the viscometer. Nevertheless it must be assumed that the shape factor $f(r)$ in Eq. (2) is changed by shear-induced deformation.

Further quantitative studies of the deviation of particles describing springy and snake orbits from the equations of motions of ellipsoids and rigid rods would be of value.

Studies of the viscosity of suspensions of very flexible filaments which form coils would also be of great interest. A highly sensitive viscometer would have to be used to enable viscosities to be measured at sufficiently low concentrations to prevent entanglement and aggregation of the particles. But even in the presence of entanglement, such experiments may prove to be of interest in connection with the flocculation of pulp suspensions.

In this context, experiments in the Couette apparatus to study the disturbance to the field of flow caused by helices and coils should also be profitable to determine the extent to which they are "free draining". Such experiments would be of value in connection with the theory of viscosity of "free-draining" and "partially draining" coiled macromolecules. This

could be done by studying the flow lines inside and outside the coils by means of small tracer particles in the suspending medium.

C. THE WEISSENBERG EFFECT

In the viscosity measurements of Nawab and Mason (1), the effect of flexibility of the particles was not apparent. However, it was noticed that suspensions of filaments of axis ratios, at which it was predicted from observations in the Couette apparatus (Section C.2.iii of Part III) that the particles would be flexible on shearing in the viscometer, the suspensions crept up the inner cylinder of the viscometer. This effect was noticed to a slight extent at axis ratio 174 and became more pronounced at the higher axis ratios.

This phenomenon was identified with the Weissenberg effect (11) which is commonly exhibited by visco-elastic gels and solutions (11).

The effect was attributed to recoverable elastic properties of the system, which cause tangential tensile stresses in the liquid when it is sheared. It had not previously been reported for suspensions, though it has since been found to occur also with suspensions of flexible pulp fibres (12). It is not however known whether the effect will occur in dilute solutions of flexible filaments, where particle interactions are negligible.

By means of the theory of shear-induced bending developed in Part II, it is possible to predict with some accuracy whether particles

at a given r and $G\eta$ will bend during shearing. The theory should therefore prove useful in further work on the Weissenberg effect to ascertain whether it is produced by flexible rotations of the individual particles (and not by rigid rotations) or whether concentrations, at which particle interactions are significant, are required.

D. THE FLEXIBILITY OF PULP FIBRES

The study of the flexibility of Douglas Fir pulps of different yields (Part IV) was conducted concurrently with studies of flocculation in suspensions of samples of the identical pulps (12). Comparison of the results with the flexibility measurements indicated that the friction losses occurring during turbulent flow of the suspensions through a pipe decreased with increasing fibre flexibility. The tensile strengths of fibre "networks" (12) in suspensions and wet webs tended to increase with flexibility.

The results of Part IV also suggested that the increase in tensile strength and the decrease in bulk with beating were also to some extent associated with increasing fibre flexibility.

It is apparent that fibre flexibility plays an important part in determining the macroscopic characteristics of fibre assemblies.

However, further work is required under more standardized conditions before definite correlations with fibre flexibility can be established. When the properties of assemblies are to be compared with fibre flexibility, it is emphasized that pulps fractionated to similar fibre

length distributions should be used in the experiments on the assemblies, since it has been shown that the ability of fibres to bend is extremely sensitive to fibre length.

Apart from establishing the role of fibre flexibility in determining the characteristics of pulp suspensions and of paper, further work on the factors which influence the flexibility of individual fibres would be of interest. The following experiments are suggested:

1. Flexibility measurements of fibres of the same species, from which different chemical components (e.g. hemicelluloses, lignin etc.) have been removed by carefully controlled laboratory methods.
2. Experiments to compare the flexibility of early- and late-wood fibres.
3. Flexibility measurements of fibres conditioned at various relative humidities, suspended in a non-hygroscopic medium, such as a high viscosity silicone oil.
4. A study of the effect of ultrasonic beating on fibre flexibility. By using this method of beating, the occurrence of localized damage to the cell walls can be avoided.

E. SUMMARY OF RECOMMENDATIONS FOR FURTHER WORK

1. Extension of the theory of deformation of thread-like particles beyond the conditions of critical bending.
2. A quantitative study of the preferred orientations of deformable thread-like particles, and of orientation distributions both in the XY- and

XZ-planes.

3. Further studies of the mechanisms of helix and coil formation.
4. Experiments to determine the disturbance to the field of flow caused by coiled filaments, using tracer particles in the suspending medium.
5. Quantitative studies of the effect of moisture-content on the flexibility of wood-pulp fibres.
6. Systematic experiments to determine:
 - (i) The effect of fibre flexibility on the rheological properties of fibre assemblies, e.g. suspensions, networks, wet webs and paper sheets.
 - (ii) The effect on fibre flexibility of the removal of chemical components from the fibres.
 - (iii) The effect on fibre flexibility of various pulping methods and mechanical treatments.
 - (iv) The flexibility of different species of fibres.

REFERENCES

1. Nawab, M.A. and Mason, S.G., J. Phys. Chem. In Press.
2. Jeffery, G.B., Proc. Royal Soc. (London) A 102:117 (1922).
3. Guth, E., Kolloid Z. 74:147 (1936).
4. Guth, E., Phys. Rev. 53:926A (1938).
5. Burgers, J.M., Second Report on Viscosity and Plasticity. North Holland Publishing Co., Amsterdam (1938), Ch. III, 10.
6. Eisenschitz, R., Z. Phys. Chem. A 158:84 (1932).
7. Trevelyan, B.J. and Mason, S.G., J. Colloid Sci. 6:354 (1951).
8. Mason, S.G. and Manley, R.St.J., Proc. Royal Soc. (London) A 238:117 (1956).
9. Bartok, W. and Mason, S.G., J. Colloid Sci. 12:243 (1957).
10. Nawab, M.A., Ph.D. Thesis, McGill University, Montreal (August, 1957).
11. Weissenberg, K., Proc. First Int. Cong. Rheology, Holland, 29 (1948) and Nature 159:310 (1947).
12. Forgacs, O.L., Robertson, A.A. and Mason, S.G. Pulp Paper Mag. Can. 59:117 (1958).

CLAIMS TO ORIGINAL RESEARCH

1. The axial spin of rigid cylindrical particles in laminar shear has been shown to be in quantitative agreement with that predicted from Jeffery's theory for prolate spheroids, provided that the experimentally determined "equivalent ellipsoidal axis ratio" was used.

2. A theory was developed for the critical conditions beyond which a thin cylindrical particle will deform under the stresses exerted by the liquid. The results of experiments to test the theory were in good agreement with those predicted.

3. The motions of thread-like particles undergoing various degrees of deformation were studied. It was shown that the rotational orbits of deformable particles differ increasingly from those of rigid cylinders as the particles become more flexible. Highly flexible particles form helices and coils which in some respects behave like deformable spheres.

4. A method of measuring the flexibility of pulp fibres was developed, based on the rotational orbits of the individual fibres in liquid shear. The scope of the method was illustrated by means of experiments which show the changes in fibre flexibility during pulping, beating and drying.

APPENDIX I

Particle Motions in Sheared Suspensions

6. General Behaviour of Wood Pulp Fibres

A. P. Arlov¹, O. L. Forgacs and S. G. Mason

Physical Chemistry Division, Pulp and Paper Research Institute of Canada, Montreal

Rotationsrörelser hos träfibrer i vätskesuspension i laminär rörelse beskrives. Det visas att rotationens natur bestäms av fibrens flexibilitet. Styva fibrer roterar i cirkulära elliptiska banor i stort sett på samma sätt som styva släta stavar, för vilkas rörelse en väl utvecklad teori finnes. Flexibla fibrer roterar på ett betydligt mer komplicerat sätt. Det har befunnits möjligt att urskilja ett fåtal olika typer av rotationsbanor, vilka kan tjäna som karakteristikum på fiberflexibilitet. Till skillnad från styva fibrer visar isolerade flexibla fibrer en tendens att övergå till två "preferred" slag av rotationsbanor, karakteriserade av två banparametrar, nämligen de som motsvarar rotation kring fiberaxeln endast samt rotation endast kring en mot denna vinkelrät axel. I utspädda suspensioner är situationen mera likartad den som gäller för styva stavar, där samverkan mellan partiklarna ofta ändrar banparametrarna. Omloppstiden är hos flexibla fibrer betydligt mindre än hos styva med samma dimensioner, och produkten av omloppstid och hastighetsgradient, som är konstant hos styva stavar, tilltager hos flexibla partiklar med växande hastighetsgradient, vilket kan tillskrivas den med hastighetsgradienten växande deformationen.

The rotations and spins executed by wood-pulp fibres suspended in a liquid subjected to laminar shear are described. It is shown that the type of rotation depends upon whether the fibres are rigid or flexible. When rigid, the fibres spin and rotate in spherical elliptical orbits in the same general manner as smooth rigid rods for which the theory is well developed. When the fibres are flexible, the rotations are much more complicated. It has been found possible, however, to make a simple classification of types of rotational orbits, which, it is suggested, may serve as a quantitative method of measuring the spectrum of fibre flexibilities.

Unlike rigid fibres, isolated flexible fibres show a pronounced tendency to assume one of two preferred rotational orbit constants, one corresponding to pure spin without rotation and the other to pure rotation without spin. On the other hand, in dilute suspensions the steady state distribution of orbit constants of fibres is similar to that in suspensions of rigid rods of comparable axis ratio where, it has been shown, the distribution is determined by interaction effects.

Periods of rotation T of flexible fibres are substantially lower than for rigid rods of corresponding axis ratio. The product TG of rigid rods remains constant over a range of velocity gradients G whereas with flexible fibres it increases appreciably with increasing G , an effect which has been shown to be associated with the accompanying increase in the amount of fibre deformation during rotation.

Die Rotationsbewegungen von Holzfasern in Flüssigkeitssuspensionen mit Lamellenströmung werden beschrieben. Es zeigt sich, dass die Natur der Rotation von der Faserflexibilität bestimmt wird. Steife Fasern rotieren in zirkulären, elliptischen Bahnen ungefähr in derselben Weise wie steife, glatte Stäbe, für deren Bewegung eine gut ausgebaute Theorie existiert. Flexible Fasern rotieren auf eine bedeutend kompliziertere Art. Es konnten einige verschiedene Typen von Rotationsbahnen bestimmt werden, welche als Charakteristikum für die Faserflexibilität gelten können. Zum Unterschied von steifen Fasern zeigen isolierte flexible Fasern eine Tendenz, zwei vorgezogene Rotationsbahnen zu beschreiben. Diese sind charakterisiert durch zwei Bahnparameter, die einerseits einer Rotation um die Faserachse und andererseits einer Rotation um eine zu dieser senkrechten Achse entsprechen. In verdünnten Suspensionen ist die Situation ähnlich jener bei steifen Fasern wo das Zusammenwirken zwischen den einzelnen Partikeln die Bahnparameter oft ändert. Die Umlaufzeit bei flexiblen Fasern ist bedeutend kürzer als bei steifen mit denselben Dimensionen. Das Produkt von Umlaufzeit und Geschwindigkeitsgradient, welches bei steifen Fasern konstant ist, steigt bei flexiblen Fasern mit wachsendem Geschwindigkeitsgradienten, was der mit dem Geschwindigkeitsgradienten steigenden Deformation zugeschrieben werden kann.

Introduction

Particles in liquid suspensions subjected to laminar shear undergo rotational and translational movements. Previous papers in this series have dealt with rotations, collisions and other interactions, and orientation of simple particles such as rigid and fluid spheres (1, 2) and smooth rigid cylinders (2, 3) in very dilute suspensions. Most of the phenomena observed can be explained by hydrodynamical theory.

This paper describes similar observations on wood-pulp fibres. While there are many points of similarity

to rigid cylinders, the phenomena are complicated by the irregularities in the shape of fibres and by their tendency to undergo bending during rotation.

The phenomena described are of interest in connection with flow, aggregating and other properties of pulp suspensions (4, 5).

Experimental method

The experimental work was conducted by means of the two twin-cylinder Couette devices previously described (1, 2). In each apparatus, two precision-bore concentric cylinders are rotated in opposite directions by driving mechanisms which enable the

¹Present address: Norwegian Pulp and Paper Research Institute, Oslo.

APPENDIX II

A. THE COUETTE APPARATI

The experimental observations were made using two twin-cylinder Couette devices which were constructed by the Design and Shops Group of the Pulp and Paper Research Institute of Canada. The essential features of the apparati have been described previously in the scientific literature (1, 2). For completeness of this thesis, a description of the apparati is given, including some modifications which were made in the course of the present work. Some additional notes on the materials and the experimental technique are also given.

1. Principles of the Apparatus

The Couette devices were designed to permit observations of individual particles in suspension subjected to laminar shear. In each apparatus, two co-axial cylinders are rotated in opposite directions about the vertical axis by means of drives, the speeds of which could be varied independently. The suspension is placed in the annulus between the two cylinders.

A particle in a liquid which is subjected to laminar shear moves with the same translational velocity as the shear stratus of the undisturbed liquid which is replaced by its centre. Since the cylinders are rotated in opposite directions a stationary layer is established. By adjusting the speeds of the cylinders, this layer can be made to coincide with the centre of a particle located anywhere in the suspension.

The principle of the arrangement is shown in Fig. 1. Referred to the co-ordinate system used throughout these studies and shown in Fig. 1 of Part II, the X-axis at any point in the liquid is parallel to the direction of flow, the Y-axis is the direction of the gradient across the annulus and the Z-axis is normal to the XY-plane.

2. Effective Shear Rate

The shear rate (G) created by the rotating cylinders is not constant across the gap, but decreases across the gap between the inner and outer cylinders. However, it was shown by Mason (1) that for particles whose dimensions were small compared with the width of the annulus, the effect of non-uniformity of the gradient could be neglected. But it cannot be neglected in calculating the velocity gradient in the stationary layer.

At a radial distance R between the two cylinders, it may readily be shown (1) that the velocity gradient G_R is given by

$$G_R = \frac{2(\omega_a + \omega_b)}{\left(\frac{1}{R_a^2} - \frac{1}{R_b^2}\right) R^2} \quad (1)$$

where G_R = the velocity gradient at R .

R_a = radius of the outer cylinder.

R_b = radius of the inner cylinder.

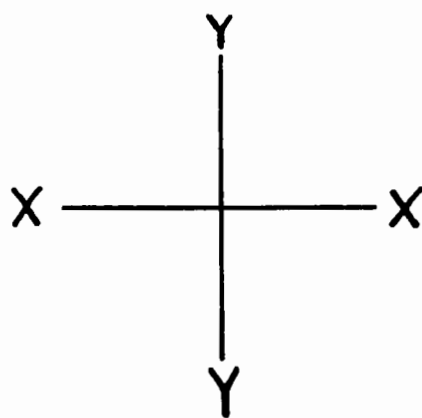
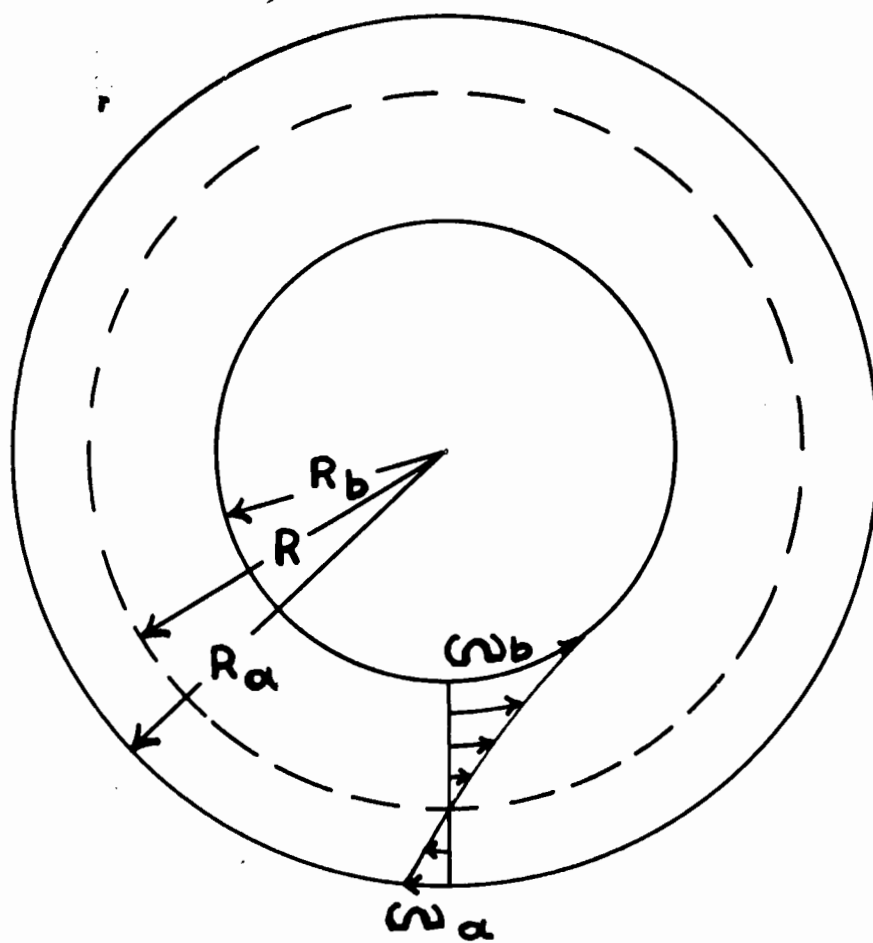
ω_a = angular velocity of the outer cylinder.

ω_b = angular velocity of the inner cylinder.

Appendix II

FIGURE 1

Principle of the Couette Apparati



At the stationary layer, Eq. (1) becomes

$$G = \frac{2 \left(\frac{R_a^2}{R_b^2} \omega_a + \omega_b \right)}{\frac{R_a^2}{R_b^2} - 1} \quad (2)$$

whence G can be calculated from the radii and angular velocities of the cylinders.

3. Apparatus No. 1

The Apparatus No. 1, Fig. 2, to observe particle motions by viewing along the Y-axis (normal to the planes of shear) was first used by Trevelyan (1) and later by Manley (3) and Bartok (2).

Details of the apparatus are shown in the cross-sectional diagram Fig. 3. The cylinders 1 and 2 were of precision-bore pyrex tubing. The outer cylinder was mounted on a brass block 3 containing a drainage hole 4. The inner cylinder was suspended from a brass block 5 and fitted with a pyrex plug 6 at the lower end. The blocks were geared to separate driving mechanisms. Each driving mechanism consisted of a Graham continuously-variable-speed drive. Connected to the input was a 3600 r.p.m. synchronous motor and to the output a 50:1 speed reducer which was interchangeable with a 25:1 reducer. The output of each reducer was coupled to a driving shaft 10 and 12 of the apparatus proper. Direct-reading tachometers (not shown in Figs. 2 and 3) were driven off the shafts.

The dimensions of the cylinders and the relationship for calculating G obtained from Eq.(2) are given in Table I.

The microscope was readily movable in three dimensions, so that any particle in the annulus could be focussed.

4. Apparatus No. 2

A second apparatus, Fig. 4, arranged for viewing along the Z-axis, was first used by Bartok (2) and is shown schematically in Fig. 5. To permit illumination from below, the outer cylinder had a bottom and a cover plate of glass. Two interchangeable inner cylinders of different diameters were available. Dimensions of the cylinders together with the relationships for calculating G are given in Table I.

The microscope could be focussed vertically. As in Apparatus No. 1, it was mounted integrally with the light source and could be rotated through 180° about the axis of the cylinders.

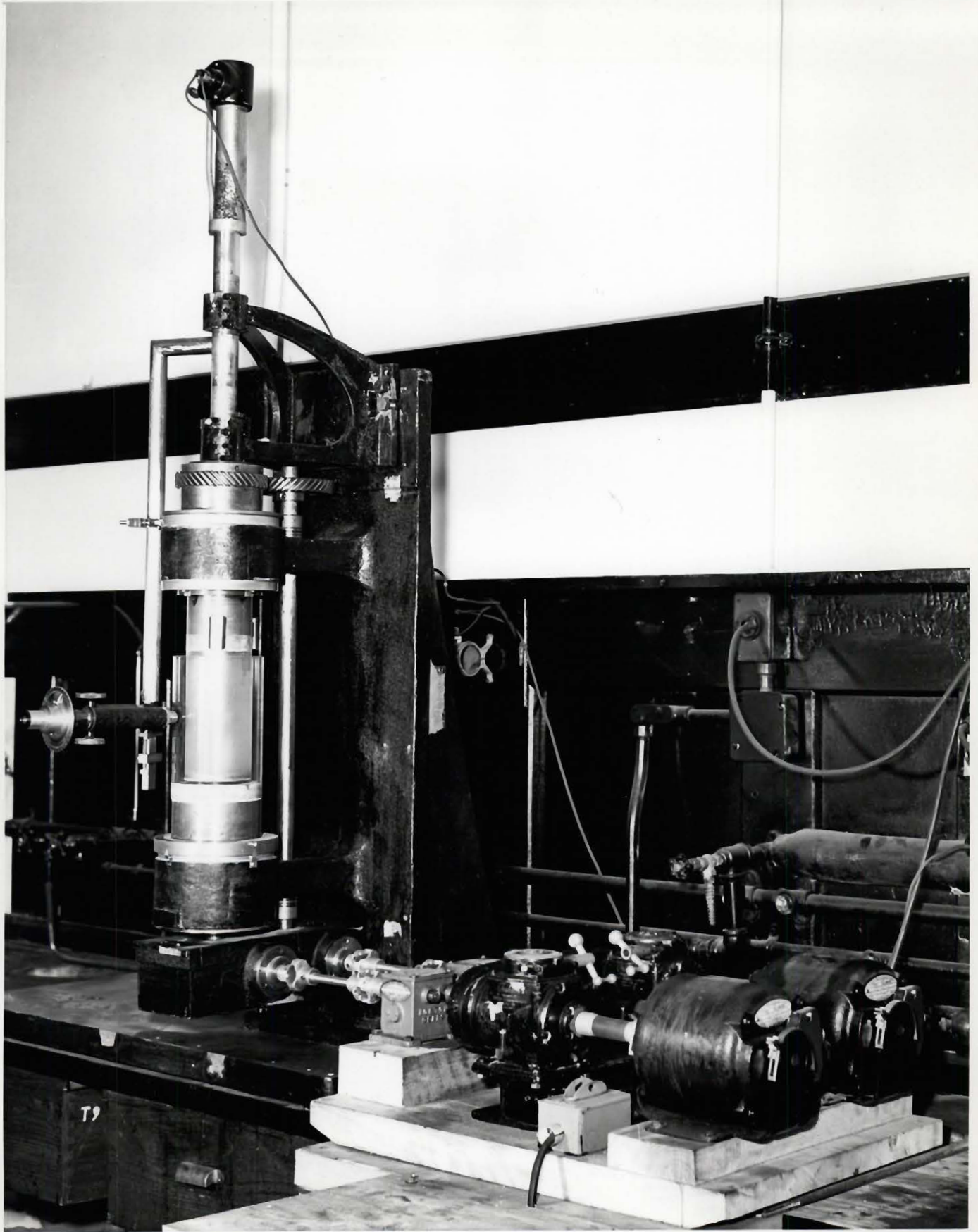
The driving mechanisms were similar to those in the first apparatus. Three speed reducers of ratios 50:1, 25:1 and 12.5:1 were available.

The experiments in Part II of this thesis required an accurate knowledge of the viscosity of the suspending medium in the annulus. It was found that the proximity of the light source to the outer cylinder as shown in Fig. 4 and 5 caused appreciable temperature-gradients in the liquid, thus establishing convection currents. This difficulty was overcome by

Appendix II

FIGURE 2

Photograph of the Apparatus No. 1. The microscope is aligned for viewing along the Y-axis.

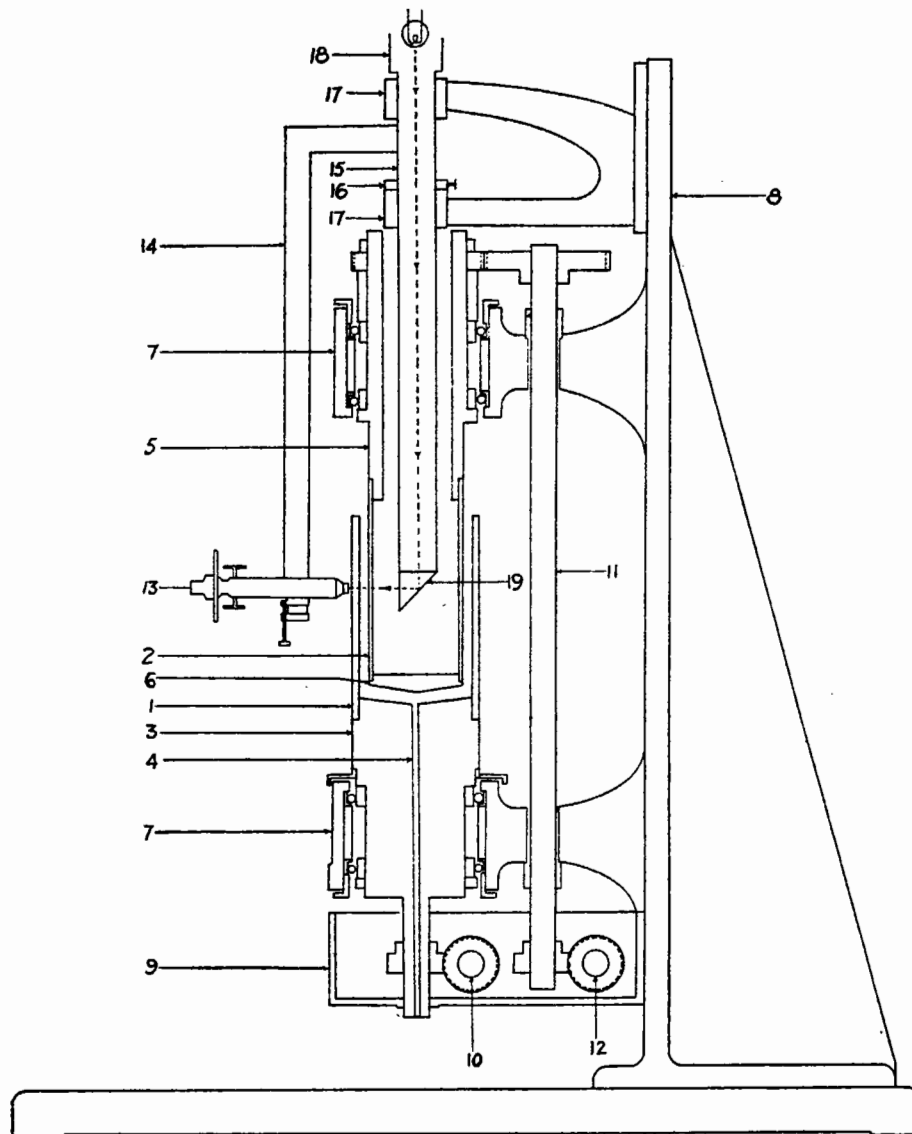


Appendix II

FIGURE 3

Schematic diagram of the Apparatus No. 1.

After Trevelyan and Mason (1).



Appendix II

FIGURE 4

Photograph of the Apparatus No. 2.
The microscope is aligned for viewing
along the Z-axis.



Appendix II

FIGURE 5

Sectional diagram of the Apparatus No. 2.

After Bartok and Mason (2).

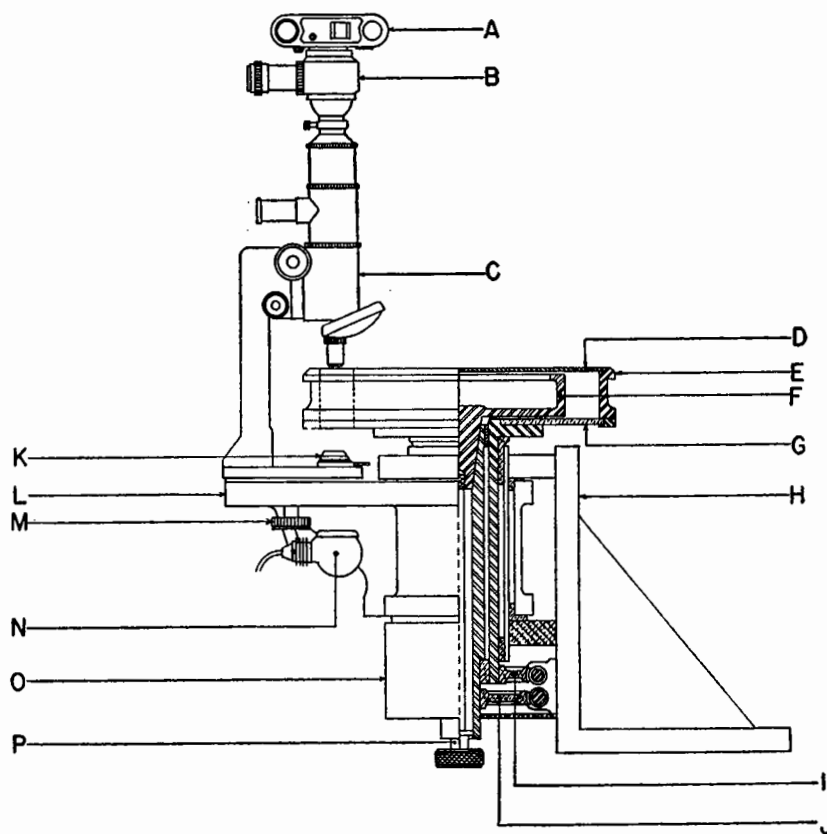


FIG. 5. Cross-sectional view of the concentric cylinder apparatus for observations along the Z -axis. Legend: *A*—camera; *B*—beam splitter; *C*—microscope; *D*—glass cover plate; *E*—outer cylinder; *F*—inner cylinder; *G*—bottom glass plate; *H*—apparatus mount; *I*—outer cylinder worm drive; *J*—inner cylinder worm drive; *K*—iris diaphragm; *L*—microscope swivel mount; *M*—traversing knob; *N*—light source; *O*—gear housing; *P*—inner cylinder release rod.

Appendix II

T A B L E I

Dimensions and Speeds of Couette Cylinders

Apparatus	Outer Cyl. Inner dia. in.	Inner Cyl. Outer dia. in.	Inner Cyl. Height in.	Relationship for G^x sec. ⁻¹	With 25:1 Reducer [*] :	
					Range of R.P.M.	Range of G
No. 1	4.498	3.698	7	$0.646 N_a + 0.437 N_b$	0 to 7.5	0 to 8.1
No. 2	11.995	9.017	2	$0.4815 N_a + 0.2721 N_b$	0 to 7.5	0 to 5.6
		10.515	2	$0.9044 N_a + 0.6950 N_b$	0 to 7.5	0 to 10

^x N_a and N_b are R.P.M. of outer and inner cylinders respectively.

^{*} Maximum values of R.P.M. and G with 50:1 or 12.5:1 reducers are obtained by dividing or multiplying given values by 2 respectively.

using a "Zirconarc" lamp (Fish-Schurman Corp., New Rochette, N.Y.) mounted horizontally about 24 ins. below the cylinders. The beam was reflected by means of a plane mirror tilted to 45° and located vertically below the axis of the microscope. Despite the greater working distance, this powerful source provided ample illumination for black and white or colour photo- and cine-micrography even with polaroid filters.

5. Avoidance of Wall Effects and End Effects.

In both apparatus, observations of particles close to the cylinder walls were avoided. In the Apparatus No. 1, end effects were avoided by using only the central 4 ins. of the vertical length of the annulus for observations.

In the Apparatus No. 2, distortion of the shear field due to the bottom of the annulus was eliminated by floating the suspending medium on a layer of an immiscible liquid of much lower viscosity.

Corn syrup ($\rho = 1.38 \text{ g/cc}$) was floated on carbon tetrachloride ($\rho = 1.60 \text{ g/cc}$) and castor oil (300 oil), ($\rho = 0.99 \text{ g/cc}$) was floated on a 20% solution of cadmium nitrate ($\rho = 1.19 \text{ g/cc}$). Nevertheless, circulation effects across the annulus occurred at G greater than 10 sec.^{-1} , so that particles could not be kept stationary in the microscope field without changing the location of the stationary layer. This indicated an upper limit of 10 sec.^{-1} to the range of gradients which could be used for precise measurements of particle rotations in the Apparatus No. 2.

6. Precision of Calculated Values of G

In both Apparati, experiments to test Eq. (2) by comparing observed and predicted periods of rotation of rigid spheres (1, 2) revealed that values of G calculated from Eq. (2) were accurate to several parts in a thousand.

B. PHOTOGRAPHIC TECHNIQUES

Most of the observations were made through a Zeiss stereomicroscope, with built-in interchangeable objectives. The following magnifications with the associated field diameters were available using a 10x eyepiece: 6.3x, 32mm.; 10x, 20mm.; 16x, 12.5mm.; 25x, 8 mm.; 40x, 5mm.

Photomicrographs were taken by means of a "Robot Royal" camera, mounted directly to a photographic (monocular) tube which was fitted with a beam-splitter.

Several demonstration films of the motions of pulp fibres (Part IV) were made using a "Bolex" 16mm. cinecamera. The camera was mounted on a framework which was attached to the microscope swivel mount, and aligned with but not attached to the camera. The particle image seen through the beam-splitter was focussed on the position of the film by means of a gate-focuser in the camera, without using a camera objective. Very satisfactory results were obtained with suspensions in corn syrup using Super Anscochrome film (120 ASA). Since wood-pulp fibres are birefringent, contrast was greatly improved by using polarized light.

This arrangement did not permit the integral mounting of the heavy camera on the microscope; therefore individual particles were focussed separately at the beginning of each sequence.

C. PREPARATION OF FILAMENT SAMPLES

To obtain filaments of the required lengths, the continuous threads were first wound tautly across a framework consisting of two parallel sets of pins 8 cm. apart.

The mounted threads were embedded in "Tissuemat" wax. To ensure close contact between the threads and the embedding medium, the threads were first thinly coated with a solution of the wax in xylene by means of a small paint-brush and dried to form a thin film of wax on the surface of the material.

The block of wax between the pins was removed and sectioned to required lengths in a sliding microtome. The wax was dissolved by washing the sections in xylene. The xylene was removed with ethanol and the specimens were dried from anhydrous ether. Although xylene acts as a mild swelling agent on most polymeric materials, no dimensional changes of the filaments were observed provided prolonged contact with the solvent was avoided. An alternative embedding agent, "Carbowax" (Polyethylene Glycol made by the Union Carbide Co., N.Y.: a 8:3 mixture of grades 4000 and 1500 respectively was found suitable) was also used. This material was water soluble, and proved very satisfactory for Dacron, which does not swell appreciably in water.

The lengths of the sectioned filaments were measured accurately using a projecting microscope. Standard deviations for the mean length of the samples were between 8 and 11%.

D. MEASUREMENT OF THE PERIODS OF ROTATION

The periods of rotation T (Part III) of thread-like particles rotating in the XY-plane were timed in the Apparatus No. 2, by visual observation, using a stopwatch.

A hair-line in the microscope eyepiece was aligned with the Y-axis. With straight rigid particles, the watch was started when the axis of the filament was parallel with the hairline and stopped when the particle reached the same position after a rotation through $\phi = 360^\circ$. With curved particles and those undergoing springy or snake rotations, the period was timed between the positions in which the imaginary line joining the two ends of a particle was parallel with the hairline and the corresponding position after a 360° rotation.

For measurements of T in the Apparatus No. 1 (Part II), the hairline was aligned with the Z-axis, and timings were again taken between positions in which the particle axis, or the line joining the ends, was parallel with the hairline.

Both these positions corresponded to orientations of the particles at which their angular velocity was greatest, and where consequently small errors in judging the position of the particle at the beginning and end of the periods made their least contribution to the

value of T.

The periods of curved particles which underwent axial spin (Part II) fluctuated between certain limits, as the result of the varying shape the particles presented in the field of flow in the course of rotation in the spherical elliptical orbit. For such particles, a mean value of T was calculated from timings over at least ten rotations.

E. VISCOSITIES OF SUSPENDING MEDIA

The viscosities of corn syrup and castor oil used in the present work were determined at various temperatures, using a DRAGE (A.G. Epprecht, Chemical Institute, Zurich, Switzerland) rotating cylinder viscometer. The results, which are given in Table II, were in good agreement with those obtained by the "falling-sphere" method (4). Both the corn syrup and the castor oil exhibited Newtonian behaviour over the gradients of 0 to 100 sec.⁻¹.

The viscosity of CHP (Cyclohexanol Phthalate) which was considered as an alternative non-aqueous suspending medium is included in Table II. This liquid was rejected as a suspending medium because of the high temperature dependence of its viscosity, but was used as the internal phase in experiments with fluid drops (Part III).

Appendix II

T A B L E IIViscosities of Suspending Media

Liquid	Method	t°C.	η poises
Corn Syrup Sample 1 [*]	Drage	18.2	111.4
		20.4	86.9
		24.2	57.0
Corn Syrup Sample 2 [*]	Falling Sphere	21.0	80.5
		25.5	49.3
		30.9	27.8
Castor Oil	Drage	19.2	44.6
		25.0	26.2
		30.0	17.6
GHP	Falling Sphere	20.0	238.0
		25.5	85.9
		28.0	54.1

^{*} Samples 1 and 2 were obtained from different batches.

REFERENCES: APPENDIX II

1. Trevelyan, B.J. and Mason, S.G., J. Colloid Sci. 6, No. 4:354 (1951).
2. Bartok, W. and Mason, S.G., J. Colloid Sci. 12, No. 3:243 (1957).
3. Manley, R.St.J. and Mason, S.G., Can. J. Chem. 33:763 (1955).
4. Reilly, J. and Rae, W.N., "Physico-Chemical Methods", Vol. I, Fifth Ed., p. 677, Methuen and Co. Ltd., London (1954).

APPENDIX III

GLOSSARY

For the benefit of readers not familiar with papermaking, a brief note on the composition of wood is given, together with a glossary of the specialized terms used in Part IV.

1. The Structure of Wood

CELLULOSE is the principal constituent of wood (45-55%). Associated with it, in varying amounts, are LIGNIN (24-28%), a group of polysaccharides known as HEMICELLULOSES (14-30%), pectic substances, fats, waxes, gums, essential oils and small quantities of other substances. From the papermaking point of view, the most important of these are cellulose, lignin and the hemicelluloses.

Cellulose is a polysaccharide composed of linear chains of glucopyranose residues, D.P. 3000 to 5000. These chains form the main structural units of fibres.

Hemicelluloses are polysaccharides of lower D.P., and form part of the system penetrating the amorphous regions of the cellulose fabric.

Lignin is a highly complex aromatic polymer. It forms the greater portion of the middle lamella between the fibres, and cements these together; it also occurs in the amorphous regions of the fibre wall. In order to isolate the fibres the lignin must be partially removed. This may be achieved by cooking the wood in acid or alkaline liquors which react preferentially with the lignin to render it soluble.

2. Chemical Pulping

Sulphite Pulping: A method of chemical pulping in which the wood is cooked in a liquor containing NaHSO_3 and SO_2 . The amount of lignin removed may be varied by varying the temperature, the pH and the time of cooking.

Kraft (Sulphate) Pulping: A method of chemical pulping in which the wood is cooked under pressure in an alkaline liquor containing NaSH and NaOH . The amount of lignin removed may be varied by varying the maximum temperature and the time.

Yield: The estimated percentage by weight of oven-dry pulp, obtained from the original oven-dry wood, after chemical pulping.

3. Chemical Tests

Klason Lignin Estimation: A standard method of estimating the lignin content of wood or wood pulps by dissolving the carbohydrate fraction with 72% H_2SO_4 . The residual material is known as Klason lignin.

Pentosan Estimation: The hemicelluloses in softwoods contain a high percentage of pentosans (five carbon sugars). Estimation of the pentosan content therefore serves as a guide to the hemicellulose content. In the standard method (Tappi T 450 sm-40) the furfural produced by the action of hot 3.5 N HCl on the sample is separated by distillation.

4. Mechanical Treatment and Physical Tests

Beating: Mechanical treatment given to papermaking fibres suspended in water to mix and prepare them for forming in the paper machine

into paper of the desired characteristics. The "Valley Beater" used in this work was of the widely used Hollander type. The suspension is circulated in a vat containing a heavy roll rotating against a bed-plate. The roll and bed-plate contain horizontal metal bars, set on edge. As the result of beating, the structure of the fibre walls is loosened and disrupted (fibrillated) and the fibres swell.

Freeness: The quality of a pulp suspension that determines the rate at which it parts with water when being formed into a sheet on a wire screen or perforated plate.

In the Canadian Standard Freeness test, a 0.3% suspension is used in a standard instrument. Freeness forms a convenient though somewhat arbitrary measure of the extent to which a pulp has been beaten.

Bulk: This term is a measure of the density of paper. It is defined as

$$\text{Bulk} = \text{Thickness (microns)} / \text{substance (gm./m}^2\text{)}$$